A Theoretical and Experimental Study of the Optical Forces from a Laser Beam

by Hongyan Zhao

A thesis submitted to

the Faculty of Graduate Studies and Research
in partial fulfillment of the requirements for the degree of

Master of Science

Department of Physics &

Department of Biomedical Engineering

McGill University

Montreal, Quebec, Canada

September, 1991

© Hongyan Zhao, 1991

ABSTRACT

7

養

A practical geometric optics method for derivation of the optical forces from light rays was described. By this method, the forces from a G.P.W. (Gaussian Plane Wave) and a general TEM₀₀ laser beam were calculated and studied. For a G.P.W. beam, there were two forces which acted on small particles located inside the electromagnetic field; one, called the scattering force, directed in the beam propagation direction, pushed particles axially. The other, called the gradient force, due to the non–uniformity of the electromagnetic field, acted like an optical well and confined the particles to the beam axis. The forces from a general TEM₀₀ beam behaved differently due to the profile of the beam. It was shown that axial confinement was also possible for a highly focused TEM₀₀ beam, therefore providing the possibility of single beam trapping. The relationship between the forces and the profile of a TEM₀₀ laser beam was investigated comprehensively.

Three experimental stations were designed and built. Both upward and downward accelerating experiments were constructed to confirm the existences of the scattering force and the gradient force in a G.P.W. beam. Furthermore, the scattering force was studied quantitatively. A single beam trapping experiment was designed to verify the possibility of axial constraint of small particles by a highly focused TEM₀₀ laser beam. The single beam trapping conditions found in the experiment were in agreement with the results of the theoretical analysis.

RÉSUMÉ

Une méthode pratique d'optique géometrique pour déterminer la force optique de rayons de lumière est décrite. Par cette méthode, les forces d'une O.P.G. (Onde Plane Gaussienne) et d'un faisceau laser (TEM₀₀) ont été calculées et étudiées en profondeur. Pour un faisceau O.P.G., il y a deux forces qui agissent sur les petites particules à l'intérieur du champ électromagnétique; la premiére, nommée la force de dispersion, dirigée dans la direction de la propagation du faisceau, pousse les particules dans le sens axial. La deuxière, nommée la force de gradient, due à la non-uniformité du champ électromagnétique, agit comme un puits optique et retient les particules dans l'axe du faisceau. Les forces du faisceau TEM₀₀ se comportent différemment selon le profil du faisceau. Il a été démontré qu'il est possibile de retenir les particules dans le sens axial avec un faisceau TEM₀₀ hautement focalisé, offrant la possibilité d'un unique faisceau de capture. Le rapport entre la force et le profil du faisceau TEM₀₀ laser a été étudié en détail.

Trois stations expérimentales ont été concuees et construites. Des expériences avec des accélérations vers le haut et vers le bas ont été faites afin de confirmer l'existence d'une force de dispersion et d'une force graduée dans un faiseau O.P.G.. En plus, la force dispersée fut étudiée de manière quantitative. Une expérience pour la capture par faisceau unique a été élaborée pour vérifier la possibilité de contrainte axiale des petites particles par un faisceau laser TEM₀₀ hautement focalisé. Les conditions obtenues expérimentalement pour la capture par faisceau unique furent en accord avec les résultats de l'analyse théorique.

ACKNOWLEDGEMENTS

I would like to express my deepest appreciation to my thesis supervisor, Professor Ian W. Hunter, for his guidance, encouragement and patience during my studies at the department of Biomedical Engineering. I admire his deep insight into many scientific subjects and his enthusiasm and vigor for research. His completeness and thoroughness of scientific thought have had a profound influence on me.

Special thanks are due to Mr. Serge Lafontaine for his valuable advice and suggestions. He is a wonderful person full of scientific knowledge. He is also a nice friend who is willing to give his help at any time.

Thank Professor Arthur Ashkin for many telephone discussions with him which had given me valuable ideas and encouraged me to accomplish those experiments.

Thank my co-supervisor in Department of Physics, Professor Zaven Altounian, for his encouragement and support. He is a kind professor to talk with.

Thank Professor Lynette Jones, for her kind help in data analysis.

I would like to thank Dr. Yangming Xu, for his help in the many discussions on this work.

Thank my fellow students in the Biorobotics Laboratory, particularly Colin Brenan and Paul G. Charette, for their creative ideas and the helpful discussions we had. Their valuable help was evident in every aspect of my thesis work. I would like to thank Telly Doukoglou, for his kind help in solving computer problems, Stev Thomson for his help in machining. Without their efforts, this dissertation would have been impossible.

Thank my very good friends, Jon Bart Macneil, Paul Henri and Steve Kacani for their kind help in writing this thesis.

Thank Sylvain Martel, for being a good co-researcher and translating the English abstract of this thesis into French.

Last but not least, I would like to thank my husband, Jiantao Ma, for his help in every aspect of this thesis. Thank my parents and my sisters for their encouragement, continuous support and understanding over these two years.

The financial support from the Department of Physics in the form of a Reinhardt bursary and from McGill University in the form of CIDA fellowship is greatly appreciated.

Glossary of Abbreviations and Symbols

CW Continuous Wavelength G.P.W. A Plane Wave with Transverse Gaussian Intensity Distribution. N.A. Numerical Aperture Fundamental Gaussian Beam TEM_{oo} \vec{E} **Electric Field Vector** \vec{B} Magnetic Field Vector λ Light Wavelength Light Velocity с š **Energy Flow** \ddot{T} Electromagnetic Stress Tensor E **Electric Permittivity** Inverse Magnetic Permeability μ Beam Waist Radius ω \vec{k} Beam Propagation Direction Ryleigh Size z_R Laser Power R **Energy Reflection Coefficient** \boldsymbol{T} **Energy Transmission Coefficient VAF** Variance Accounted for RSS Residual Sum of Squares SC Sample Multiple Correlation Coefficient Particle Radius Q $n(n_s, n_m)$ Refractive Index (of sphere and medium respectively)

 β_k

Regressed Parameters

Contents

Chapter 1	
Introduction	
1.1 Prologue	
1.2 Survey of the Relevant Literature	2
1.3 Introduction of the Theoretical Model for Deriving the Forces	
1.4 Physical Properties of Gaussian Beams	10
1.4.1 Analytical Expressions of a TEMoo Beam	10
1.4.2 Transformation and Magnification by a Simple Lens	12
1.4.3 The Relation Between the Force and the Beam Profile	14
1.5 Scope of Thesis	1.5
Chapter 2	
Theoretical Study of the Optical Forces from a Laser Beam	16
2.1 The Force Element from a Single Ray	16
2.2 Forces on the Sphere by a G.P.W	19
2.2.1 Equations of the Force	19
2.2.2 Results and Discussions	22
2.2.2.1 Results from the Numerical Integration of Fz (Qz)	22
2.2.2.2 Results from the Numerical Integration of Fy (Qy)	23
2.2.3 Summary	25
2.3 Radiation Forces from a TEMoo Beam	
2.3.1 Equations of the Forces	25
2.3.1.1 The Propagating Direction of	
a Specified Ray in a TEMoo Beam	27
2.3.1.2 The Angular Coordinates of the Specified Ray	28
2.3.1.3 The Expressions of Qz and Qy	29
2.3.2 Results and Discussions	32
2.3.2.1 The Force along the Beam Axis	32
2.3.2.2 The Transverse Force	40
2.3.3 Summary	45
2.4 Summary	46
Chapter 3	
Experimental Study of the Ontical Forces from a Laser Ream	47

3.1 Upward Accelerating Experiment	47
3.1.1 Apparatus	48
3.1.2 Experimental Equipment and Design Specifications	49
3.1.3 Observations	51
3.1.4 Data Acquisition	52
3.1.5 Theoretical Model	53
3.1.6 Data analysis	55
3.1.7 Discussion	65
3.2 Downward Accelerating Experiment	66
3.2.2 Design Specification	67
3.2.3 Observations	69
3.2.4 Data Acquisition	69
3.2.5 Theoretical Model	70
3.2.6 Data Analysis	70
3.2.7 Discussions	77
3.3 Single Beam Trapping Particles	77
3.3.1 Apparatus	78
3.3.2 Observations	79
3.3.3 Conclusions	80
3.4 Summary	81
Chapter 4	
Conclusions	82
4.1 Summary	82
4.2 Limitations and Recommendations for Future Work	83
4.2.1 Computation	83
4.2.2 Experiments	83
Appendix 1	
Fresnel Coefficients	85
Appendix 2	
Derivation of the Angular Coordinates	
in the Particle Coordinate System of a Specified Ray	86
Appendix 3	
Computer Programs	91
Bibliography	104

List of Figures

Figure 1.1: Schematic diagram of the force derivation by a geometric
optics model
Figure 1.2: Propagating Gaussian beam (from: Yariv, 1975) 12
Figure 1.3: Force components on a particle placed at point P in a focused
TEMoo beam (from: Ashkin, 1989) 14
Figure 2.1: Schematic diagram of the ray path through a sphere of radius ρ
and index n_s
Figure 2.2: O-XYZ coordinate system fixed at the center of the sphere.
Point P is on the spherical surface. Point B is the projection of
point P on the XY plane. The wave propagates along the
opposite direction of Z axis
Figure 2.3: Value of Qz over the ratio of the particle size and beam waist
radius
Figure 2.4: Value of Qy over the ratio of the offset from Z-axis and beam
waist radius 24
Figure 2.5: Value of Qy over the ratio ρ_0/ω
Figure 2.6: Particle coordinate frame O-XYZ and beam coordinates
O'-rz. The origin of O-XYZ is fixed at the center of the
sphere and the Z axis is anti-parallel to the beam axis. The
origin of O'-rz is at the center of the beam whose coordinates
in O-XYZ is (0,yo,zo)
Figure 2.7: Schematic diagram of the normal line to the equal-phase
surface
Figure 2.8: Schematic diagram of the incideny ray DC in the coordinate
system O-XYZ
Figure 2.9: Reflection plane of an incident ray
Figure 2.10: Profiles of laser beam for various waist radius
Figure 2.11: Movement of sphere in a highly focused laser beam 34
Figure 2.12: Results cf Qz for ω_0 =0.05 μ m
Figure 2.13: Results of Qz for ω_0 =0.05 μ m
Figure 2.14: Results of Qz for ω_0 =0.1 μ m

Figure 2.15: Results of Qz for ω_0 =0.2 μ m
Figure 2.16: Results of Qz for ω_0 =0.5 μ m
Figure 2.17: Results of Qz for $\omega_0=1\mu m$
Figure 2.18: Results of Qz for ω_0 =5 μ m
Figure 2.19: Results of Qz for $\omega_0=10\mu m$
Figure 2.20: Movement of sphere transverse to the beam axis 41
Figure 2.21: Results of Qy for $\omega_0=10\mu m$
Figure 2.22: Results of Qy for ω_0 =5 μ m
Figure 2.23: Results of Qy for ω_0 =3 μ m
Figure 2.24: Results of Qy for $\omega_0=1\mu m$
Figure 2.25: Results of Qy for ω_0 =0.5 μ m
Figure 2.26: Results of Qy for ω_0 =0.1 μ m
Figure 2.27: Results of Qy for ω_0 =0.05 μ m
Figure 3.1: A schematic diagram of the upward accelerating experiment
apparatus
Figure 3.2: A schematic diagram of the bar
Figure 3.3: A schematic diagram of the chamber with needle inside 51
Figure 3.4: A schematic diagram of data acquisition 53
Figure 3.5: A schematic diagram of the forces acted on a particle 54
Figure 3.6: A plot of the displacement versus time 56
Figure 3.7: A schematic diagram of downward accelerating experiment. 67
Figure 3.8: A schematic diagram of the chamber 68
Figure 3.9: A schematic diagram of single beam trapping experiment. 78
Figure A2.1: A schematic diagram of a ray incident on a sphere 86
Figure A2.2: A schematic diagram of the system of a ray incident on a
sphere and its sectional drawing when point I is in the first
quadrant
Figure A2.3: A sectional drawing for the case where I is in the second
quadrant
Figure A2.4: A sectional drawing for the case where I is in the third
quadrant
Figure A2.5: A sectional drawing for the case where I is in the fourth
quadrant
Figure A2.6: A schematic diagram of the system of a ray incident on a
sphere with β <0

List of Tables

ĺ

Take T

Table 2–1: Results of the angle and magnitude of exiting rays	18
Table 3-1: Magnitude of the parameters in the movement equation	55
Table 3-2: Data of captured particle size, laser power and	
measured velocity.	57
Table 3–3: Results of linear regression analysis	59
Table 3-4: Data of the three velocities for glass beads	60
Table 3-5: Data of PMMA latex beads: particle size,	
laser power and measured velocity	62
Table 3-6: Results of regression analysis for PMMA latex beads.	63
Table 3-7: Data of the three velocities for PMMA latex beads	64
Table 3-8: Data for glass beads: particle size,	
laser power and measured velocity	71
Table 3-9: Data for PMMA latex beads: particle size,	
laser power and measured velocity	72
Table 3–10: Regression analysis for glass beads	73
Table 3-11: Regression analysis for PMMA latex beads	74
Table 3-12: Data of the three velocities of glass beads	75
Table 3-13: Data of the three velocities of PMMA latex beads	7 6
Table 3-14: Results of beam size and divergence	
for different beam expander	79

Chapter 1

Introduction

1.1 Prologue

In the Biorobotics Laboratory of the Department of Biomedical Engineering at McGill University a prototype of a high performance micro-robot was developed in order to perform surgery, dynamic mechanical testing and manipulation of microscopic objects such as single living cells (Hunter, et al., 1990). The micro-robot (MR1) consists of two parallel drive limbs, with four linear electromagnetic actuators in each limb. The tips of the limbs can move in two overlapping spherical spaces of 1 mm uiameter. The speed and accuracy of the limb movements, under closed loop conditions, are in the excess of 1 kHz for movements of a few nm. MR1 already utilizes the current technology in electromagnetic actuators to its maximum. In order to improve the performance of micro-robot, (in building the next generation one –MR2), different kinds of actuators should be considered.

One possible solution was provided by the development of the technology of laser applications. Since the first demonstration of laser trapping of single dielectric spheres [Ashkin, 1970], experiments have been carried out which demonstrated the ability of the laser to confine, separate, orient and precisely manipulate single cells in controlled environments with neither mechanical contact nor optical damage. Among the several methods of optical trapping [Ashikin, 1971; 1987; Roosen, 1977; 1979], the single beam optical trap was the most convenient and practical one, which used only one highly focused beam to hold particles in the same manner as a pair of tweezers and depended only on optical forces for its stability.

The goal of this thesis is to study the principles of the single beam optical trap, determine the best conditions of this optical trapping theoretically and design several experimental stations to confirm those theoretical results. Chapter 1 reviews the fields of laser manipulation of small particles and the method for calculating the photon momentum from a light beam. Chapter 2 derives the forces of radiation pressure resulting from different laser beam profiles and discusses those results. Chapter 3 explains the details of the experimental apparatus and presents experimental results. Chapter 4 discusses some possible improvements to the experiment.

1.2 Survey of the Relevant Literature

Light is made up of photons which have momentum. Therefore, light can exert forces on an illuminated object. However, because light momentum is very small, there had not been practical applications of light force until the invention of lasers. The coherent, highly directional and high density properties of lasers provide radiation forces strong enough to affect the dynamics of small neutral particles. Stemming from the realization of the large magnitude of radiation pressure from lasers and the observation that radiation pressure could be utilized in a way which avoids disturbing thermal effects, in 1970, Dr. A. Ashkin first demonstrated that micro-sized particles were accelerated and trapped in stable optical potential wells using only the force of radiation pressure from a continuous laser [Ashkin, 1970]. His experiment showed that a one watt continuous wavelength (CW) argon ion laser at $\lambda = 0.5145 \ \mu m$ focused on a lossless dielectric sphere of radius $r = \lambda$ and density $10^3 \ kg/m^3$ gave a radiation pressure $0.66 \ nN$, and the resulting acceleration of the sphere $(1.2 \times 10^6 \ m/s^2)$ was 10^5 times the acceleration of gravity.

More importantly, his experiment showed that a light beam with a transverse gradient of light intensity striking a sphere of refractive index greater than the external medium exerted

not only a force along the beam propagation direction, but also a transverse component of force which pushed the particle toward the region of maximum light intensity. The force along the beam propagation is called the scattering force; it points in the direction of the incident light, and is proportional to the light intensity. It is the only force component that exists in a plane wave light beam. The transverse force, called the gradient force, exists in beams with non–uniform intensity, and is proportional to the gradient of the intensity and points in the direction of the intensity gradient. The sign of the gradient force is such that a particle with index of refraction higher than its surroundings is pulled into the high intensity region of the beam; whereas a low index particle is pushed out of the high intensity region of the beam. The characteristics of the two forces provided the possibility of studying and manipulating single particles.

Optical levitation, a technique by which single microscopic dielectric particles are captured and stably supported by a vertical laser beam against gravitational forces, proved to be a useful tool for investigating properties both of light scattering processes and of the scatterers themselves [Grehan and Gouesbet, 1980; Lettieri, et al. 1981]. It also provided a new technique of Raman–Microsampling [Thurn and Kiefer, 1984] by which the ideal sample arrangement for Raman microprobe studies would have the particle free in space without any supporting element and additionally have it perfectly centered in the middle of the laser focus where highest light intensity was present.

Optical focusing, an application to the neutral atom by the radiation pressure from lasers, was used to control the motion of atoms in various ways such as longitudinal and transverse cooling, focusing and reflection [Balykin, et al., 1986; 1988] and provided the possibility of developing a laser lens for neutral particle beams.

Roosen showed that by using two identical and oppositely directed horizontal laser beams to confine the particle to a single location, a third, vertical, beam could move the particle to a new equilibrium point [Roosen and Slansky, 1979]. This manipulation could be used in

applications where the precision micromanipulation of small particles without mechanical support is important, such as in light scattering and laser—initiated fusion experiments.

In 1976, Dr. G. Roosen, by a theoretical model, first calculated the forces on a small sphere by a plane wave but with a transverse Gaussian intensity structure, that is a Gaussian plane wave (G.P.W.). He repeated the levitation experiment of Ashkin, and obtained the results of the scattering force and the gradient force which were in good agreement with the expectation [Roosen, 1976].

Dr. G. Roosen also calculated the force on a hollow sphere by a TEM_{oo} (a kind of mode of Gaussian beams), and the force from a TEM_{o1} beam which has a different light intensity distribution from TEM_{oo} beam [Roosen, 1978]. The results further verified the conclusions, the particles in a light field are acted on by two forces: one along the direction of beam propagation, is proportional to the light intensity; the other a bounding force which confines a particle with higher refractive index than its surroundings to the high intensity area and *vice versa*.

One recent paper reported that, depending on the properties of the forces, it was possible to determine the light intensity distribution of a beam by examination of the pattern of small crystalline particles dispersed in the light field [Burns, et al. 1990]. The crystals were organized by creating an optical standing wave pattern with a regular array of intensity antinodes at the positions where the dielectric objects were ultimately desired. The standing wave was produced in water containing micrometer sized spheres which then organized themselves by occupying the periodic positions at the antinode maxima driven by optical forces. The paper reported the formation of a variety of two dimensional crystals.

Total Control

1

In 1986, according to the characteristics of the forces, Dr. A. Ashkin conceived the possibility of a single highly focused laser beam with a Gaussian intensity profile trapping small particles. He proposed that in the beam axial direction, the beam has a non-uniform intensity distribution, thus, the gradient force not only existed in the lateral direction but also in the axial direction. The gradient force and the scattering force components in the axial direction could be configured to give an axially oriented optical well. Indeed, he designed an experiment to

confirm his hypothesis. The single highly focused laser beam could trap and manipulate cells and particles from tens of microns down to submicron sizes [Ashkin and Dziedzic, 1986; 1987]. For large cells, where the beam focal volume of a few $(\mu m)^3$ was smaller than the cell, the trap acted much like laser tweezers, which exerted strong forces near the boundaries of the cell. One of the unique features of this manipulative technique is its ability to apply controlled manipulative forces inside of the cell while leaving the cell wall intact, thus providing the possibility to study the mechanical properties of living cytoplasm with minimal damage.

Optical trapping is a very interesting topic, but theoretical studies have not been fulfilled until now. In order to use this trap, it is necessary to carry out the theoretical study.

1.3 Introduction of the Theoretical Model for Deriving the Forces

Light is a transverse electromagnetic wave. The optical force acted on an object in a light field is the result of the interaction between the electromagnetic field and the object. Generally, the Lorentz formula is used to determine the forces on an object located inside an electromagnetic field.

$$\vec{f} = \iiint_{V} dV(\psi \vec{E} + \frac{\psi}{c} \vec{v} \times \vec{B})$$
 (1.1)

where \vec{E} and \vec{B} are the magnitudes of the electric field and the magnetic field respectively, ψ is the charge density distribution and \vec{v} is the velocity of a charge. However, the integration is very complicated if the electromagnetic field is time—varying and space—varying. The formula is suitable only to micro—objects whose sizes are smaller than the wavelength of the light; in this case the variation in space does not make an obvious variation inside the object. Thus, the forces is derived by time averaging over one period of the light wave. For neutral dielectric particles, the charge density distribution can be expressed by a multipole expansion. The force is obtained by calculating forces on multipoles separately. One such example, is the force on

an neutral atom, which was derived and discussed by Y. R. Shen [Shen, 1984]. He obtained results analogous to those observed by Ashikin for macro—particles, that is, there are two forces: a scattering force caused by absorption of light momentums, and a dipole force (gradient force) resulting from non-uniform light intensity. The difference is, the sign of the transverse optical well for macro—objects is decided by the relative index of refraction of the object to its surroundings, while for atoms it is decided by the comparison of the resonant frequency of the atom and the light frequency. We will not discuss the method here, but it is very important to note that the forces are also applicable to the micro—objects such as atoms and molecules.

Considering a macro-object located inside of an electromagnetic field, it is necessary to find a practical and simple way to solve the forces. Starting from Maxwell's equations, the conservation of momentum for a system consisting of an object and an electromagnetic field was obtained in the form:

$$\frac{d}{dt}\vec{P}_o + \oint_s \vec{T} \cdot \vec{n}ds - \frac{d}{dt}\vec{P}_f = 0 \tag{1.2}$$

where

To the second

A ANNA A

$$\vec{P}_f = \iiint_{\nu} d\nu \frac{1}{4\pi} (\vec{E} \times \frac{\vec{B}}{\mu}) \tag{1.3}$$

$$\ddot{T} = \frac{1}{4\pi} \left[\frac{1}{2} \left(\epsilon E^2 + \frac{B^2}{\mu} \right) \ddot{I} - \left(\epsilon \vec{E} \vec{E} + \frac{\vec{B} \vec{B}}{\mu} \right) \right] \tag{1.4}$$

 \vec{P}_o is the momentum of the object, \vec{P}_f is the electromagnetic momentum of the field. ϵ and μ are the electric permittivity and the inverse magnetic permeability of the medium in which the electromagnetic wave propagates. \vec{T} is the electromagnetic stress tenser, \vec{I} is a unit dyad. For a transverse electromagnetic wave, \vec{T} becomes:

$$\vec{T} = \frac{1}{4\pi} \left[\frac{1}{2} \left(\epsilon E^2 + \frac{B^2}{\mu} \right) \right] \vec{k} \vec{k} \tag{1.5}$$

where \vec{k} is the direction of beam propagation. $\vec{T} \cdot \vec{n}$ gives the component of the flow per unit

area of momentum through the surface ds whose normal is in \vec{n} direction. In other words, it is the force per unit area transmitted across the surface ds and acting on the object. When the object does not move relative to the electromagnetic field, the \vec{P}_f inside the object will not change, thus:

$$\frac{d}{dt}(\vec{P}_f) = 0 \tag{1.6}$$

and (1.2) becomes

$$\frac{d}{dt}(\vec{P}_o) = -\oint_s \vec{T} \cdot \vec{\kappa} ds \tag{1.7}$$

It can be seen that Equation (1.7) can be used to calculate the forces acting on the object in an electromagnetic field by enclosing the object with a boundary surface s and adding up the total electromagnetic force according the right side of (1.7).

In order to apply Equation (1.7), \vec{E} and \vec{B} must be derived by Maxwell's equations and boundary conditions first; this is very complicated for a generalized object interacting with a generalized field. Avoiding solving Maxwell's equations, a simple and practical method, called the geometric optics method, was invented to solve the force on the object by A. Ashkin and G. Roosen [Ashkin, 1970; Roosen, 1976].

The theme of the method is, a light field is made up of a bound of rays; each ray goes through the object by the geometric optics law. At the interface of the object and the light field, the ray will be reflected and refracted according to Snell's law. Instead of solving \vec{E} and \vec{B} by Maxwell's equation and boundary conditions, $\vec{T} \cdot \vec{n}$ is calculated for every incident ray and exiting ray by the Fresnel coefficients, which give the per unit area force on the object by the incident ray and the exiting ray. Therefore, integration of the individual ray forces over the boundary of the object gives the force on the object due to the light field.

The method is based on the assumptions that: the size of the object is larger than the wavelength of the light, the object is homogeneous inside, and inside the object, there is no absorption of light. By the geometric optic method, the scattering force and gradient force can be derived as follows [Ashkin, 1970].

Consider a sphere of radius Q and refractive index n_s illuminated by a G.P.W. beam. G.P.W. is chosen because it is the simplest wave with transverse non—uniform intensity distribution. As shown in Figure 1.1, the z-axis is the beam axis, and the sphere is located off the beam axis. AB is the diameter parallel to the z-axis. Consider a pair of rays, a and b, arriving at the surface symmetrically about AB.

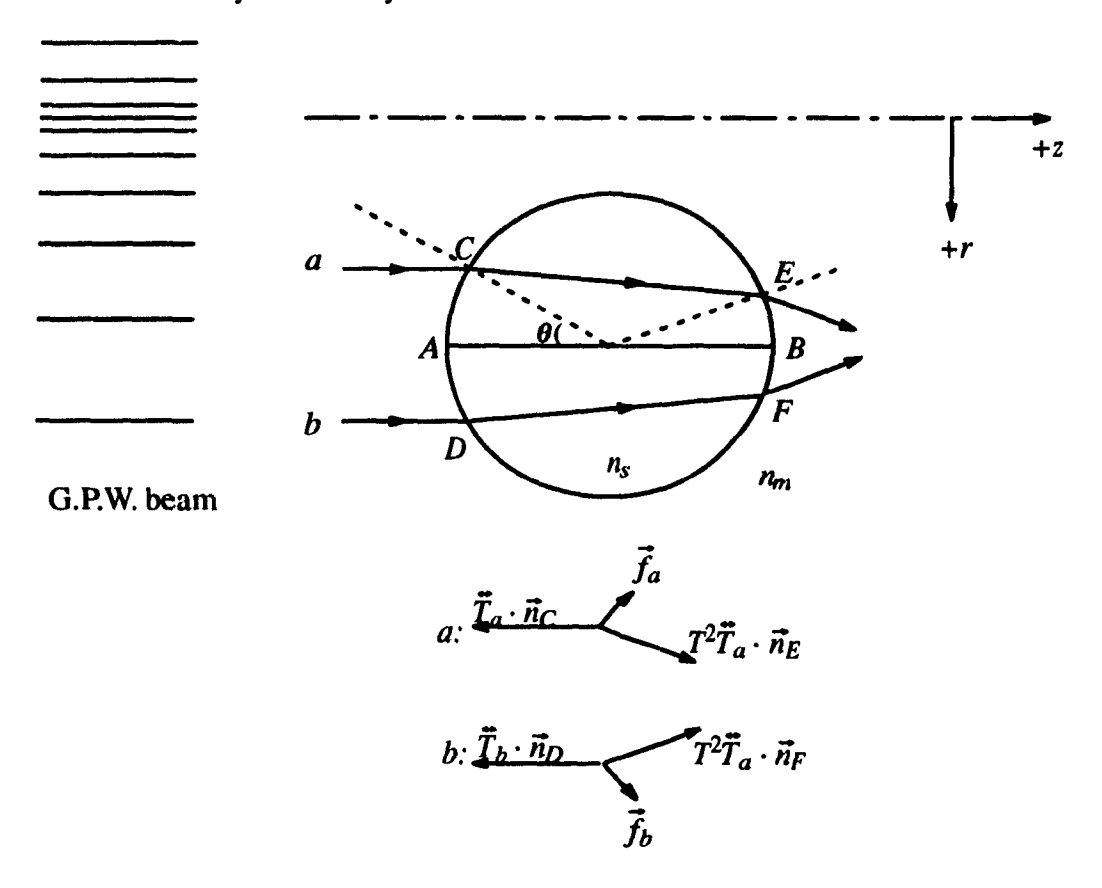


Figure 1.1: Schematic diagram of the force derivation by a geometric optics model.

To simplify the problem, it is supposed that the reflection on the surface can be neglected. The transmission coefficient is T. Ray a undergoes double refraction, and exits at point E. Assuming the stress tenser through ray a is \tilde{T}_a , then

$$\vec{T}_a = \frac{1}{8\pi} \left(\epsilon E_a^2 + \frac{B_a^2}{\mu} \right) \vec{k} \vec{k} \tag{1.8}$$

where E_a and B_a are the magnitudes of the electric field and magnetic field through ray $a.\epsilon$ and μ are the electric permittivity and the inverse magnetic permeability of the external medium. \vec{k} indicates the direction of the z-axis. At point E, exiting ray a has changed to $T^2\vec{T}_a$. At point C, ds has a direction \vec{n}_C , at point E, ds has a direction \vec{n}_E . Thus, the per unit area force acted by ray a is

$$\vec{f}_a = -\left[\vec{T}_a \cdot \vec{n}_C + T^2 \vec{T}_a \cdot \vec{n}_E\right] \tag{1.9}$$

which expands to

$$\vec{f}_a = -\left[-\cos\theta \vec{k} + T^2\cos\theta(\cos(2\theta - 2\gamma)\vec{k} + \sin(2\theta - 2\gamma)\vec{r})\right] \frac{1}{8\pi} (\epsilon E_a^2 + \frac{B_a^2}{\mu}) \tag{1.10}$$

where $\frac{\sin \theta}{\sin \gamma} = \frac{n_s}{n_m} \tag{1.11}$

It can be seen that if $n_s > n_m$, \vec{f}_a is force component along the \vec{k} and $-\vec{r}$ direction.

Similarly for ray b:

$$\vec{f}_b = -\left[-\cos\theta \vec{k} + T^2\cos\theta(\cos(2\theta - 2\gamma)\vec{k} - \sin(2\theta - 2\gamma)\vec{r})\right] \frac{1}{8\pi} (\epsilon E_b^2 + \frac{B_b^2}{\mu}) \quad (1.12)$$

The direction of \vec{f}_a and \vec{f}_b are symmetric about \overline{AB} , but the magnitude of \vec{f}_a is larger than \vec{f}_b . Their sum gives a forward \vec{k} and inward $-\vec{r}$ force. Although the magnitudes of the forces vary considerably with angle θ , qualitatively the results are alike for all θ . Therefore, as a whole, the sphere was acted on by a force in the direction of beam propagation and towards the beam axis.

It is quite obvious that the forward force results from the momentum exchanged directly from the photons propagating through the sphere; it is the scattering force. The transverse force is caused by the light gradient; it is the gradient force.

The complete calculation of the force is described in Chapter 2, the derivation presented here is just for the introduction of the geometric optics method.

1.4 Physical Properties of Gaussian Beams

It is apparent from the review in Section 1.2 that the radiation pressure strongly relies on the geometric character of the light beam, thus in order to successfully apply the lasers to our task, the properties of the laser beam must be studied first.

Gaussian beams are the most widely encountered optical beams in quantum electronics. in which the intensity distribution at planes normal to the propagation direction is Gaussian. One typical Gaussian beam which has a symmetric spherical wavefront is the TEM_{oo} , which is the simplest and lowest mode of Gaussian beams. A TEM_{oo} beam is the output of a cylindrically symmetric laser such as a helium neon or argon ion laser.

The following sections will mainly discuss the properties of the TEM₀₀ beam.

1.4.1 Analytical Expressions of a TEM₀₀ Beam

The field of a TEM_{oo} beam can be expressed as:

$$E(x,y,z) = E_o \frac{\boldsymbol{\omega}_o}{\boldsymbol{\omega}(z)} \exp(-i(kz - \boldsymbol{\eta}(z)) - r^2(\frac{1}{\boldsymbol{\omega}^2(z)} + i\frac{k}{2R(z)}))$$
(1.13)

where

$$\omega^{2}(z) = \omega_{o}^{2} (1 + (\frac{\lambda z}{\pi \omega_{o}^{2} n})^{2}) = \omega_{o}^{2} (1 + \frac{z^{2}}{z_{R}^{2}})$$
 (1.14)

$$z_R = \frac{\pi \omega_o^2 n}{\lambda} \qquad k = \frac{2\pi n}{\lambda} \tag{1.15}$$

$$R(z) = z(1 + \frac{z_R^2}{z^2}) \tag{1.16}$$

$$\eta(z) = tg^{-1}(\frac{z}{z_R}) \tag{1.17}$$

z is the distance propagated from the plane (z=0) where the wavefront is flat, λ is the wavelength of light, ω_o is the radius of the $1/e^2$ irradiance (intensity) contour at the plane where the wavefront is flat, $\omega(z)$ is the radius of the $1/e^2$ contour after the wave propagates a distance z. z_R is called the Rayleigh range, which is a fundamental beam parameter dependent only on ω_o and λ . R(z) is the wavefront radius of curvature after propagating a distance z. R(z) is infinite at z=0, passing through a minimum at $z=z_R$ and rising again toward infinity as z is further increased, asymptotically approaching the value of z itself. The plane z=0 marks the location of a Gaussian waist, or a place where the wavefront is flat. ω_o is called the waist radius.

As R(z) asymptotically approaches z for large z, $\omega(z)$ asymptotically approaches the value $\omega(z) = \lambda z / \pi n \omega_o$, where z is presumed to be much larger than $\pi \omega_o / \lambda$ so that the $1/e^2$ irradiance contours asymptotically approach a cone of angular radius

$$\theta_{beam} = \tan^{-1} \frac{\omega(z)}{z} = \tan^{-1} (\frac{\lambda}{\pi \omega_0 n})$$
 (1.18)

This value is the far field angular radius of the Gaussian TEM₀₀ beam. The vertex of the cone lies at the center of the waist.

It is important to note that for a given value of λ , the variations of beam diameter and divergence with distance z are functions of a single parameter. This is often chosen to be ω_o , the beam waist radius.

Some of these parameters are described in Figure 1.2.

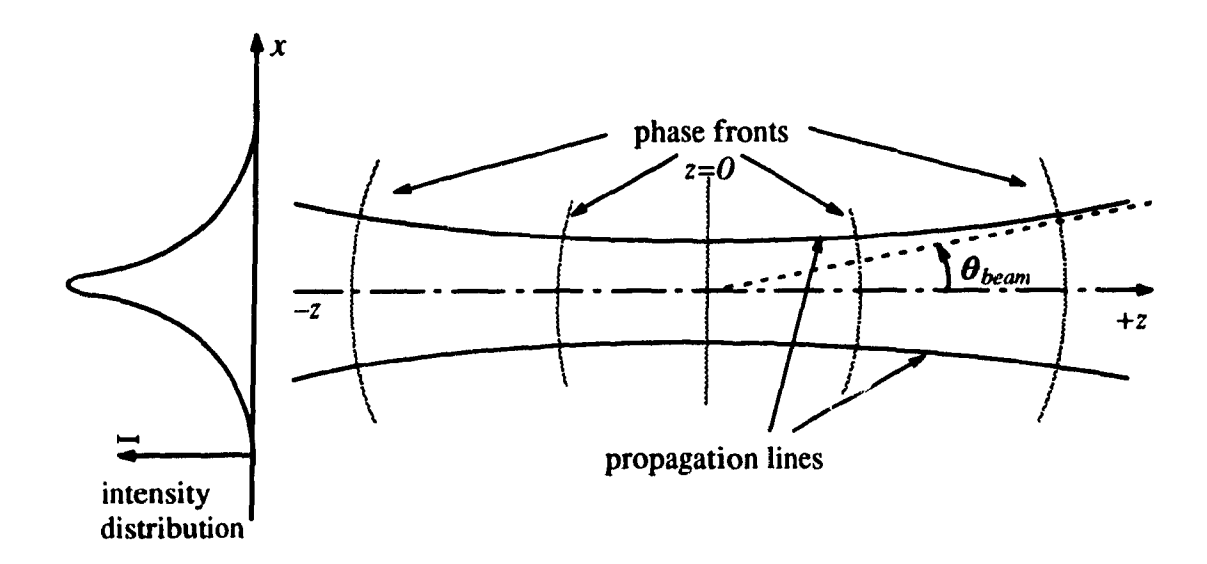


Figure 1.2: Propagating Gaussian beam (from: Yariv, 1975).

A TEM₀₀ Gaussian beam is specified by its waist radius ω_o . If ω_o is changed, the outline (or profile) of the beam will be changed because of the direct relationship between beam waist and divergence $(\theta_{beam} \propto 1/\omega_o)$.

1.4.2 Transformation and Magnification by a Simple Lens

A laser beam profile can be changed by focusing, thus, it is necessary to study the transformation of the beam by lenses.

The standard lens equation can be written in the form:

$$\frac{1}{s} + \frac{1}{s''} = \frac{1}{f} \tag{1.19}$$

where s is the object distance, s'' is the image distance and f is the focal length. For Gaussian beams, an analogous formula has been derived by assuming that the waist of the input beam represents the object, the waist of the output beam represents the image. The formula is expressed in terms of the Rayleigh range of the input beam [Shelf, 1983]

$$\frac{1}{s + z_R^2/(s - f)} + \frac{1}{s''} = \frac{1}{f} \tag{1.20}$$

When $z_R \to \infty$, this reduces to the geometric optics equation. The output beam has a beam waist radius ω_o'' , the magnification ω_o''/ω_o is given by

$$m = \frac{\omega_o''}{\omega_o} = \frac{1}{\sqrt{[1 - \frac{s}{f}]^2 + [\frac{z_R^2}{f}]^2}}$$
(1.21)

The spot size and focal position of a Gaussian beam can be determined by Equations (1.21) and (1.20). Two cases of particular interest are when s=0 (the input waist is at the first principle surface of the lens system) and s=f (the input waist is at the front focal point of the optical system). For the case of s=0, the equations for image distance and waist size reduce to:

$$s^{\prime\prime} = \frac{f}{1 + \lambda f/\pi\omega_o^2} \tag{1.22}$$

$$\omega_o^{\prime\prime} = \frac{\lambda f/\pi\omega_o}{[1 + (\lambda f/\pi\omega_o^2)]^{\frac{1}{2}}}$$
 (1.23)

For the case of s=f, the results are:

$$s^{\prime\prime} = f \tag{1.24}$$

$$\omega_o^{\prime\prime} = \lambda f/\pi\omega_o \tag{1.25}$$

These two sets of equations reduce an important conclusion: $\omega_o'' \propto 1/\omega_o$. The larger size of the input beam, the smaller the focal spot of the output beam. Therefore, in order to have a smaller focal size, it is often necessary to expand the beam before focusing it.

1.4.3 The Relation Between the Force and the Beam Profile

G.P.W. beam is the approximate case of TEM_{oo} when $R \to \infty$, that is, $\theta_{beam} \to 0$, $z_R \to \infty$. The force in such a beam profile has been discussed in Section 1.3. One of its significant characteristics is the scattering force and the gradient force are separated automatically by their directions.

However, when a TEM₀₀ beam is highly focused by a lens as shown in Figure 1.3, the focusing makes the intensity distribution change. Therefore, the force has a different characteristic from a G.P.W. beam.

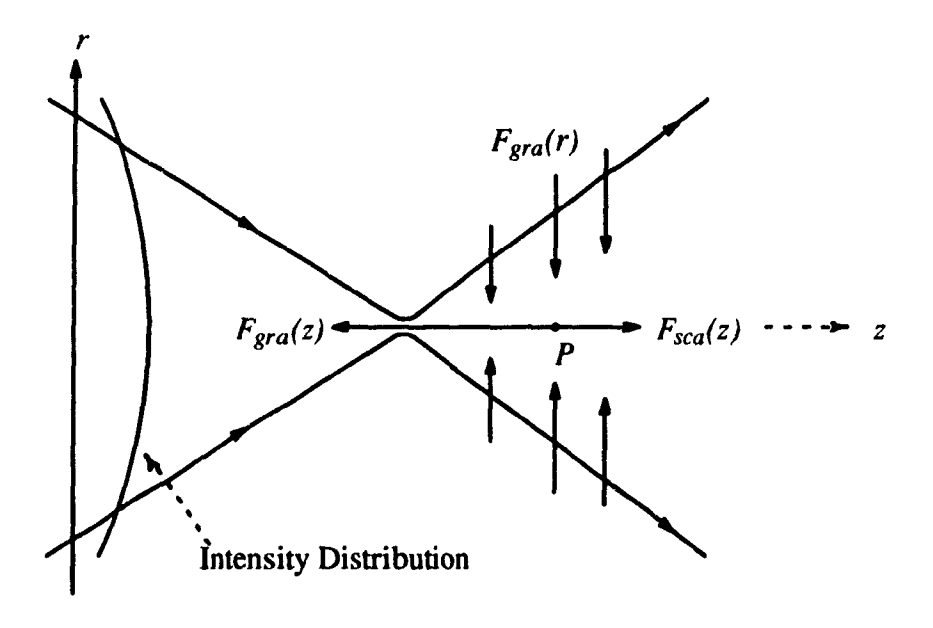


Figure 1.3: Force components on a particle placed at point P in a focused TEM₀₀ beam (from: Ashkin, 1989).

As shown in Figure 1.3, a high index of refraction particle is placed at a point P on the axis of the beam. In axial direction there is a scattering force $F_{sca}(z)$ pushing the particle in the +z direction and an axial gradient force $F_{gra}(z)$ pulling the particle back toward the beam focus in the -z direction. The condition for axial stability is that $F_{gra}(z)$ exceeds $F_{sca}(z)$ at the point of the maximum axial intensity gradient. This implies the existence of a stable equilibri-

um at some point close to the beam focus where the axial gradient force and scattering force balance. Radially, the transverse gradient force can still confine the particle on the beam axis. It is the principle underlying the operation of the single beam trap.

1.5 Scope of Thesis

As seen in the above review, in order to apply the radiation pressure and the optical trap from lasers to microsize particles, the forces from a Gaussian beam must be explored. The major contributions of this thesis are the following:

- The scattering force and gradient force from a G.P.W. beam was derived using the geometric optics method. The results indicated that the scattering force pushed the particles along the beam propagation direction, while the gradient force confined the particles to the beam axis.
- 2. The relationships between the forces as a function of object size and beam profile was derived for the case of a general TEM₀₀ Gaussian beam. The results were suitable to any profile of a TEM₀₀ beam. When the divergent angle was small, the results approached the results for a G.P.W. beam; When the divergent angle was large, the results showed the existence of a single beam trap. Finally, the theoretical particle-manipulating abilities of a single focused beam were studied.
- 3. Three experimental stations were designed and built. The first two could accelerate spherical particles up and down by using the beam from an argon ion laser which was directed upward and downward. These two experimental stations verified the existence of the scattering force and gradient force resulting from photon momentum. The third could hold spherical particles tightly by using a beam which was focused by a high numerical aperture (N.A.) lens and confirms the existence of the lateral restoring force in a TEM₀₀ beam.

Chapter 2

Parket t

Theoretical Study of the Optical Forces from a Laser Beam

As reviewed in Chapter 1, it can be seen that there are many factors which determine the force of radiation pressure from a laser beam, for example, the power and profile of the beam, the size and index of refraction of particles, *etc*. In this chapter, the relative effect of these factors is studied, especially that of laser beam profile.

First a force element contributed by a single beam of light on a transparent sphere was derived and then was applied to deriving the force from either a G.P.W. laser beam or a TEM_{oo} laser beam with an arbitrary profile. It was shown theoretically that the force could form an optical well which could be used to trap and manipulate some kind of particles. The main point demonstrated was the relation between the force and the profile of a TEM_{oo} laser beam. The possibility of trapping a particle by a single laser beam was also verified theoretically.

2.1 The Force Element from a Single Ray

In Section 1.3, an example was given where a G.P.W. impinges on a sphere under the condition that the reflection on the surface could be ignored. In the real case, both the reflection and refraction on the interface must be considered. Thus, if a ray arrives at a sphere, it will be reflected and refracted many times until the ray magnitude decreases to zero. The following will give a treatment of a force element contributed by a single ray.

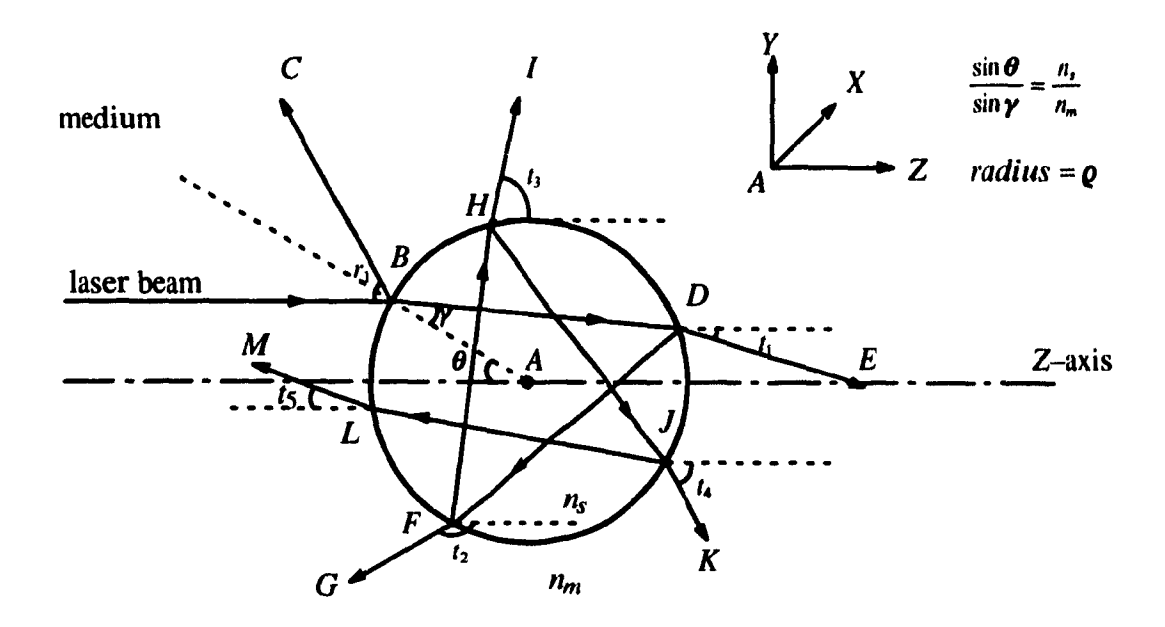


Figure 2.1: Schematic diagram of the ray path through a sphere of radius ϱ and index n_s .

Supposing that a ray with a unit energy density, that is, a unit value of T but with a direction parallel to z-axis as shown in Figure 2.1, arrives at point B on the surface of a sphere of radius Q and refractive index n_s . The external medium has a refractive index n_m . The Z-axis is parallel to the incident ray and goes through the sphere center A; the sphere is located at the coordinate system center. At point B, a factor R of the ray is reflected through BC and a factor T is transmitted to the point D. R and T are the energy flow reflection coefficient and transmission coefficient respectively. At point D, the ray is also split into two parts, one part is reflected inside the sphere while the other part is transmitted outward from the sphere. At point F, the reflected ray DF is divided into two rays again. The process of division of the ray remaining inside the sphere continues until the ray magnitude decreases to zero.

In order to calculate the sum $\sum_{i} \vec{T}_{i} \cdot \vec{n}_{i}$, the direction of every exiting ray with respect to the Z-axis is derived by Snell's law, and the magnitude is obtained according to the Fresnel coefficients. Table 2-1 lists the results of the angle and magnitude for every exiting ray.

Table 2-1: Results of the angle and magnitude of exiting rays. $(n_s/n_m = \sin \theta / \sin \gamma)$

ray	ВС	DE	FG	HI	JK	LM	•••
angle	2 0	2 θ – 2 γ	$4\gamma - 2\theta$	6y - 2 0	8γ – 2 0	10γ – 2 0	•••
magnitude	R	T^2	RT ²	R^3T^2	R^5T^2	R^7T^2	•••

Let $\vec{q} = -\sum_{i} \vec{T}_{i} \cdot \vec{n}_{i}$, Supposing the reflection plane is on the YZ-plane, the \vec{q} has two components q_{z} and q_{y} which are the sum of two convergent series.

$$q_{z} = 1 + R\cos 2\theta - T^{2}\cos 2(\theta - \gamma) + RT^{2}\cos(4\gamma - 2\theta)$$

$$-R^{2}T^{2}\cos(6\gamma - 2\theta) + R^{3}T^{2}\cos(8\gamma - 2\theta)$$

$$+ \dots + (-1)^{n-1}R^{n}T^{2}\cos(2(n+1)\gamma - 2\theta) + \dots$$

$$= 1 + R\cos 2\theta - \frac{T^{2}(\cos 2(\theta - \gamma) + R\cos 2\theta)}{1 + R^{2} + 2R\cos 2\gamma}$$
(2.1)

$$q_{y} = -R \sin 2\theta + T^{2} \sin 2(\theta - \gamma) + RT^{2} \sin(4\gamma - 2\theta)$$

$$-R^{2}T^{2} \sin(6\gamma - 2\theta) + R^{3}T^{2}(8\gamma - 2\theta)$$

$$+ \dots + (-1)^{n-1}R^{n}T^{2} \sin(2(n+1)\gamma - 2\theta) + \dots$$

$$= -R \sin 2\theta + \frac{T^{2}(\sin 2(\theta - \gamma) + R \sin 2\theta)}{1 + R^{2} + 2R \sin 2\gamma}$$

$$\vec{q} = \vec{q}_{y} + \vec{q}_{z} \qquad d\vec{f} = \vec{q}ds$$
(2.2)

These are the results of a force element from a single ray. That is, an incident optical ray parallel to the Z-axis produces two force components: q_z parallel to the original ray direction and

 q_y perpendicular to the original ray direction. The total force on the sphere produced by an incident parallel ray bundle is found by summing the force elements of one ray.

2.2 Forces on the Sphere by a G.P.W.

2.2.1 Equations of the Force

Consider a G.P.W. incident on a sphere with radius Q and refractive index n_s surrounded by an external medium which has a refractive index n_m . The electric field can be expressed as:

$$\vec{E} = \vec{E}(x, y)e^{\frac{i2\pi i}{\lambda}} \tag{2.3}$$

where

$$E(x,y) = E_0 \exp(-\frac{x^2 + y^2}{\omega^2})$$
 (2.4)

 ω is the waist radius of the beam. E_o is the electric field magnitude on the beam axis.

By definition,
$$\vec{T}(x,y) = \frac{1}{8\pi} (\epsilon E^2 + \frac{B^2}{\mu}) \vec{kk}$$

where $B = n_m E$ and $n_m = \sqrt{\epsilon \mu}$, ϵ and μ are the electric permittivity and the inverse magnetic permeability of the external medium, \vec{k} is the direction of beam propagation. We have

$$\vec{T}(x,y) = \frac{\epsilon E^2}{4\pi} \vec{k} \vec{k} = \frac{\epsilon E_o^2}{4\pi} \exp(-2\frac{x^2 + y^2}{\omega^2}) \vec{k} \vec{k}$$
 (2.5)

the energy flow is
$$\vec{s}(x,y) = \frac{c}{4\pi}\vec{E} \times \frac{\vec{B}}{\mu} = \frac{cn_m}{4\pi\mu}E^2\vec{k} = \frac{c}{4\pi}\sqrt{\frac{\epsilon}{\mu}}E^2(x,y)\vec{k}$$
 (2.6)

where c is light velocity. E_o can be obtained from the laser power:

$$P = \int \int \vec{s}(x,y) \cdot \vec{n} dx dy = 2\pi \int_{0}^{\infty} \frac{c}{4\pi} \sqrt{\frac{\epsilon}{\mu}} E_o^2 \exp(-\frac{2r^2}{\omega^2}) r dr = \frac{\omega^2 c}{8} \sqrt{\frac{\epsilon}{\mu}} E_o^2$$
 (2.7)

Thus we have
$$E_o^2 = \frac{8P}{c\omega^2} \sqrt{\frac{\mu}{\epsilon}}$$
 (2.8)

Therefore

$$\vec{T}(x,y) = \frac{2P}{\pi c\omega^2} \sqrt{\epsilon \mu} \exp(-2\frac{x^2 + y^2}{\omega^2}) \vec{k} \vec{k}$$

$$= \frac{2n_m P}{\pi c\omega^2} \exp(-2\frac{x^2 + y^2}{\omega^2}) \vec{k} \vec{k} \tag{2.9}$$

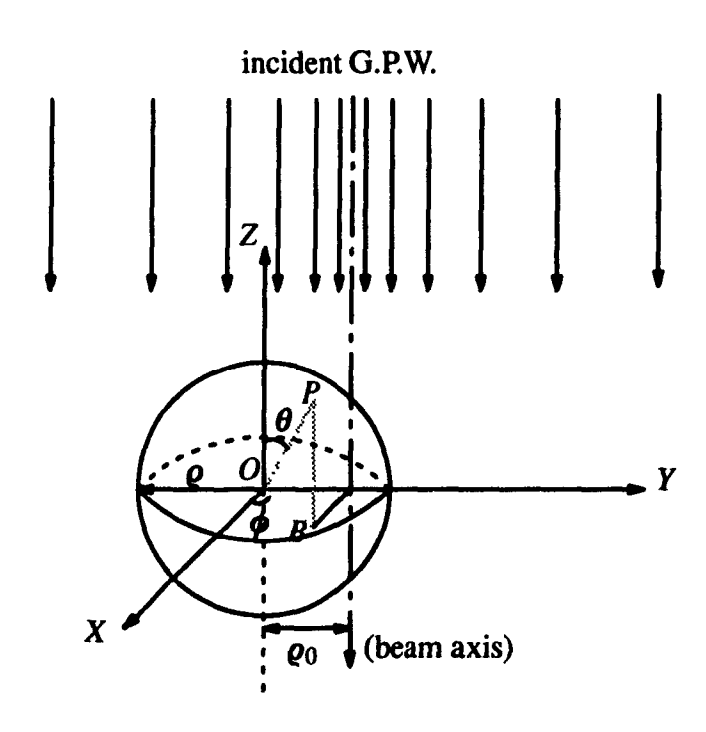


Figure 2.2: O-XYZ coordinate system fixed at the center of the sphere. Point P is on the spherical surface. Point B is the projection of point P on the XY plane. The wave propagates along the opposite direction of Z axis.

With coordinate system shown in Figure 2.2, for an arbitrary point P on the surface of the sphere, the electric field is:

$$E^{2} = E_{o}^{2} \exp\left(-2 \frac{(\boldsymbol{\varrho}^{2} \sin^{2} \boldsymbol{\theta} + \boldsymbol{\varrho}_{o}^{2} - 2\boldsymbol{\varrho} \boldsymbol{\varrho}_{o} \sin \boldsymbol{\theta} \sin \boldsymbol{\phi})}{\boldsymbol{\omega}^{2}}\right)$$
(2.10)

where ϱ_o is the offset of the beam axis from Z-axis, the beam axis lies on the YZ plane and is anti-parallel to Z-axis.

Having obtained the results of \vec{q} for a single ray, the equation of the force for a G.P.W. beam is derived by integration over the top half surface of the sphere:

$$\vec{F} = \frac{2n_m P}{\pi c} \vec{Q} \tag{2.11}$$

where

$$\vec{Q} = Q_z \vec{z} + Q_y \vec{y} + Q_x \vec{x}$$

$$Q_z = -\int_0^{\frac{\pi}{2}} \int_0^{2\pi} d\theta d\phi \frac{\varrho^2}{\omega^2} \sin\theta \cos\theta q_z \exp\left(-2\frac{\varrho^2 \sin\theta^2 + \varrho_o^2 - 2\varrho\varrho_o \sin\theta \sin\phi}{\omega^2}\right)$$
(2.12)

$$Q_{y} = \int_{0}^{\frac{\pi}{2}} \int_{0}^{2\pi} d\theta d\phi \frac{\varrho^{2}}{\omega^{2}} \sin\theta \cos\theta \sin\phi q_{y} \exp\left(-2\frac{\varrho^{2} \sin\theta^{2} + \varrho_{o}^{2} - 2\varrho\varrho_{o} \sin\theta \sin\phi}{\omega^{2}}\right)$$
(2.13)

$$Q_x = 0 (2.14)$$

The force F acting on the particle by the G.P.W. has been decomposed into three components along the X, Y, and Z directions. The component along the propagation direction of the wave is called the scattering force F_z and the Y-axis component is called the gradient force F_y . The last component F_x is always zero due to symmetry. F_z and F_y are proportional to Q_z and Q_y separately. Hence, Q_z and Q_y describe the behavior of F_z and F_y . We will study Q_z and Q_y instead of F_z and F_y .

2.2.2 Results and Discussions

Equations (2.12) and (2.13) can be rewritten as

$$Q_z = Q_z(\frac{\varrho}{\omega}, \frac{\varrho_o}{\omega}, n) \tag{2.15}$$

$$Q_{y} = Q_{y}(\frac{\varrho}{\omega}, \frac{\varrho_{o}}{\omega}, n)$$
 (2.16)

where

1

 ϱ/ω : the ratio of the sphere radius to laser beam waist;

 ϱ_o/ω : the ratio of the distance between the center of the sphere and the beam axis to the beam waist;

n: $n = n_s/n_m$ is the relative index of refraction of the sphere to the external medium. At present, no analytical integrations of Q_z and Q_y exists, thus numerical solutions of Q_z and Q_y are found as a function of Q/ω , Q_o/ω and Q_z .

2.2.2.1 Results from the Numerical Integration of F_z (Q_z)

 Q_z was calculated over the ratio ϱ/ω by setting $\varrho_o = 0$. As the beam axis is anti-parallel to the Z-axis, Figure 2.3 is a plot of the data of $-Q_z$ for several values of index n. The following conclusions can be made.

- 1. Q_2 is always in the opposite direction of the Z-axis and tends to move particles along the beam propagation direction.
- 2. Figure 2.3 shows that Q_z , or the Z component of the force, increases when particle size ϱ/ω increases until ϱ is equal to or larger than ω . After this point F_z approaches to a constant value. It is easy to understand this. When the radius of sphere is smaller than the waist, the larger the particle is, the more photons the sphere will receive and

- the larger F_z will be; when ϱ is equal to or larger than ω , the sphere receives almost the same amount of photons, thus the force F_z approaches a constant value.
- 3. Figure 2.3 also shows that for the same ϱ/ω , the magnitude of Q_z increases when n increases. Large n means that the ray will be deflected to a great extent, which causes a large F_z .

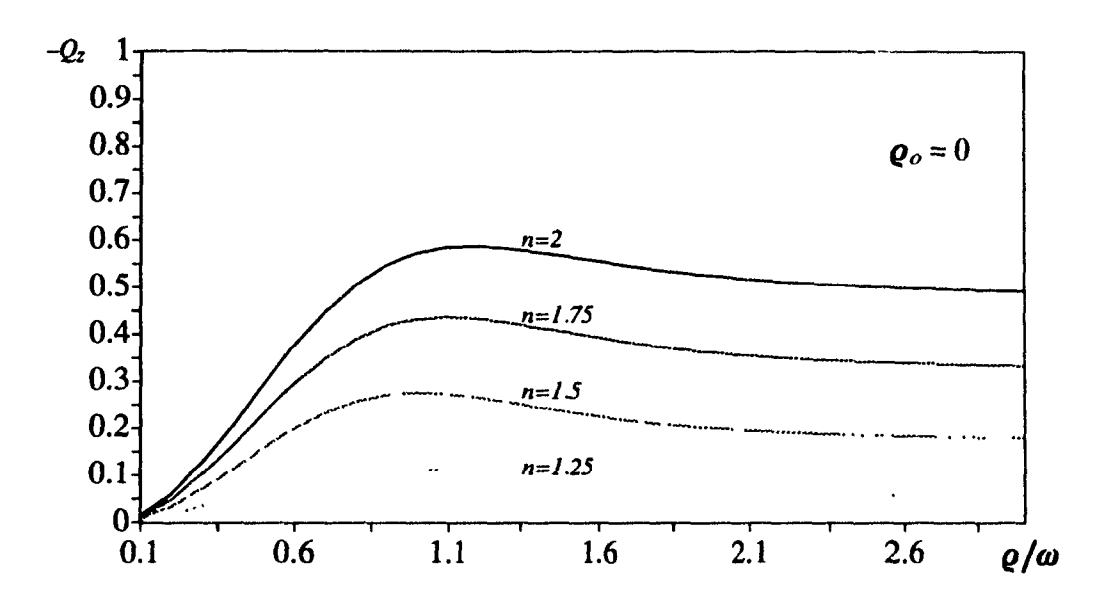


Figure 2.3: Value of Q_z over the ratio of the particle size and beam waist radius.

2.2.2.2 Results from the Numerical Integration of F_y (Q_y)

 Q_y was calculated over the offset of the sphere from the beam axis ϱ_o/ω by setting $\varrho = \omega$. The calculations were then made for different refractive index n. The following comments are based on Figure 2.4 to 2.5.

1. For n > 1, Q_y is positive, for n < 1, Q_y is negative. This indicates that when the refractive index of the sphere is larger than its medium, the force component F_y will try to pull the particle towards the beam axis. When the index of the sphere is smaller than its medium, F_y will push the particle away from the beam axis.

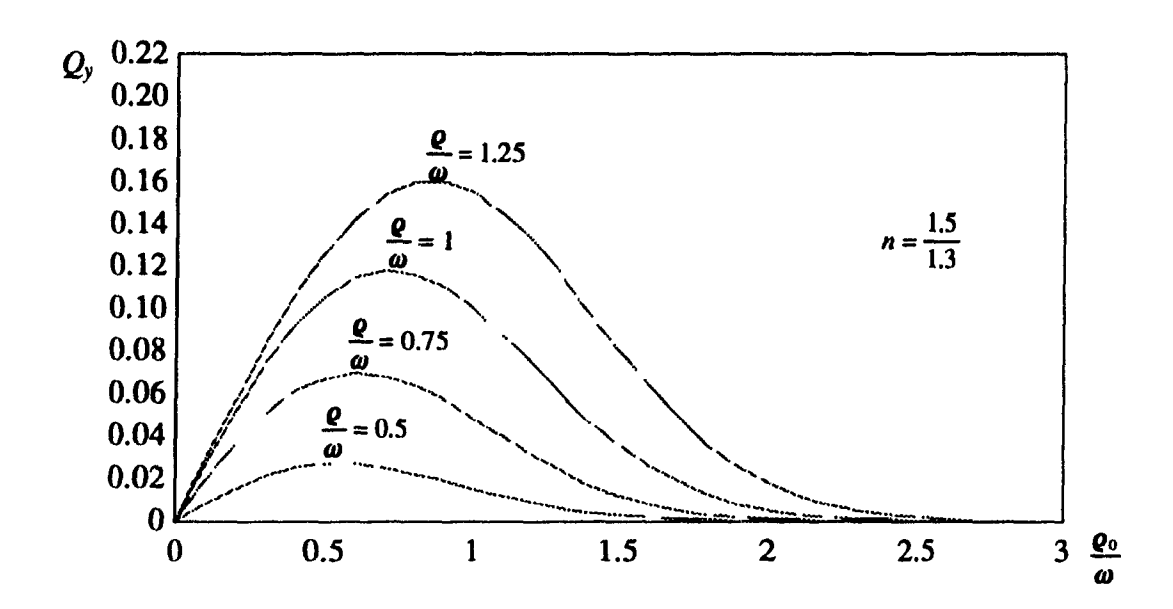


Figure 2.4: Value of Q_y over the ratio of the offset from Z-axis and beam waist radius.

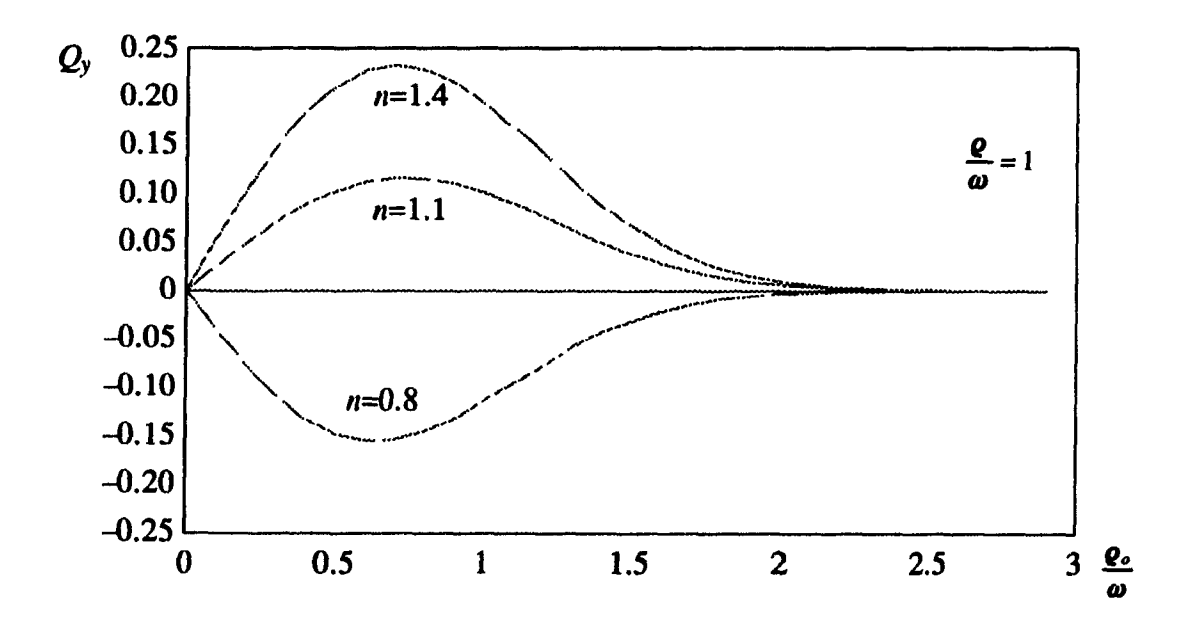


Figure 2.5: Value of Q_y over the ratio Q_o/ω .

- 2. A large size particle has a higher maximum Q_y , which means that large particles will have a deep trap and can be confined tightly.
- 3. When the difference of index of refraction n between the particle and the external medium is large, the optical well is deep, so it will be easier to capture particles with large n_s .

2.2.3 Summary

Section 2.2 theoretically studied the characteristics of the forces from a G.P.W. on a sphere.

The numerical solutions of the forces showed that the Y component of the force forms an optical well which can trap particles when the index of refraction of the particle is larger than its surrounding. The Z component of the force has nothing to do with the optical well but can push particles along the beam propagation direction. The fact that larger size and higher refractive index of the particle help to form a deeper optical well means that a large size particle with high index n_S may be confined tightly and be manipulated easily.

These results agree with those of G. Roosen (Roosen, 1976).

2.3 Radiation Forces from a TEM₀₀ Beam

2.3.1 Equations of the Forces

Consider a TEM_{oo} mode laser beam incident on a sphere with a radius ϱ and refractive index n_s , surrounded by an external medium with refractive index n_m . The same method as that of previous section is applied and \vec{Q} is similarly defined as $\vec{F} = 2n_m P \vec{Q}/\pi c$. However, the derivation of the new \vec{Q} is more complex, since the different rays in a TEM_{oo} beam propagate in different directions.

TEMoo mode laser beam

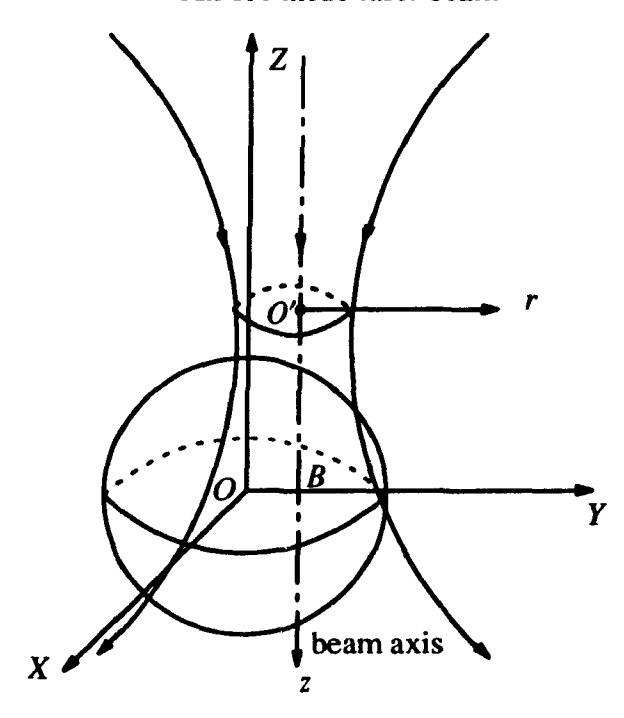


Figure 2.6: Particle coordinate frame O-XYZ and beam coordinates O'-rz. The origin of O-XYZ is fixed at the center of the sphere and the Z axis is anti-parallel to the beam axis. The origin of O'-rz is at the center of the beam whose coordinates in O-XYZ is $(0,y_0,z_0)$.

Figure 2.6 shows the coordinate frames. Due to symmetry the force contribution along the X-axis is zero in such a coordinate system.

The algorithm for deriving \vec{Q} is summarized as follows:

- 1. In the beam coordinate system O'-rz, find the direction of a ray from the TEM₀₀ beam through a given point on the surface of the sphere.
- 2. Express the direction of the ray by angular coordinates α' and β' in the particle coordinate system (see Figure 2.8),
- 3. Set up another relative reference O-X'Y'Z' in which the coordinate center is still at point O, Z' is parallel to the incident ray and the Y'Z'-plane is the reflection plane of this ray. Apply the results of q_y and q_z in Formula (2.1) and (2.2) to q_z' and q_y' , project q_z' and q_y' on Z-axis and Y-axis to obtain the contribution of this single ray to \vec{Q} .

2.3.1.1 The Propagating Direction of a Specified Ray in a TEM₀₀ Beam

A TEM_{oo} beam is expressed as:

$$E(x, y, z) = E_o \frac{\boldsymbol{\omega}_o}{\boldsymbol{\omega}(z)} \exp(-i(kz - \boldsymbol{\eta}(z)) - r^2(\frac{1}{\boldsymbol{\omega}^2(z)} + i\frac{k}{2R(z)}))$$
 (1.13)

The last part is referred as the phase of the electromagnetic wave and expressed as

$$P(z,r) = z + \frac{r^2}{2R(z)}$$

The equation P(z, r)=constant gives an equal-phase surface. In the plane wave case, the equal-phase surface is a plane, so all rays are incident on the sphere with the same direction. For a TEM_{oo} beam, different rays hit the sphere in different directions.

Supposing C(x, y, z) is a point on the surface of the sphere and also on a certain equalphase surface of the electromagnetic field of the TEM_{oo} beam. As shown in Figure 2.7 the normal line of this equal-phase surface is the direction of the laser beam incident on the point C.

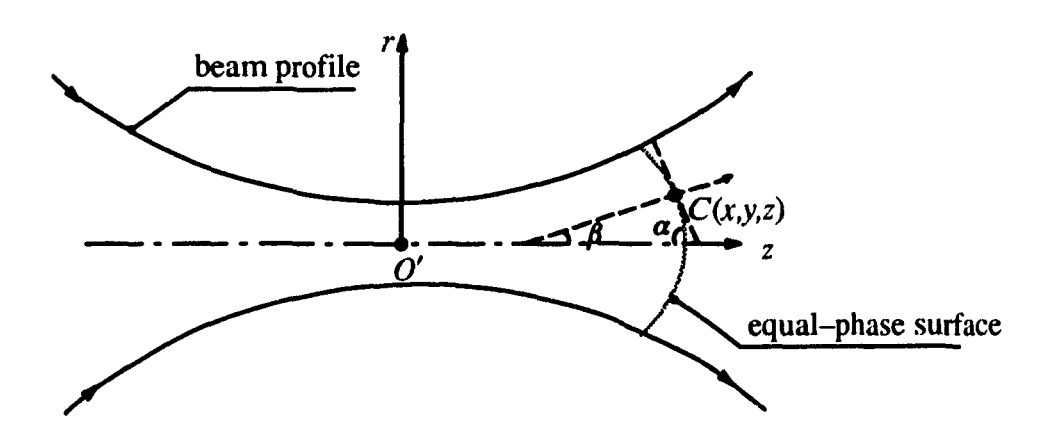


Figure 2.7: Schematic diagram of the normal line to the equal-phase surface.

Assume the normal line has an angle β with the z-axis and $\alpha = 90^{\circ} - \beta$.

Since
$$\tan \alpha = \frac{dr}{-dz}$$

* em.

therefore
$$\tan \beta = -\frac{dz}{dr}$$

Because
$$P(z,r) = z + \frac{r^2}{2R(z)} = constant$$

$$dP = \frac{\partial P}{\partial r}dr + \frac{\partial P}{\partial z}dz = 0$$

$$\frac{dz}{dr} = -\frac{\frac{\partial P}{\partial r}}{\frac{\partial P}{\partial z}}$$

$$\tan \beta = \frac{\frac{\partial P}{\partial r}}{\frac{\partial P}{\partial z}} = \frac{\frac{r}{z}}{(1 + \frac{z_R^2}{z^2}) - \frac{1 - \frac{z_R^2}{z^2}}{1 + \frac{z_R^2}{z^2}} \frac{r^2}{2z^2}}$$
(2.17)

To this point, the direction of a ray impinging on a known point on the surface of the sphere has been obtained in the beam O'-rz coordinate system. In the following section, the direction of this specified ray will be transferred to the particle coordinate system.

2.3.1.2 The Angular Coordinates of the Specified Ray

Assume that the spherical coordinates of point C are (ϱ, θ, ϕ) . As shown in Figure 2.8, DC is the direction of a ray hitting at point C, EF is a diameter parallel to DC. The direction of EF, expressed by β' and α' , is the direction of the incident ray in the particle coordinate system.

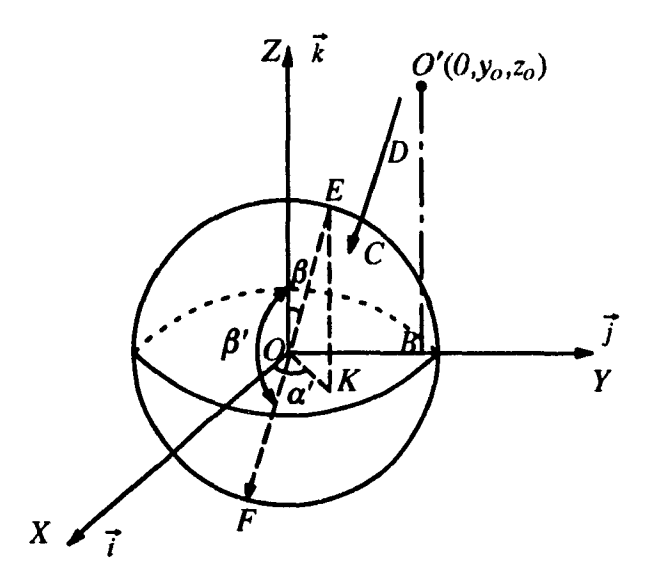


Figure 2.8: Schematic diagram of the incident ray DC in the coordinate system O-XYZ.

 β' and α' are derived by solid geometric relations. Details about the derivation are given in Appendix 2. The results of β' and α' are:

for
$$\beta > 0$$
, $\beta' = 180^{\circ} - \beta$, $\alpha' = 270^{\circ} + a\sin\frac{\varrho \sin\theta \cos\varphi}{r}$ (2.18)

for
$$\beta > 0$$
, $\beta' = 180^{\circ} - \beta$, $\alpha' = 270^{\circ} + a\sin\frac{\varrho \sin\theta \cos\phi}{r}$ (2.18)
for $\beta < 0$, $\beta' = 180 + \beta$, $\alpha' = 90^{\circ} + a\sin\frac{\varrho \sin\theta \cos\phi}{r}$ (2.19)

Therefore
$$\vec{EF} = \sin \beta' \cos \alpha' \vec{i} + \sin \beta' \sin \alpha' \vec{j} + \cos \beta' \vec{k}$$
 (2.20)

Formula (2.20) is the angular expression of \vec{EF} in the particle coordinate system, that is, the expression of the direction of the ray hitting on point C in the particle coordinate system.

2.3.1.3 The Expressions of Q_z and Q_v

A reference coordinate system O-X'Y'Z' was set up, with the Z'-axis along \vec{EF} . The Y'Z'-plane

is the reflection plane. For the incident ray DC, the incident angle is η . The reflection plane is shown in Figure 2.9.

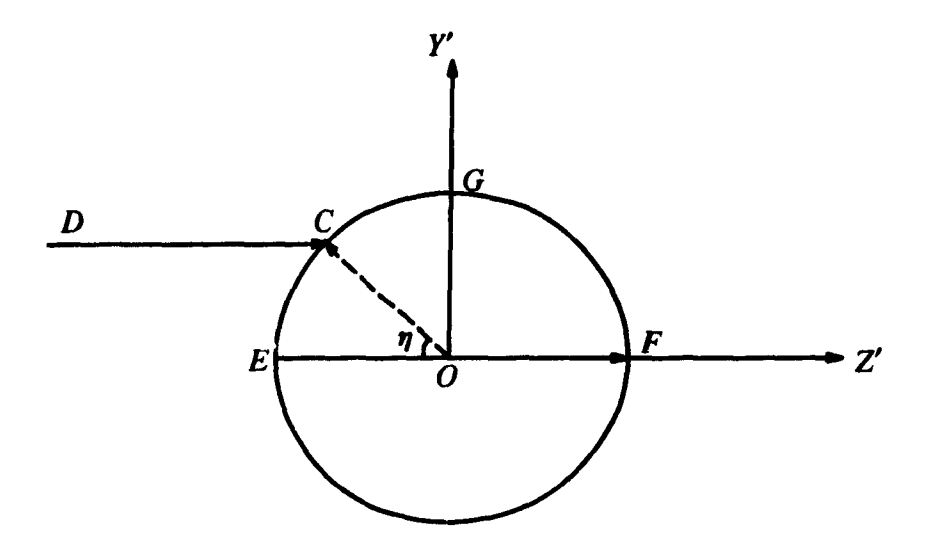


Figure 2.9: Reflection plane of an incident ray DC.

7 is derived by

$$\cos \eta = -\frac{\vec{OC} \cdot \vec{EF}}{|\vec{OC}| \cdot |\vec{EF}|}$$

$$= -(\sin \theta \cos \phi, \sin \theta \sin \phi, \cos \theta) \cdot (\sin \beta' \cos \alpha', \sin \beta' \sin \alpha', \cos \beta')$$

$$= -\sin \theta \sin \beta' \cos(\alpha' - \phi) - \cos \theta \cos \beta' \tag{2.21}$$

where \vec{OC} is a unit vector.

If $\cos \eta < 0$, the ray has no contributions to the force. To derive the angular expression of the direction of \vec{OG} in the particle system, define

$$\vec{OH} = \vec{OC} \times \vec{OE}$$

therefore

$$\vec{OG} = \vec{OE} \times \vec{OH}$$

$$\vec{OG} = \vec{OE} \times (\vec{OC} \times \vec{OE}) = (\vec{OE})^2 \vec{OC} - (\vec{OE} \cdot \vec{OC}) \vec{OE} = \vec{OC} - \cos \eta \vec{OE}$$

$$= (\sin \theta \cos \phi + \cos \eta \sin \beta' \cos \alpha') \vec{i}$$

$$+ (\sin \theta \sin \phi + \cos \eta \sin \beta' \sin \alpha') \vec{j}$$

$$+ (\cos \theta + \cos \eta \cos \beta') \vec{k}$$
(2.22)

For a single ray \vec{DC} , its contribution to \vec{Q} is:

$$dQ_z = ds \frac{\cos \eta}{\omega_o^2} \left[q_z (\vec{EF} \cdot \vec{k}) + \frac{q_y (\vec{OG} \cdot \vec{k})}{\sin \eta} \right] \frac{E^2}{E_o^2}$$
 (2.23)

$$dQ_{\gamma} = ds \frac{\cos \eta}{\omega_o^2} \left[q_z (\vec{EF} \cdot \vec{j}) + \frac{q_y (\vec{OG} \cdot \vec{j})}{\sin \eta} \right] \frac{E^2}{E_o^2}$$
 (2.24)

The factor $\sin \eta$ in the last term arises from the fact that \overrightarrow{OG} is not a unit vector. \overrightarrow{OG} has a length of $\sin \eta$. Integrations of dQ_y and dQ_z over all the points on the surface of the sphere gives the force acting on the sphere by a TEM₀₀ beam:

$$Q_{z} = \int_{0}^{a} \int_{0}^{2\pi} \frac{\varrho^{2} \sin \theta}{\omega(z)^{2}} d\theta d\phi \cos \eta [q_{z}(\vec{EF} \cdot \vec{k}) + \frac{q_{y}(\vec{OG} \cdot \vec{k})}{\sin \eta}] \cdot \exp(-\frac{2r^{2}}{\omega^{2}(z)})$$
 (2.25)

$$Q_{y} = \int_{0}^{a} \int_{0}^{2\pi} \frac{\varrho^{2} \sin \theta}{\omega(z)^{2}} d\theta d\phi \cos \eta [q_{z}(\vec{EF} \cdot \vec{j}) + \frac{q_{y}(\vec{OG} \cdot \vec{j})}{\sin \eta}] \cdot \exp(-\frac{2r^{2}}{\omega^{2}(z)})$$
 (2.26)

where

$$r^2 = \rho^2 \sin \theta^2 \cos \phi^2 + (\rho \sin \theta \sin \phi - \gamma_0)^2 \tag{2.27}$$

r is the distance of a point (Q, θ, ϕ) from the beam axis. Given the formula of \vec{Q} , the force \vec{F} acting on the sphere is deduced by $\vec{F} = 2n_m P \vec{Q} / \pi c$.

2.3.2 Results and Discussions

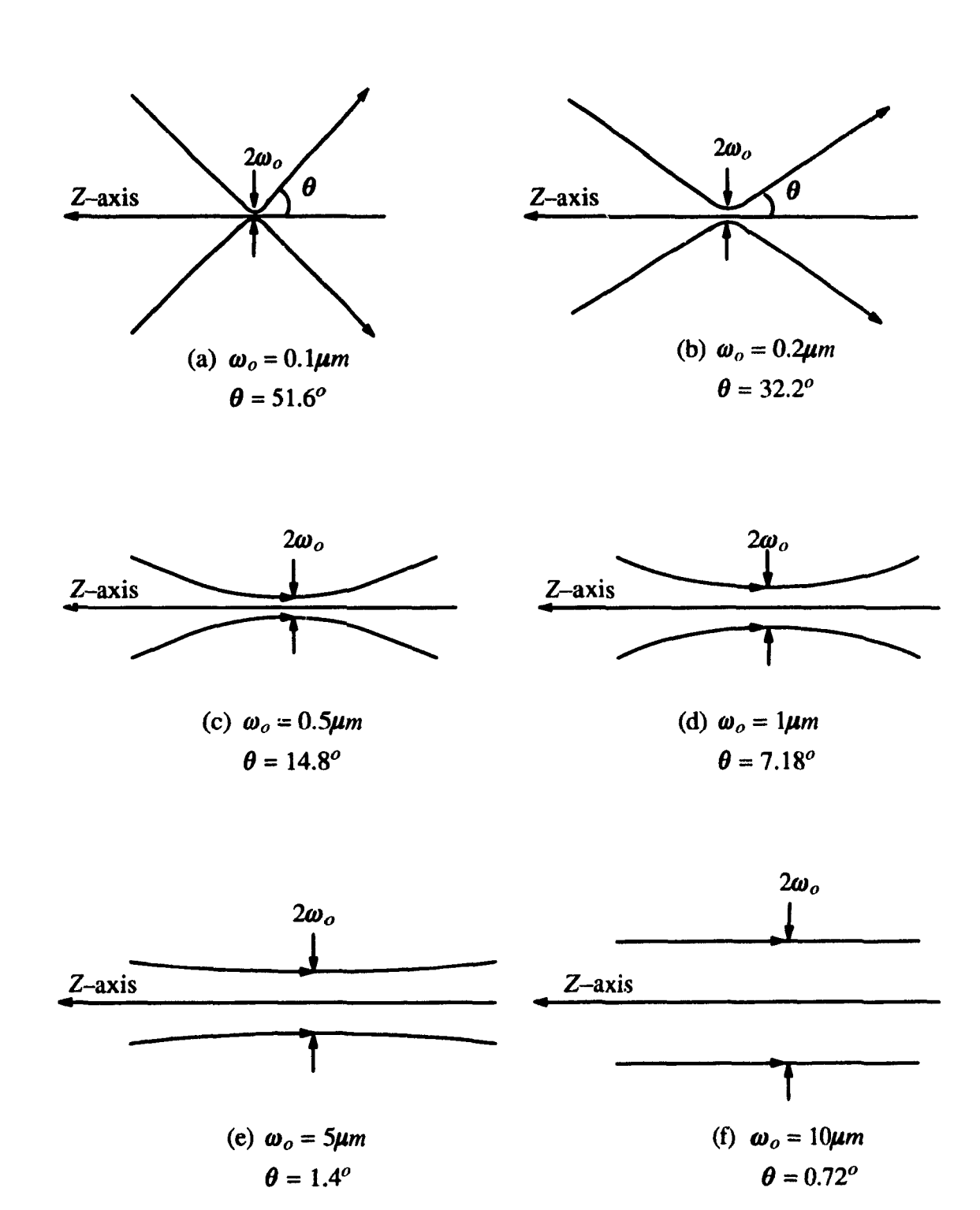
1

Section 1.4 reviewed the characteristics of TEM₀₀ mode laser beam and pointed out that a single highly focused beam could trap particles in its focal point. The profile of a TEM₀₀ mode laser beam is uniquely described by the beam waist radius ω_o when the beam wavelength and the index of the medium are given. Figure 2.10 shows the relation of beam profile and beam waist radius. To explore the possibility of particle trapping using a single beam, \vec{Q} is calculated for several beam waist radii ω_o . The following discussion is split into two parts. The first part deals with the force along the beam axis and the second part deals with the force perpendicular to the beam axis.

2.3.2.1 The Force along the Beam Axis

Assume that the relative index of refraction of the sphere to its medium is 1.5/1.3, laser wavelength is 514.5 nm and the offset of the sphere from beam axis is zero. For several different ω_0 , Q_z is calculated over the longitudinal displacement z_0 of the sphere from the beam center (the focal point).

Figures 2.12-2.19 are the results of Q_z for different ω_o . In each figure (except Figure 2.13(b)) there are four curvatures. Each curvature corresponds to the case when a fixed size sphere moves from the left side of the focal point to the right side of the focal point as shown in Figure 2.11(a).



~! !#

Figure 2.10: Profiles of laser beam for various waist radius

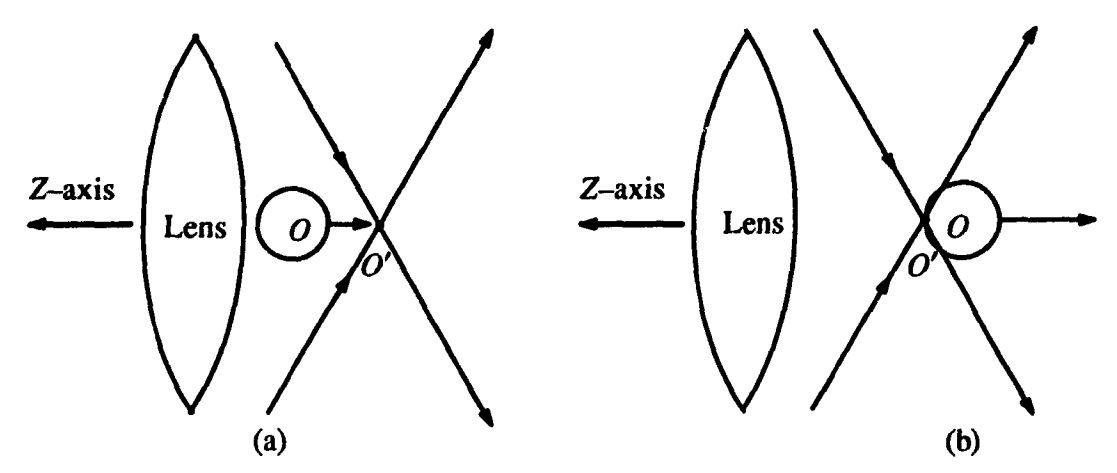


Figure 2.11: Movement of sphere in a highly focused laser beam.

The following comments are made from these figures.

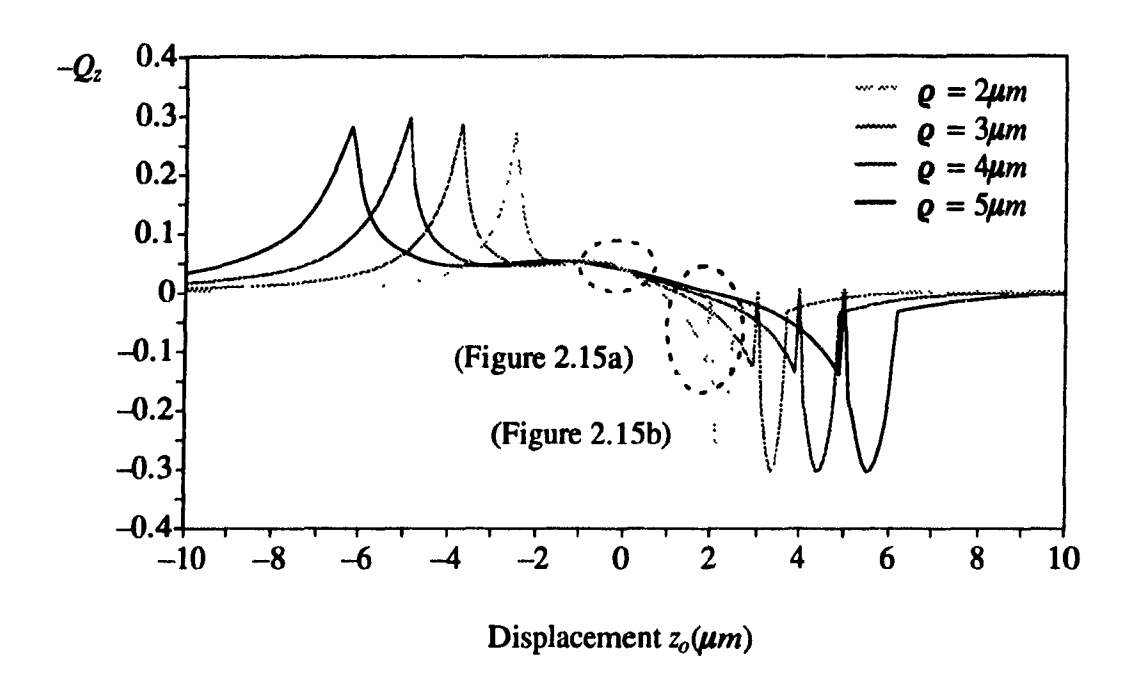
I

- 1. When the beam divergent angle θ is large enough (Figure 2.12 and 2.14), Q_z changes steeply. When the sphere is on the left side of the focal point (z_o is negative), F_z pushes the particle toward the focal point. When the sphere is on the right side of the focal point, F_z pulls the particle back. This can be explained by the following. When particle O is on the left side of the beam center O', both the scattering force (in the beam propagation direction) and the gradient force (directed toward the high density area) point toward O'. When particle O is on the right side of O', the scattering force pushes it forward while gradient force pulls it back, resulting in the balance of the two forces. The zero force position is somewhere on the right side of O', and is dependent upon particle size.
- 2. In Figure 2.13(a), the data comes from a small range (z_0 from $-1\mu m$ to $1\mu m$) in Figure 2.12. In this range the sphere is very close to the focal point. The force behavior is similar to a spring force which is proportional to the displacement away from the equilibrium point, $F_z \approx k(z+z_0)$ (that is why sometimes it is called the restoring force). Modelling the force-displacement relationship as a linear equation, for laser power of 100 mW, a particle with radius $2\mu m$ has an elastic coefficient 8.535 $\mu N/m$, a particle with

radius $5\mu m$ has an elastic coefficient 4.998 $\mu N/m$. The system is underdamped in this range of z_0 , and the particle will vibrate. However, the range is so small, that macroscopically, the particle appears to be stationary. It is by this principle that a single beam trap works.

- 3. When the sphere is exactly on the focal point O', the force values are the same for all sizes of particles.
- 4. When θ is very large, for each curvature, there are two peaks. The peak on the left side behaves like a wall and will prevent the particle from moving away, while the peak on the right side is not expected. It occurs when the sphere is on the right side of O', but its front surface is tangent with the focal point (see Figure 2.11(b)). In such a case, the surface of the sphere is nearly flat corresponding to O'. Thus most of the photons incident on the sphere surface are parallel to the beam axis. The forces are large and the same for all sizes of particles. The sharp peak is not a singular point. It can be seen in Figure 2.13(b) that the peak is continuous.
- 5. From these figures, it can be seen that a smaller size particle has a smaller confining range. Thus, a smaller size sphere can be confined tightly.
- 6. The spring-like range disappears when θ is smaller. Those curvatures tend to be straight lines. Therefore, F_z will accelerate the spheres instead of holding them.

Upon explanation of the results of the forces along the beam axis for different kinds of beams, the character of the force is very obvious. No matter what the power of light is, what the size of the particle is, the restoring force exists only when the beam is highly focused. That is, its existence depends only on the profile of the beam. Of course, the higher the power of laser beam is, the larger the force is. These results will be experimentally verified in Chapter 3.



1

1

Figure 2.12: Results of Q_z for $\omega_o = 0.05 \mu m$.

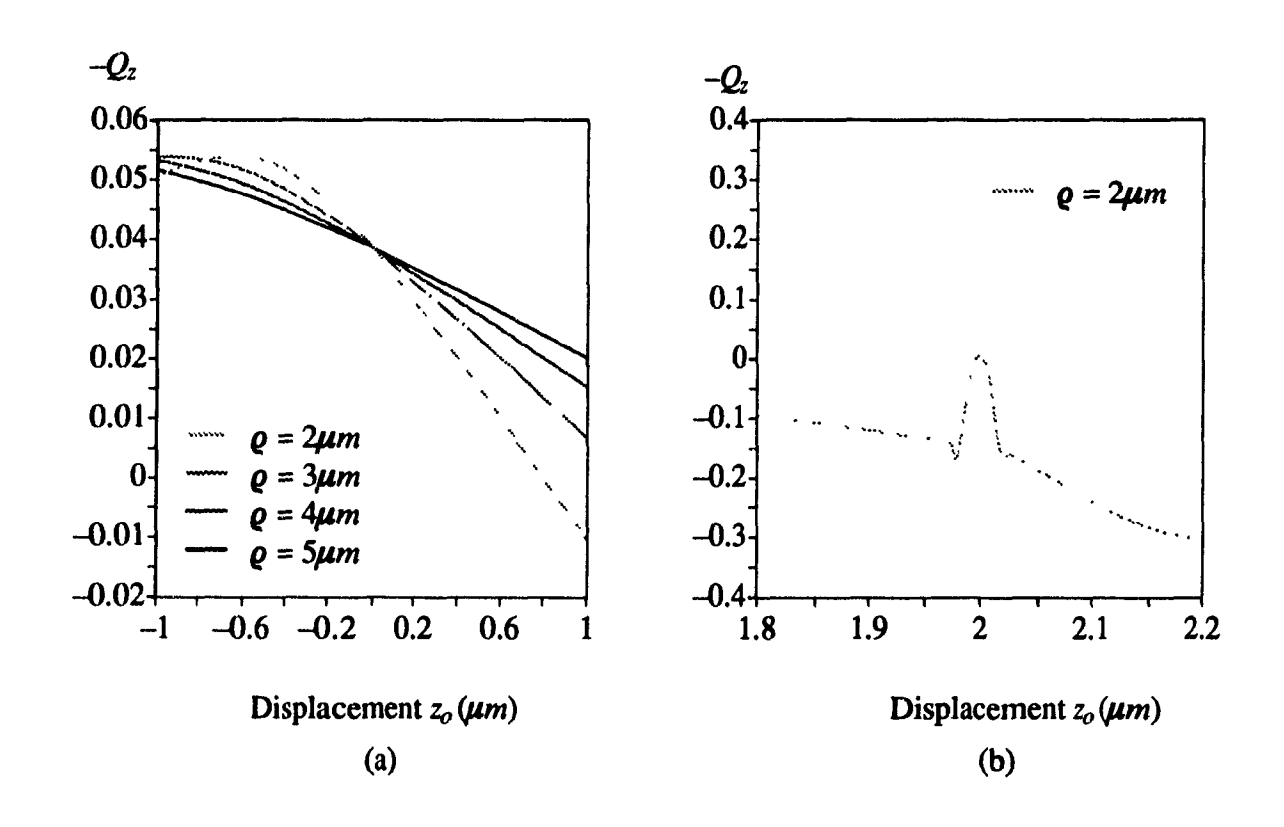


Figure 2.13: Results of Q_z for $\omega_o = 0.05 \mu m$.

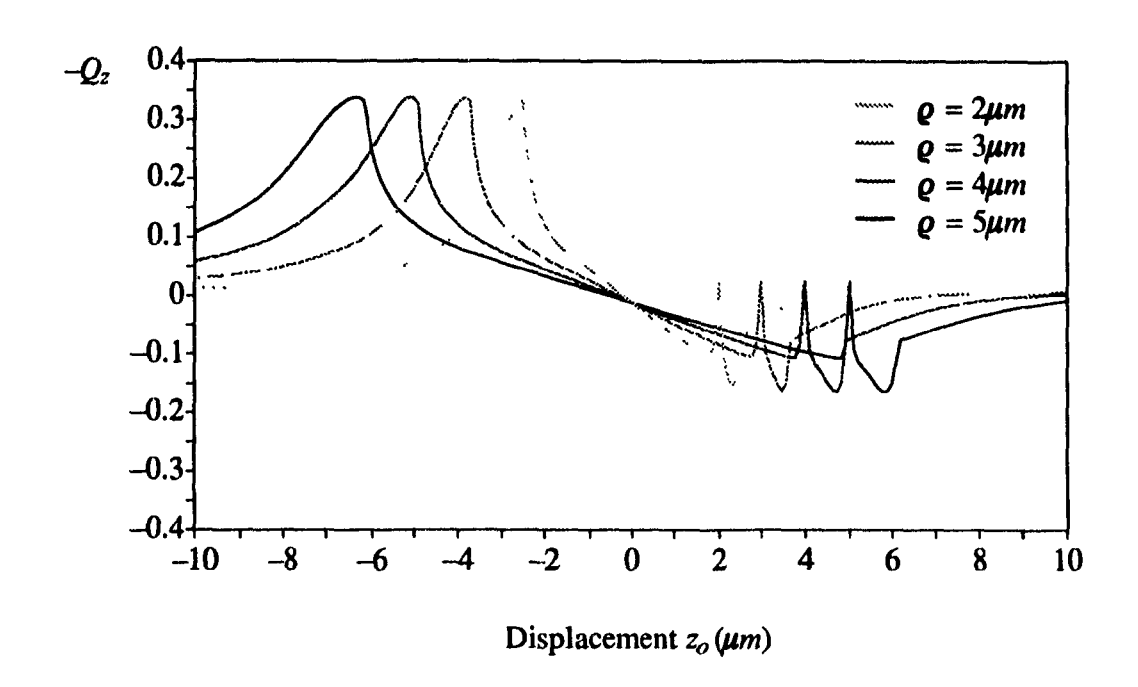


Figure 2.14: Results of Q_z for $\omega_o = 0.1 \mu m$.

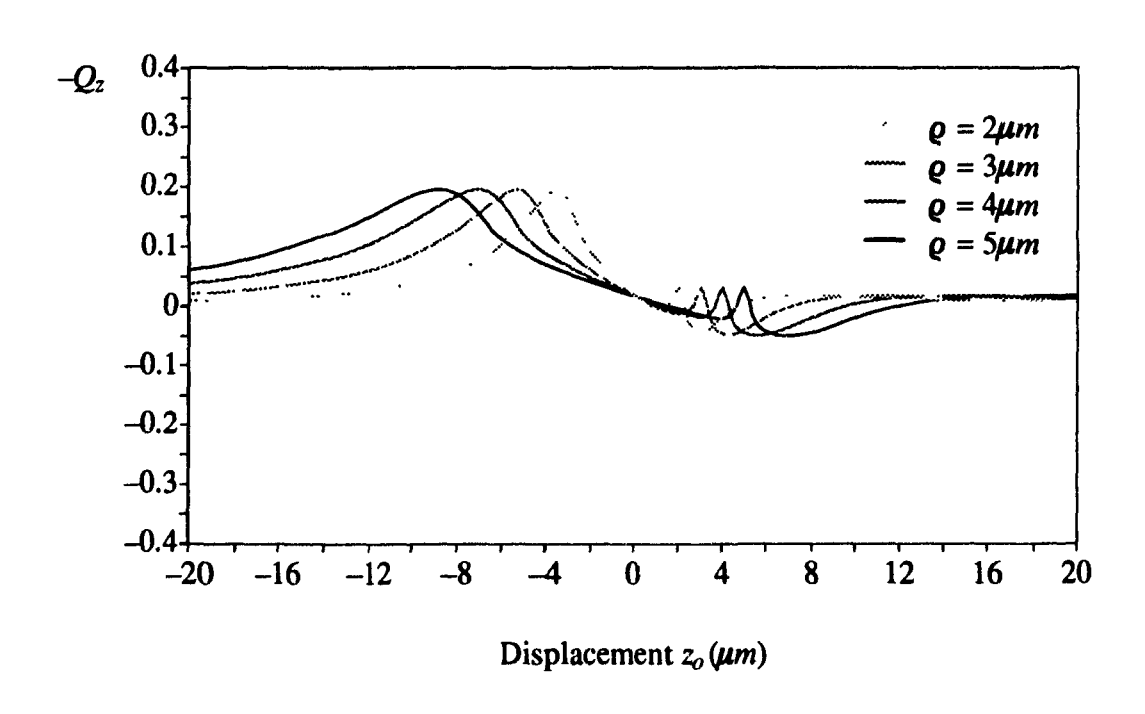


Figure 2.15: Results of Q_z for $\omega_o = 0.2 \mu m$.

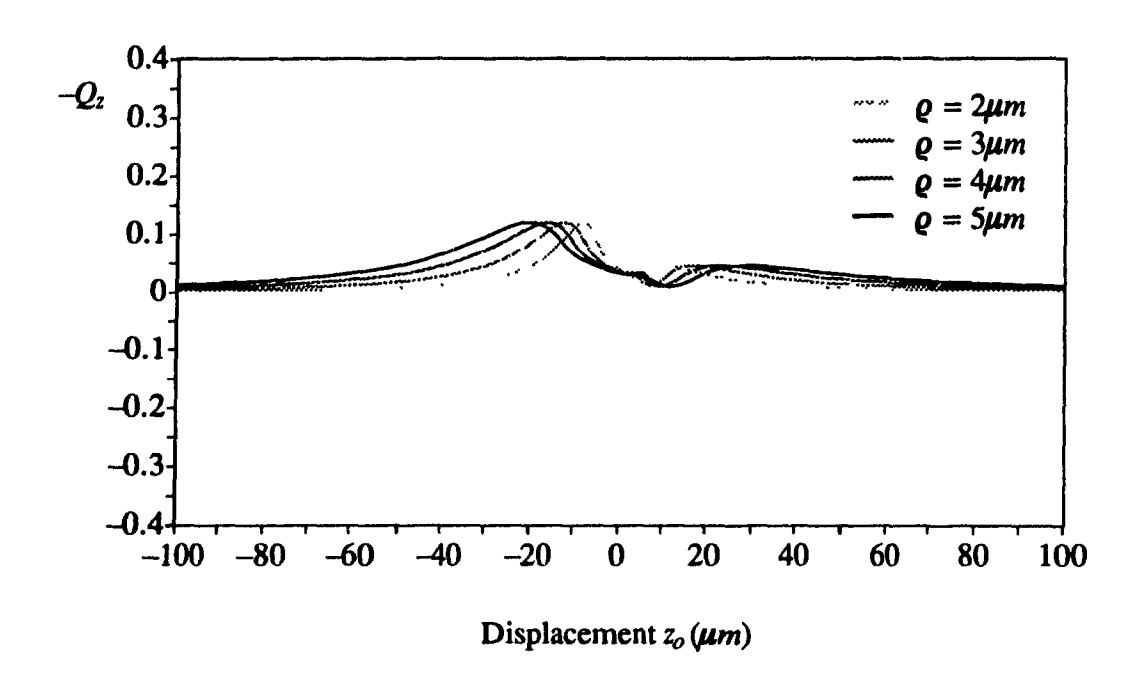


Figure 2.16: Results of Q_z for $\omega_o = 0.5 \mu m$.

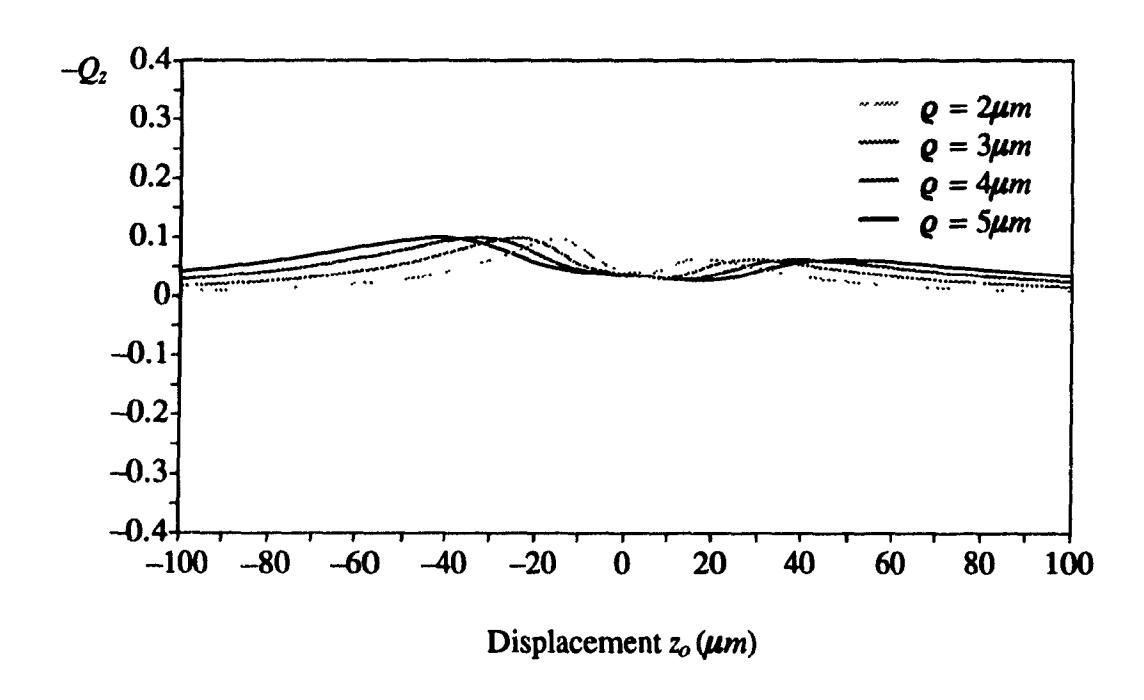


Figure 2.17: Results of Q_z for $\omega_o = 1 \mu m$.

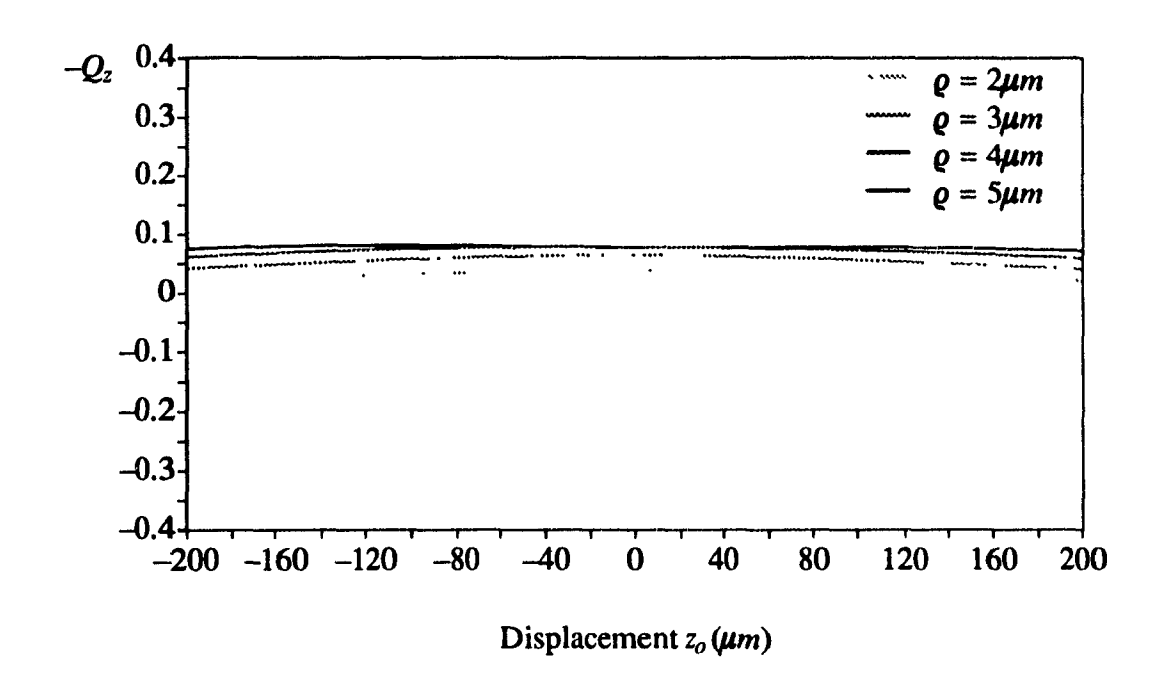


Figure 2.18: Results of Q_z for $\omega_o = 5\mu m$.

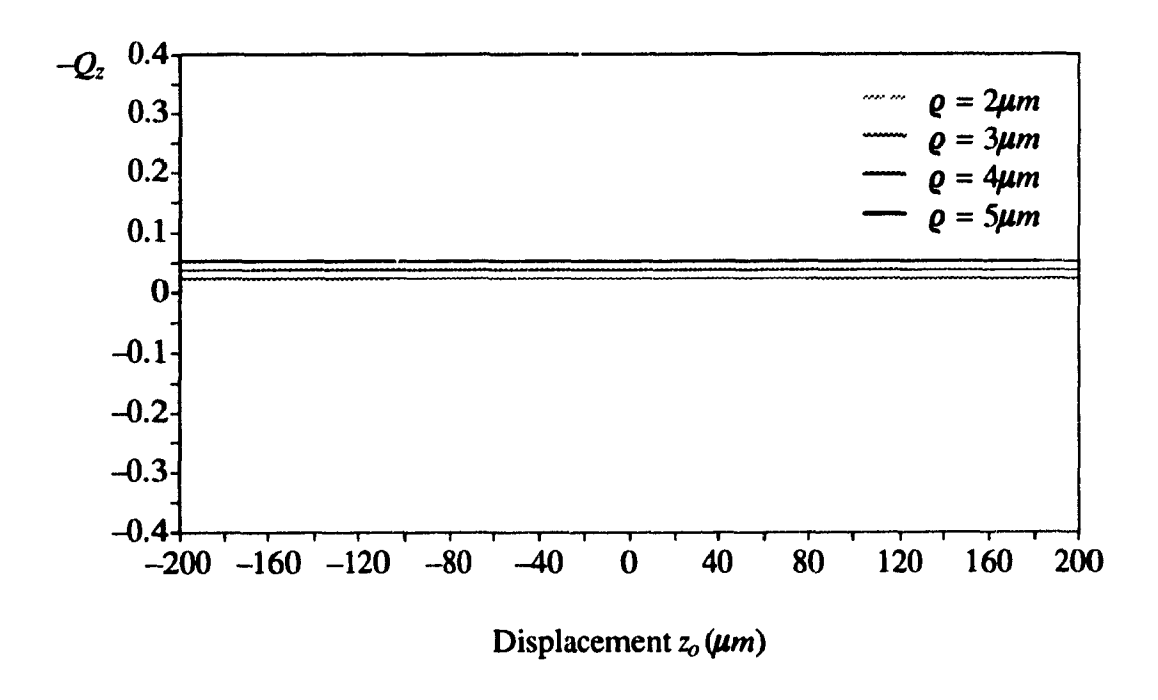


Figure 2.19: Results of Q_z for $\omega_o = 10 \mu m$.

2.3.2.2 The Transverse Force

It has been shown that a highly focused TEM₀₀ beam exerts a restoring force in its axial direction. The transverse force is studied in this section in order to obtain the stable trapping conditions.

Assume that the sphere is placed on the $z_o=0$ plane (Figure 2.20(a)). Q_y was calculated numerically over the transverse displacement of the sphere from the beam axis for different waist radius ω_o (a certain profile) and for four different sizes of particles. The results are shown in Figures 2.21–2.27.

The characteristics of Q_y are:

- 1. When θ is small (Figure 2.21), the behavior of F_y is the same as that in the parallel beam case.
- 2. When θ becomes larger (Figures 2.22–2.24), the peak value in each curvature increases. In the mean time, the positions of the four peaks of different size spheres separate gradually. Thus, as θ increases, a small size particle has a narrow and shallow optical well, a large particle has a wide and deep optical well.
- 3. When θ is even larger (Figure 2.25), the four peaks do not increase in magnitude, but approach the same value and are totally separated.
- 4. When θ is very large (Figures 2.26–2.27), an unexpected valley appears. The valley occurs when the bottom of the sphere surface is tangent with the focal point (see Figure 2.20(b)).

The characteristics of Q_y show that the transverse optical well always exists no matter what profile the laser beam has. It is the transverse optical well that confines the particle to moving along the axis. This is why Q_z is calculated for only when particle is on the axis.

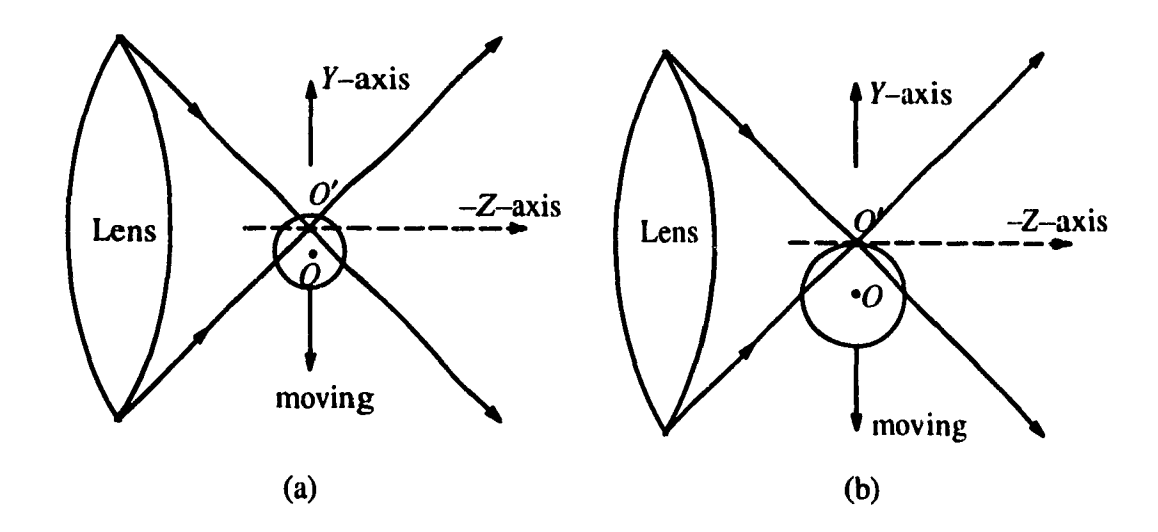


Figure 2.20: Movement of sphere transverse to the beam axis.

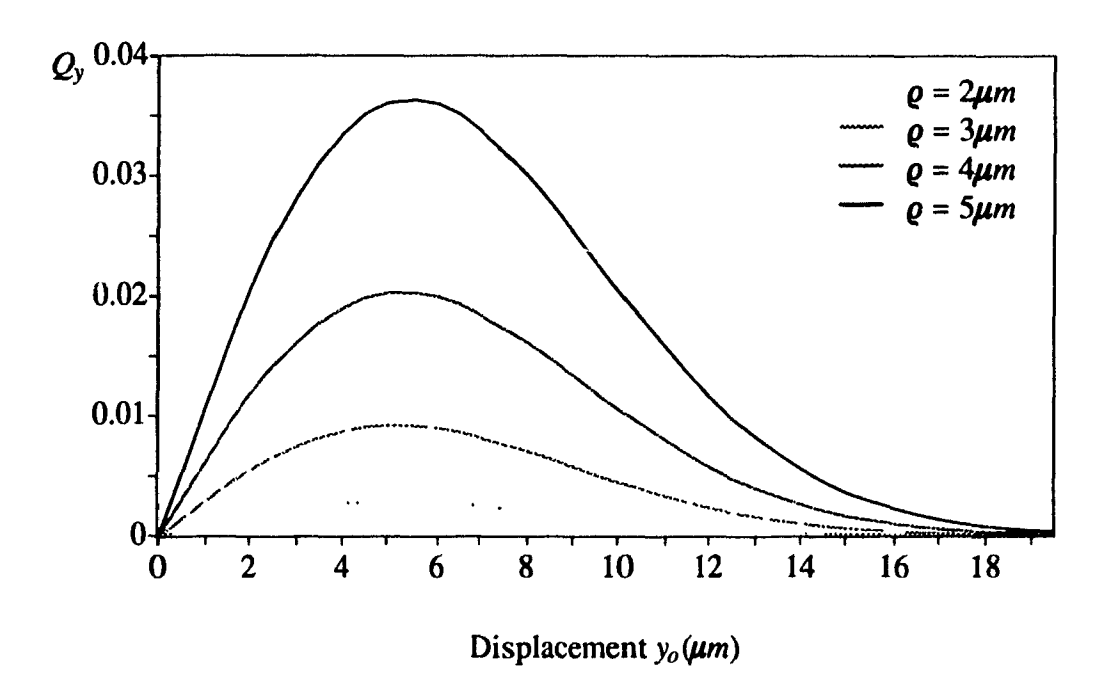


Figure 2.21: Results of Q_y for $\omega_o = 10 \mu m$.

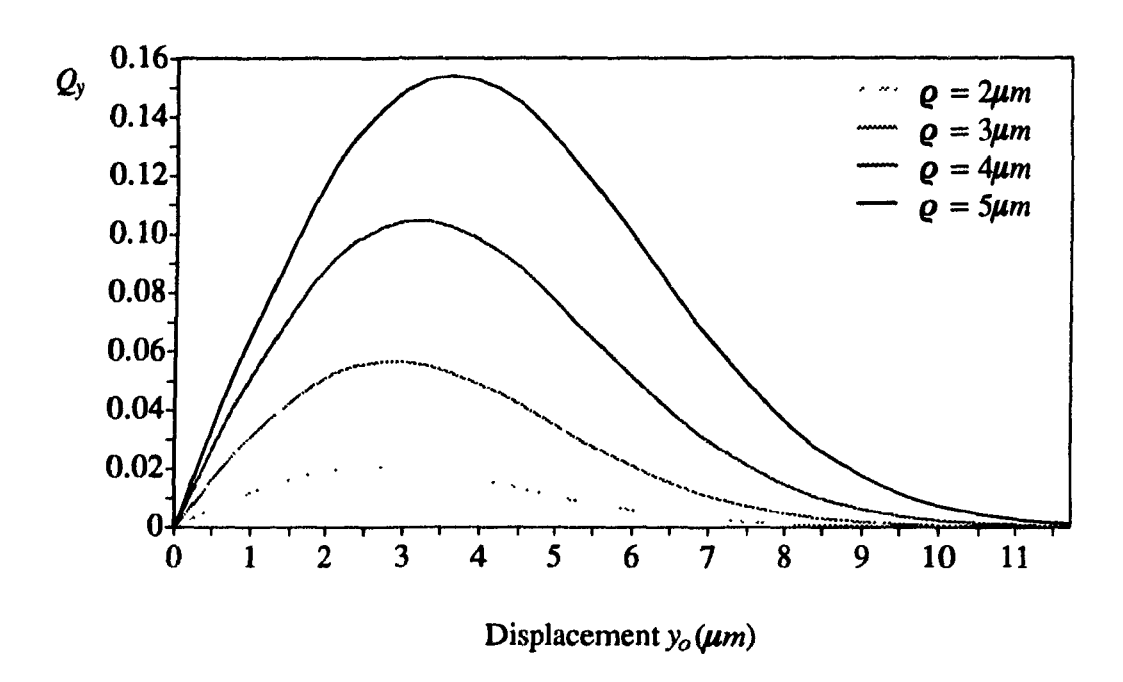


Figure 2.22: Results of Q_y for $\omega_o = 5\mu m$.

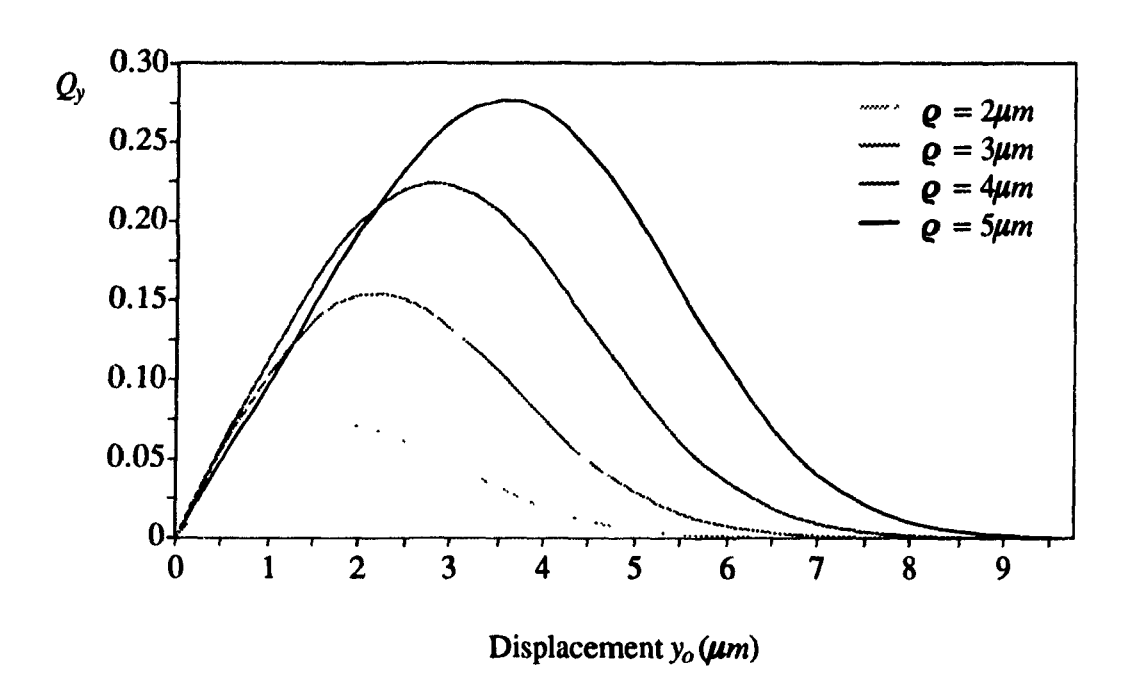


Figure 2.23: Results of Q_y for $\omega_o = 3\mu m$.

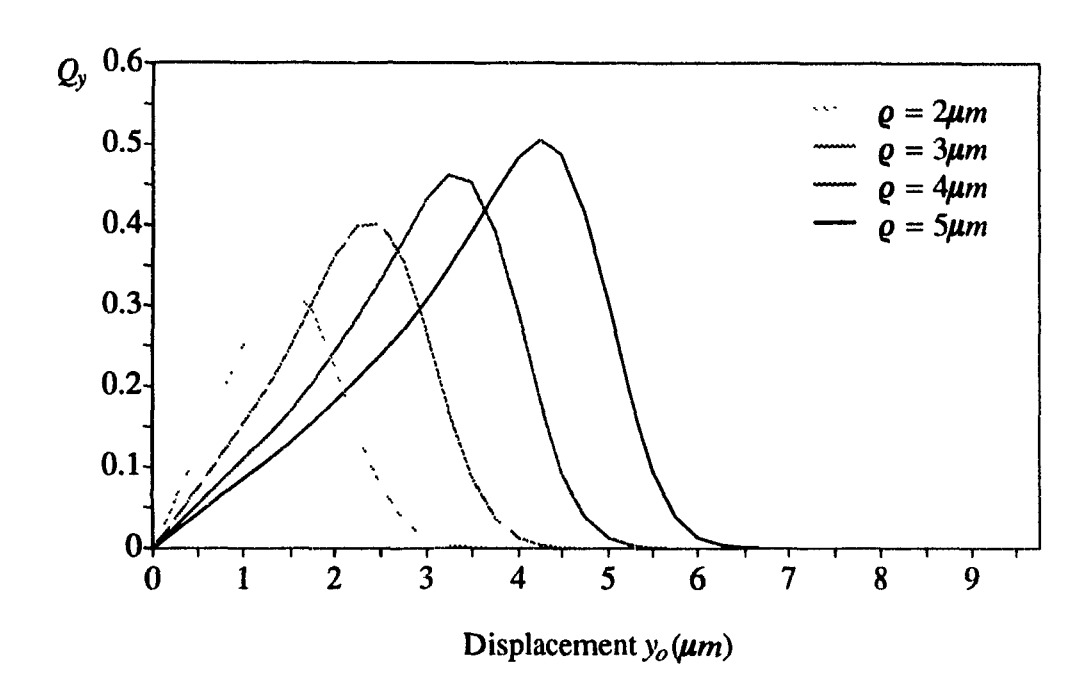


Figure 2.24: Results of Q_y for $\omega_o = 1 \mu m$.

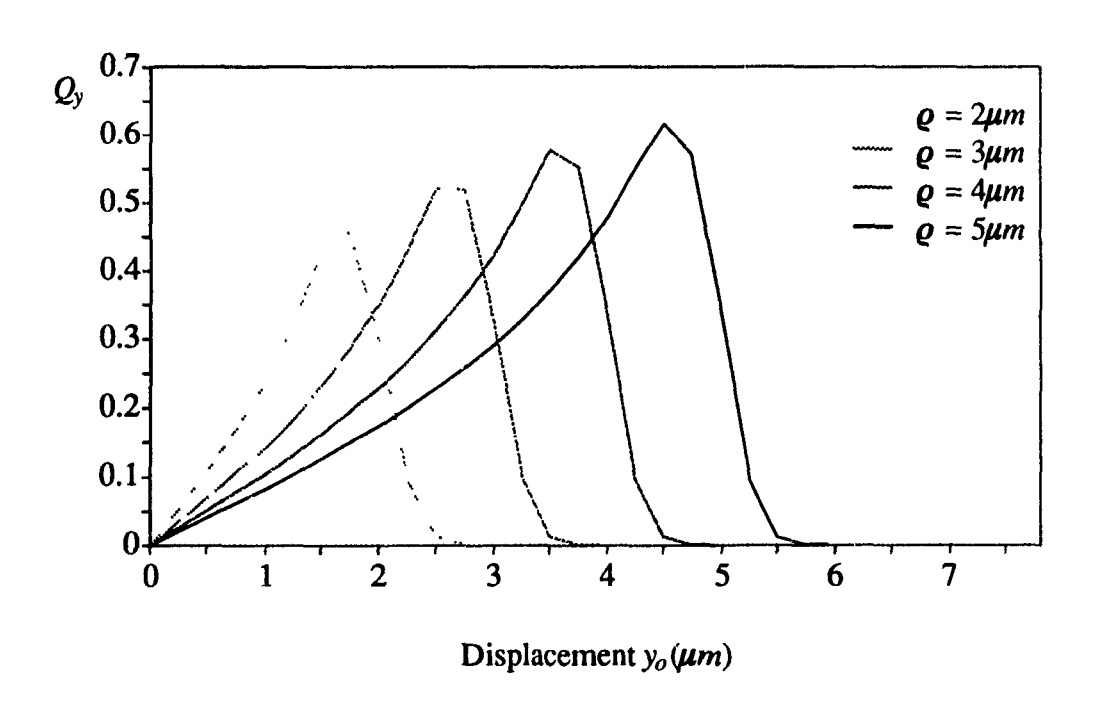


Figure 2.25: Results of Q_y for $\omega_o = 0.5 \mu m$.

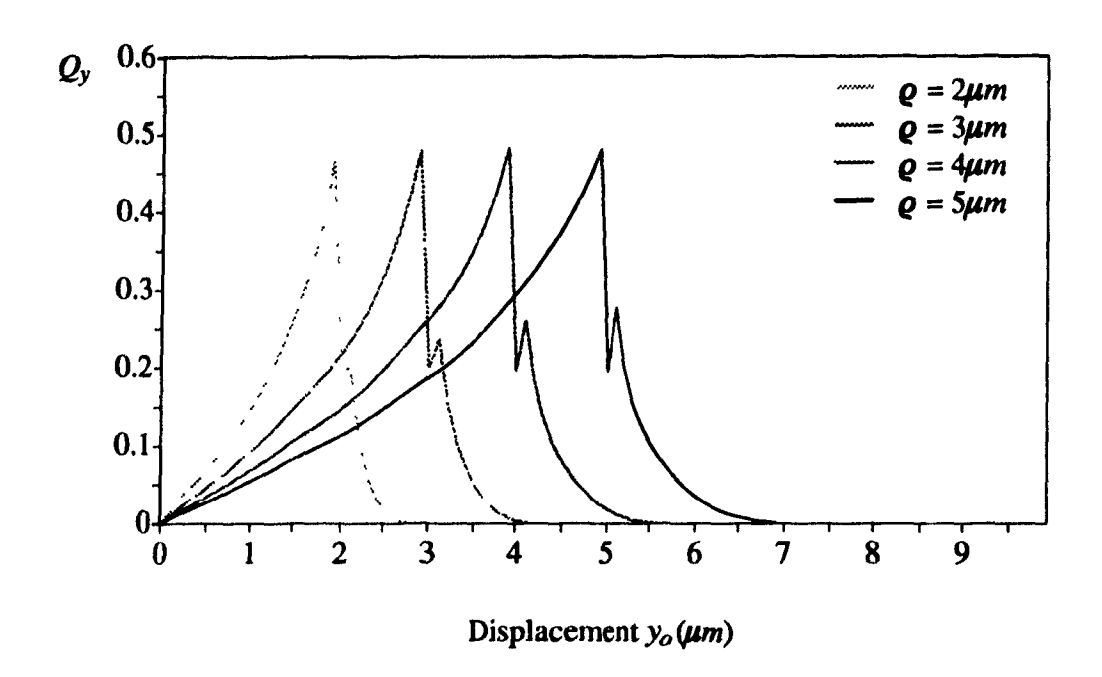


Figure 2.26: Results of Q_y for $\omega_o = 0.1 \mu m$.

K.

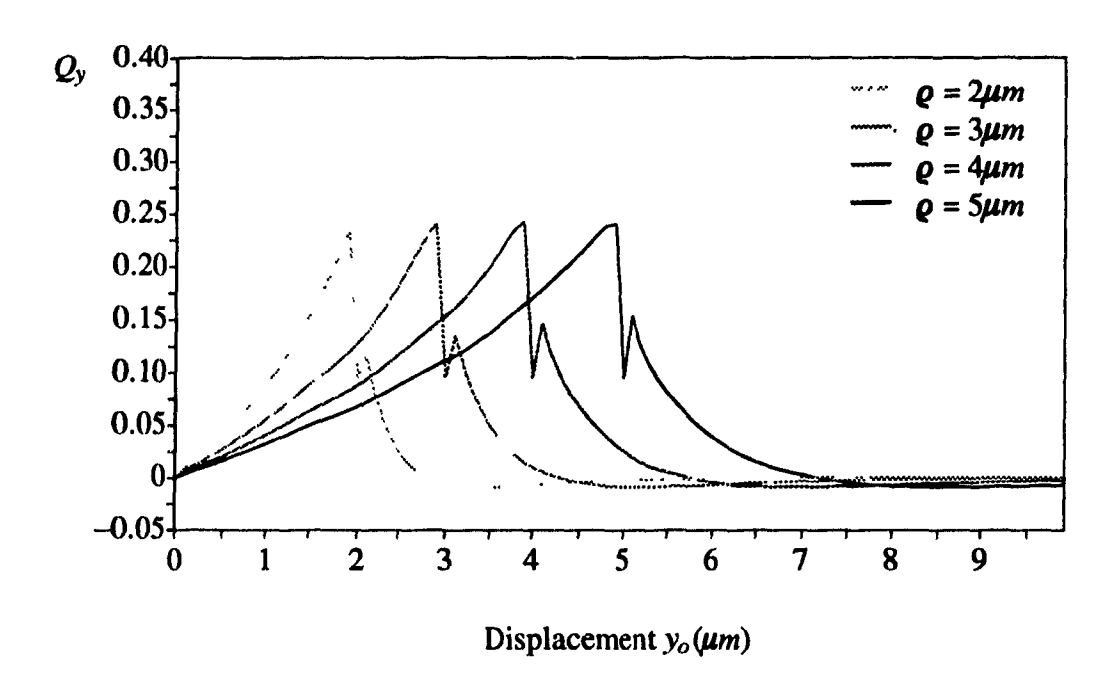


Figure 2.27: Results of Q_y for $\omega_o = 0.05 \mu m$.

2.3.3 Summary

The forces acting on a particle by a TEM₀₀ mode laser beam behave in a different way depending on the profile of the laser beam. When the beam waist radius ω_o is small ($\omega_o < 0.1 \mu m$), the axial force F_z is like the restoring force of a spring and can confine the particle axially at a certain place around the waist of laser beam. The equilibrium position is determined by the profile of the laser beam and the size of the particle. The beam has a large restoring force, or a strong elastic coefficient, for small particles. Smaller particles are confined to a smaller range around the waist of the beam. For a large beam waist radius ω_o , the laser beam tends to be a parallel beam, and the axial restoring force disappeared. This is the case of the G.P.W. beam.

The transverse force F_y always forms a transverse optical well and has the same characteristics as that in the G.P.W. beam.

The axial restoring force and the transverse optical well make the single beam trapping possible.

2.4 Summary

This chapter has presented theoretical studies of the radiation pressures from either a G.P.W. laser beam or a TEM₀₀ laser beam with an arbitrary profile.

The force acting on spheres by the G.P.W. beam is decomposed into three components. The X component is zero due to symmetry of the coordinate system O-XYZ (as shown in Figure 2.4). The component in the axial direction will accelerate the sphere along the beam propagation direction. The lateral component forms an optical well and can confine the spheres to the beam axis when the particles have a higher index of refraction than that of the external medium. When the radius of the particle is smaller than the beam waist radius both the axial force and the lateral force increase as the size of the particle increases. The fact that a larger size and higher index of refraction of the particle help to form a deeper optical well means that a large size particle with high index n may be confined tightly and be manipulated easily.

The characteristics of the forces from a TEM₀₀ beam strongly depend on the profile of the laser beam. When the beam waist radius is small ($\omega_o < 0.1 \mu m$), the axial force is like the restoring force of a spring and forms an optical well which could confine the particle axially to a certain place on the back of the beam waist. Smaller particles have a strong elastic coefficient. The axial optical well disappears when the waist of the laser beam is large. This is the case of the G.P.W. beam. The lateral force always forms an optical well and has the same behavior as that of the G.P.W. beam. Therefore as a whole, a single highly focused TEM₀₀ laser beam can form axial and lateral optical traps which will confine a particle to a single location instead of displacing them. Smaller particles will be confined easily and tightly.

Chapter 3

Experimental Study of the Optical Forces from a Laser Beam

The goal of this chapter is to examine the optical forces from a laser beam experimentally.

Three optical stations were designed and built in the laboratory.

As explained in Chapter 2, with a collimated laser beam, it is possible to confine particles transversely on the beam axis by the gradient force and accelerate them along the beam propagating direction by the scattering force. Therefore, by measuring the velocity of particles, the theoretical results in Chapter 2 may be confirmed experimentally. For this purpose, two experimental stations were designed to investigate the processes in which small particles were moved up by an upward directed laser beam and pushed down by a downward directed laser beam.

Due to the important role of beam profile characteristics, this chapter also presents an additional experiment, which shows the behavior of small particles when they are placed in laser beams with different beam profiles.

3.1 Upward Accelerating Experiment

This section reports the observation of acceleration of freely suspended particles in water by the forces from an argon ion laser. The experiment, performed on glass beads and PMMA latex beads which are predicated to be accelerated up by a vertically directed upward laser beam, is used to determine the existence of both the scattering force and the gradient force, investigate the magnitude of the scattering force and the stability of transverse trapping.

3.1.1 Apparatus

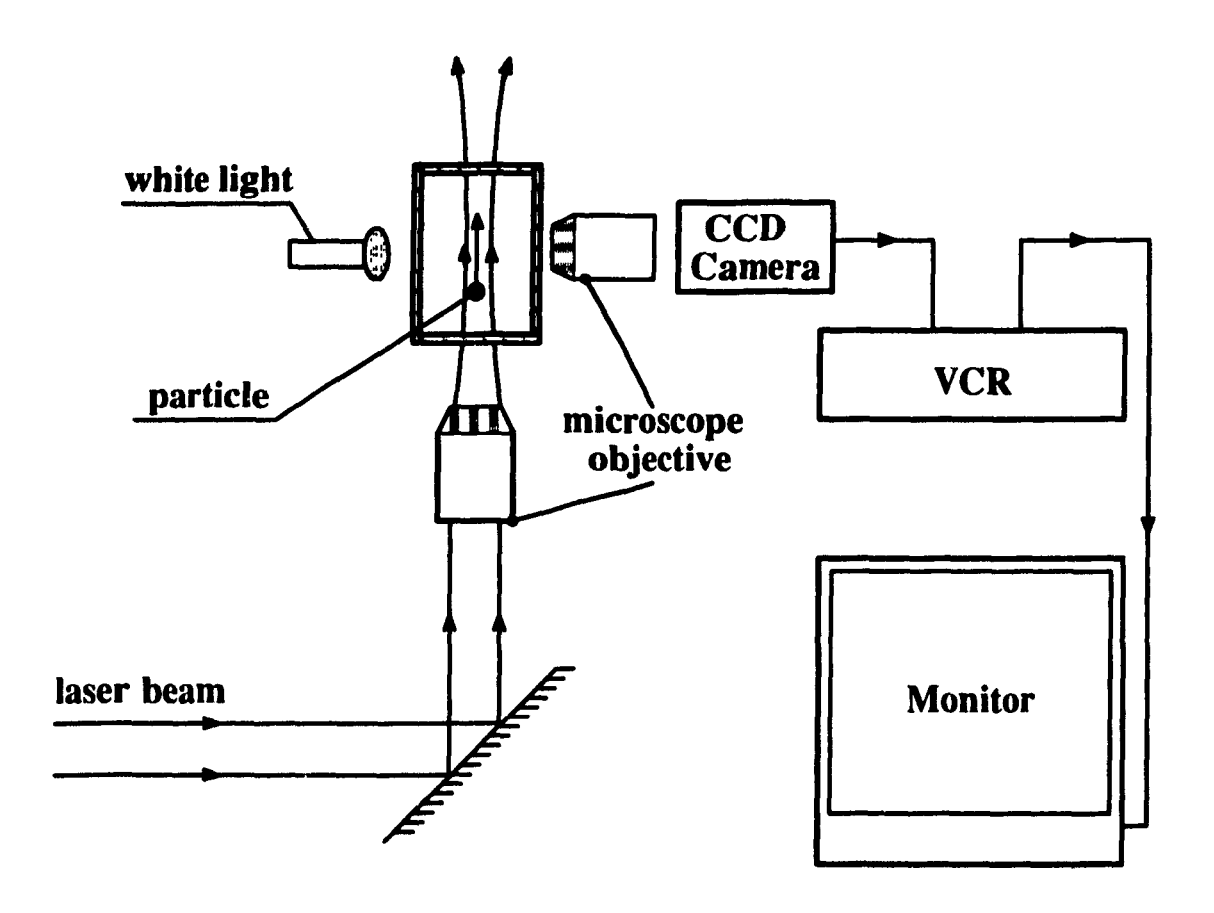


Figure 3.1: A schematic diagram of the upward accelerating experiment apparatus.

Using the apparatus shown schematically in Figure 3.1, the laser beam from an argon ion laser was guided ve rically by a mirror. After being focused by a microscope objective, the beam passed through a chamber containing distilled water. On one side of the chamber, a white light source was used to illuminate the particles, on the opposite side, a microscope objective was used to enlarge the image. A C.C.D. (Charge Coupled Device) camera was used to send the image to the VCR for recording. A color monitor was used to display what happened in the chamber.

3.1.2 Experimental Equipment and Design Specifications

1. Optical table

The entire experiment was accomplished on a Basic Table (63–500 series, TMC). The table has a patented Gimbal Piston isolator and provided the best isolation in all directions for even the lowest input level encountered. The table had M6 holes with 25 mm center to center spacing.

2. Laser

The optical beam was obtained from an argon ion laser (Model 75, Optikon). The laser beam with a single mode TEM_{oo} had a maximum power of 150 mW at $\lambda = 0.5145 \ \mu m$. The beam diameter was 0.9 mm and divergence was 0.8 mrad. The amplitude power stability under a current control mode was less than \pm 3%.

3. Mirrors

Two round flat mirrors (MPG006, MEILES GRIOT) were used to guide the laser beam vertically upward. They were fixed on two Flexure Mirror Mounts (MFM-075, Newport), allowing angular adjustments in two dimensions.

4. Bar

A hollow square bar of aluminum was used to hold objectives and mirrors vertically, as shown in Figure 3.2. The bar has three columns of holes on one of its faces. These holes were used to mount different types of optical elements and also permitted vertical movement.

5. Objectives

There were two microscope objectives in this set up. One, called the focal lens, was used for focusing the beam, the other, called the view lens, was used for observing the motion of the particles.

The focal lens was an objective with a magnification of 4x, having a focal length of 30.03 mm and working distance of 18 mm. After being focused by this lens, the beam radius

in water was changed from $0.9 \, mm$ to $8.22 \, \mu m$. With such a beam radius, the optical force could be improved but the collimation of the laser beam was not greatly affected (the divergence was $14.9 \, mrad$). With the long working distance, the chamber could be located at a convenient distance from the front of the objective.

The view lens was chosen to be the same as the focal lens. Considering that the view lens must focus on inside of the chamber, which can not be constructed very small, the view lens was required to have a long working distance. Furthermore, it was expected that the view lens could observe a relatively large area, thus, a low magnification and long working distance objective was needed.

6. Chamber

The chamber was constructed using two parallel glass plates. These two glass plates were used for observing the movement of the particles. The bottom was also made of a glass plate which allowed the beam to pass through with minimal absorption. The size of the chamber was 22 mm wide on side. In the experiment, the chamber was held by a metal plate which was fixed on a stereotaxic mount. So the chamber could be moved in three dimensions.

In the experiment, the view lens was required to focus on the laser beam axis. For this purpose, a tiny needle was positioned at the beam center, which was observed on monitor (see Figure 3.3). It was found that if the needle coincided the center of the beam, a strong scattering light pattern could be seen on the screen. The pattern was very sensitive; a tiny motion of the needle would cause a large change of the scattering light. Once the view lens focused on the needle, it focused on the center of the beam.

7. C.C.D camera and color monitor

The C.C.D camera had a small volume but a high resolution. The color monitor was used to observe what happened inside the chamber. With this camera and monitor, it was possible to observe and record continuously.

8. Particles

The particles used were glass beads and PMMA latex beads, obtained from Polysciences

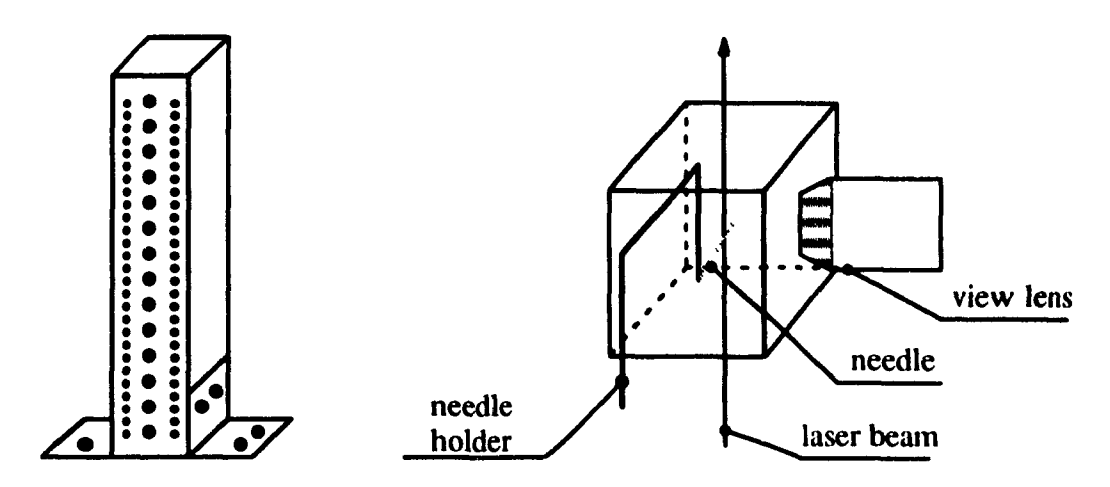


Figure 3.2: A schematic diagram of the bar.

Figure 3.3: A schematic diagram of the chamber with needle inside.

Inc.. The glass beads ranged in diameter from 3 μm to 10 μm , and had a specific gravity of 2.48 and index of refraction of 1.513. The PMMA latex beads varied from 1 μm to 10 μm in diameter, and had a gravity density of 1.19 and index of refraction of 1.49.

9. Power meter

The power meter used for measuring the optical power going through the chamber was a Digital Power Meter (Model 815, Newport). It had an absolute accuracy of \pm 3% over the range 50–85 nm.

10. Filter

A filter was placed in front of the view lens in order to filter the strong scattering light effect.

With the filter, the captured particle appeared as a bright dot on the screen.

3.1.3 Observation

In the experiment, the chamber was filled with distilled water. First some glass beads were disseminated into the water. As the glass beads were heavier than the water, in order to suspend

them, a glass tube was used to make some turbulence in the water. After the water calmed down, the laser was turned on.

The results were observed on the color monitor. If one particle was captured, it became very bright with strong scattering light and moved upward quickly. If the beam was blocked, the particle, which appeared as a black dot, would stop moving. Taking off the block would cause the particle to move again. The observation of the particle moving straight upward stems from the radial inward force, that is, the gradient force. To check for the stability of capture, the beam was moved transversely; it was found that the particle moved transversely with the laser beam. When the beam was moved back, the particle moved back with the beam. However, for a rapid movement of the beam, the particles would leave the beam.

It was also observed that when one particle was captured and accelerated up, another particle was attracted into the beam and moved following the first one. When this occurred, the first one would slow down or even drop downward. It also happened that the second one would strike the first one (as the first one moved slowly), at which point the two would combine and move up together. If the beam was blocked, the two particles (sometimes more than two) would stop moving, separate and wander off, apparently by Brownian motion.

Manipulation of one captured particle at different laser powers was also possible. Once one particle was captured, an increase in laser power would quickly accelerate the particle, attenuating the laser power would slow it, and even stop it.

For operation with PMMA latex beads, similar effects were observed.

The behavior of the particles was in qualitative agreement with that expected from the theory.

3.1.4 Data Acquisition

To demonstrate quantitatively the force of acceleration, the movement of the particles was recorded on a Hi8 video tape.

The data was acquired by setting the laser power at different magnitudes, from 100 mW down to 30 mW. For each laser power, the movements of particles were recorded. After some data were collected, data analysis was done by computer control.

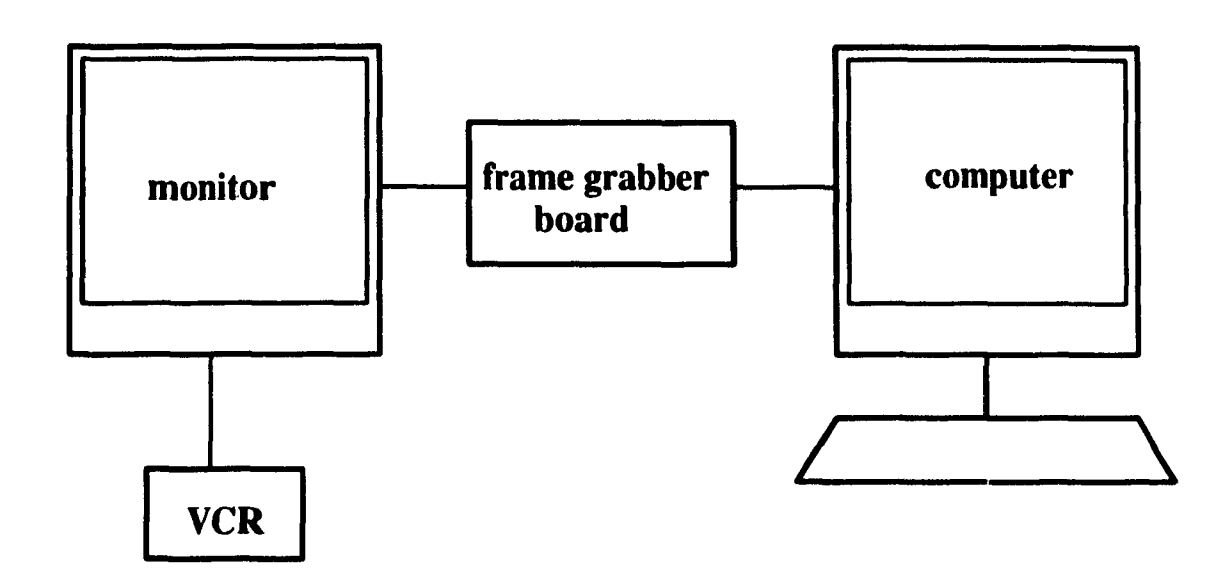


Figure 3.4: A schematic diagram of data acquisition.

Figure 3.4 is the schematic diagram of the experimental control for quantitative analysis. Using the frame by frame function of the VCR, it was possible to proceed through the display one frame at a time. The time period between two frames was 1/30 s. The position of the captured particle was recorded and saved as a file. At the beginning of the experiment, an image of the needle of known size was displayed on the screen. By comparing particle position with the needle size, the displacement of the particle in real space was obtained.

3.1.5 Theoretical Model

Theoretically, when a particle is placed in water, it will be acted on by gravity and the buoyancy of water. If the particle is captured by a laser beam, it will be acted on by another upward

optical force and will start to move upward. When it is moving, there is a resistance due to the viscosity of the water. Besides, there is another random force caused by the motion of water, which can not be estimated. As a matter of fact, before the laser beam is turned on, the particles seem to stay there motionless. Thus, we take

$$\vec{mg} + \vec{F}_{buov} + \vec{F}_{rand} = 0 \tag{3.1}$$

where mg is the gravity of the particle, F_{buoy} is the buoyancy of the water and F_{rand} is the random force. The formula of the movement of the particle is

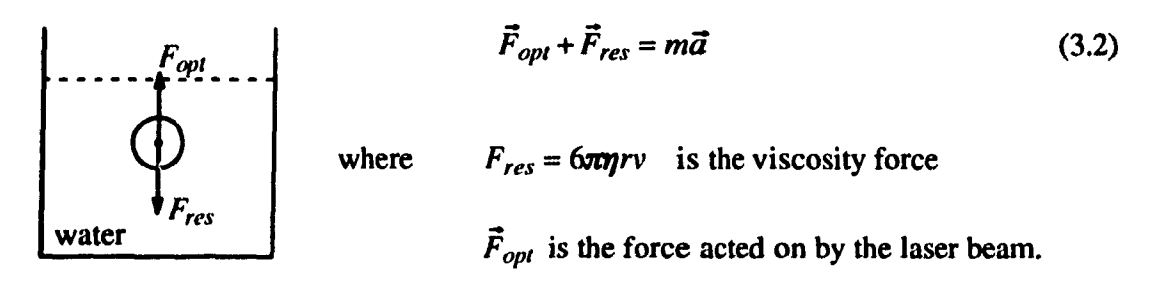


Figure 3.5: A schematic diagram of the forces acted on a particle.

Taking the upward direction as the positive x-axis, we have:

$$F_{opt} - 6\pi \eta r \frac{dx}{dt} = m \frac{d^2x}{dt^2} \tag{3.3}$$

Solving this equation, we get
$$x = at + be^{-t/\tau} - b$$
 (3.4)

where
$$a = \frac{F_{opt}}{6\pi\eta r} \qquad b = \frac{F_{opt}m}{(6\pi\eta r)^2} \qquad \tau = \frac{m}{6\pi\eta r}$$
 (3.5)

which included the initial condition t = 0, x = 0 and v = 0.

Given the values of beam waist radius, the refractive index of the particle, the force exerted on particles by laser beam was calculated by the same method as in Chapter 2. Applying the calculated force to equation (3.5), a, b and τ were obtained theoretically. As an example,

Table 3-1 gives the results of a, b and τ for the case where laser power was 100 mW and the particle was a glass bead.

Table 3–1: Magnitude of the parameters in the movement equation.

radius of the particle	a (µm/s)	b (µm)	τ (s)
$\varrho = 1 \mu m$	13,44851859	0.00007263	0.00000540
$\varrho = 2 \mu m$	25.50433144	0.00055098	0.00002160
$\varrho = 3 \mu m$	35.03534941	0.00170300	0.00004861
$\varrho = 4 \mu m$	41.36071161	0.00357415	0.00008641
$\varrho = 5 \mu m$	44.32576704	0.00598496	0.00013502

From Table 3-1, it can be seen that τ is very small. Here, it is noted again that τ represents the characteristic time for the captured particle to reach its maximum velocity. Since τ is only on the order of 0.1 ms, once one particle is observed to be captured and accelerated by laser beam, it has already reached its maximum velocity. For this reason, we are more interested in the maximum velocity of the captured particle.

3.1.6 Data analysis

This experiment was carried out for both glass beads and PMMA latex beads. The results for glass beads are mainly discussed in this section, while the results of PMMA latex beads are listed afterwards as a subsidiary illustration.

In Figure 3.6, the * is the data point where a glass particle was captured and moved up by the laser beam. Recall that the displacement of the particle in real space was obtained by comparison with needle size. A needle with a diameter of 96 μm is equivalent to 59.9 on the computer screen. Thus, the displacement of the particles in micrometers is the displacement

on the screen multiplied by a factor 96/59.9.

1

The state of the s

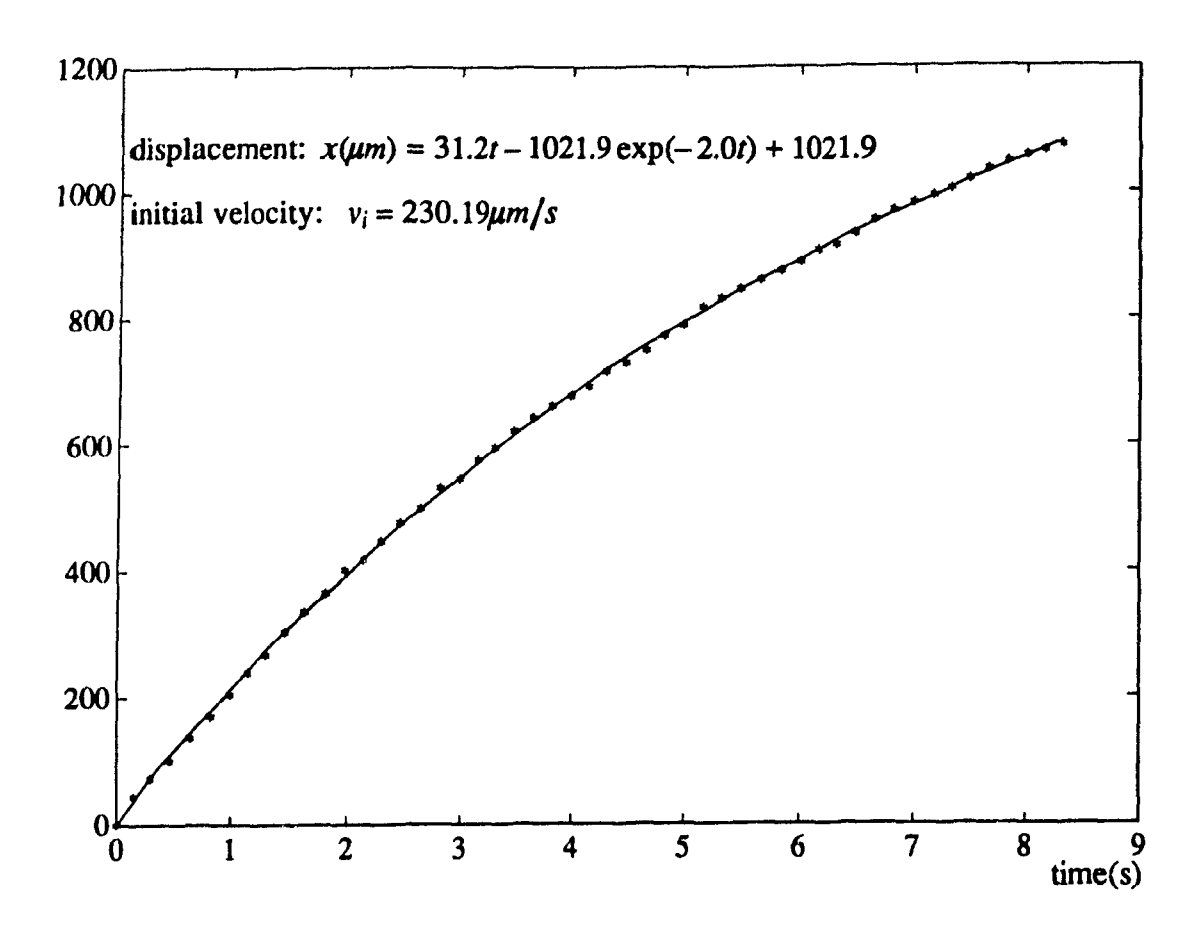


Figure 3.6: A plot of the displacement versus time.

From the function (3.4), it is thus expected that the data of the displacements of the captured particle could be connected as a straight line since τ is too small. However, when the effect of absorption laser light by water and the shadowing effect due to some other particles staying behind the measured one are considered, the captured particle is expected to slow down, stop and even be kicked off the beam. For this reason, only the initial velocity may be used to compare with the theoretical results. Since light absorption by water varies exponentially with the distance away from the light source, a function of the form $x = pt + qe^{-rt} + s$ was chosen to fit the data. In Figure 3.6, the solid curve is the fitted result.

An initial velocity of 230 $\mu m/s$, and a particle radius of 6.8 μm which was obtained by the image on the screen, was used for the fitting.

Table 3–2 presents results of particles size, laser power and the measured velocities for other captured particles using a similar treatment.

Table 3-2: Data of captured particle size, laser power and measured velocity.

	particle radius ϱ (μm)	laser power P (mW)	velocity v (μm/s)
1	6.8	100.59	230
2	7.6	100.59	293
3	6.4	100.59	286
4	5.2	100.59	182
5	6.8	100.59	279
6	7.6	86.64	266
7	6.8	79.88	188
8	7.6	73.96	265
9	6.4	73.96	209
10	6.8	66.36	148
11	5.2	66.36	176
12	6.0	58.75	186
13	5.6	58.75	180
14	5.2	58.75	133
15	5.2	50.72	116
16	4.8	50.72	111
17	4.4	50.72	113
18	4.4	50.72	99
19	5.6	45.22	124
20	5.2	45.22	97.4
21	6.0	45.22	194
22	4.8	38.88	80.4
23	4.8	38.88	76
24	6.0	30.03	97.3
25	5.2	30.03	50.5

In order to obtain a relationship between the variables: velocity, laser power and particle size, and predict the value of the velocity from a set of values of the independent variables: particle size r and laser power P, a regression analysis was employed to accomplish the following tasks:

- a. to obtain best estimates of the unknown regression parameters;
- b. to test hypotheses about these parameters;

Sales A

N. Committee

c. to determine the adequacy of the assumed model.

Taking the data in Table 3–2 as an example, two assumed models were used: one is the simplest linear model $v = \beta_0 + \beta_1 \varrho + \beta_2 P$, and the second is the second order linear model $v = \beta_0 + \beta_1 \varrho + \beta_2 P + \beta_3 \varrho P + \beta_4 \varrho^2 + \beta_5 P^2$. The parameters and their standard errors in both models are computed by the computational methods provided by the NAG software on regression analysis. Table 3–3 presents the results of all the estimated parameters, their standard errors, t-statics, residuals and the correlation coefficients.

The *t*-statistic is defined as $\hat{\boldsymbol{\beta}}_k / \sqrt{Se\hat{\boldsymbol{\beta}}_k}$, where $\hat{\boldsymbol{\beta}}_k$ is the estimated value of parameter $\boldsymbol{\beta}_k$, $Se\hat{\boldsymbol{\beta}}_k$ is the standard error of $\boldsymbol{\beta}_k$. The t-statistic is used to determine whether the parameter $\boldsymbol{\beta}_k$ is significant or not in the model. *RSS* is the residual sum of squares, $RSS = \sum_i (\hat{v}_i - v_i)^2$, where \hat{v}_i is the estimated velocity from the regression model, v_i is the actual velocity from the experiment. *SC* is the sample multiple correlation coefficient, $SC^2 = 100(1 - RSS / \sum_i (v_i - \bar{v}_i)^2)$, where \bar{v}_i is the mean of v_i . *SC* is a useful measure of how well an estimated regression fits the observation.

Table 3-3: Results of linear regression analysis.

		parameters	standard error	<i>t</i> —statistic	RSS	SC
first model	$oldsymbol{eta}_o$	-137.35	33.64	23.679		
$v = \boldsymbol{\beta}_o + \boldsymbol{\beta}_1 \boldsymbol{\varrho} + \boldsymbol{\beta}_2 \boldsymbol{P}$	β_1	32.03	7.208	11.93	1.59e+4	93.45%
	β_2	1.8244	0.306	3.29		
second model	β_o	-7.43	9.22	2.446		
$v = \boldsymbol{\beta}_o + \boldsymbol{\beta}_1 \boldsymbol{\varrho} + \boldsymbol{\beta}_2 \boldsymbol{P}$	β_1	21.77	27.05	4.185		
$+\mathcal{E}_{3}\varrho P+\beta_{4}\varrho^{2}+\beta_{5}P^{2}$	β_2	2.85	2.68	1.743	1.654	02 5 9 <i>a</i>
$ + r_3 \mathbf{Q} \mathbf{P} + \mathbf{p}_4 \mathbf{Q}^2 + \mathbf{p}_5 \mathbf{P}^2 $	β_3	0.0683	0.49	0.097	1.55e+4	93.58%
	β_4	4.00	4.97	1.796		
	β 5	-0.0105	0.013	0.092		

Based on the t-test, it was shown that at a 95% significance level, all the parameters in model 1 are significant. While in model 2, only the parameters β_0 and β_1 are significant. By the F-test, $F = [(RSS_1 - RSS_2)/(\mu_1 - \mu_2)]/[RSS_2/\mu_2]$, it was shown further that at a 95% significance level, the parameters β_3 , β_4 and β_5 in model 2 which do not exist in model 1 are not needed. The results indicated that a simple linear model was an appropriate model for the data in Table 3–2. An additional test was made to judge whether Q or P was significant. The result is at an 80% significance level, P is more significant than Q. Since the significance level is not high, both particle size Q and laser power P did affect the motion of the particles.

In order to compare the experimental results with the theoretical calculations, Table 3-4 presents three velocities for a certain particle at a fixed laser power: 1.velocity directly from measurement; 2.velocity from the regression model; 3.velocity from the calculation.

Table 3-4: Data of the three velocities for glass beads.

	particle size	laser power	original velocity	regressed velocity	calculated velocity
	ρ (μm)	P (mW)	v_o ($\mu m/s$)	$v_r (\mu m/s)$	v_c ($\mu m/s$)
1	6.8	100.59	230.00	263.98	148.64
2	7.6	100.59	293.00	289.60	133.12
3	6.4	100.59	286.0	251.16	155.35
4	5.2	100.59	182.00	212.73	167.95
5	6.8	100.59	279.00	263.98	148.64
6	7.6	86.64	266.00	264.15	114.66
7	6.8	79.88	188.00	226.19	118.03
8	7.6	73.96	265.00	241.02	97.88
9	6.4	73.96	209.00	202.58	114.23
10	6.8	66.36	148.00	201.52	98.06
11	5.2	66.36	176.00	150.28	110.80
12	6.0	58.75	186.00	162.02	94.03
13	5.6	58.75	180.00	149.21	96.54
14	5.2	58.75	133.00	136.39	98.09
15	5.2	50.72	116.00	121.74	84.69
16	4.8	50.72	111.00	108.93	85.06
17	4.4	50.72	113.00	96.12	84.34
18	4.4	50.72	99.00	96.12	84.34
19	5.6	45.22	124.00	124.52	74.31
20	5.2	45.22	97.40	111.71	75.50
21	6.0	45.22	194.00	137.33	72.38
22	4.8	38.88	80.40	87.33	65.20
23	4.8	38.88	76.00	87.33	65.20
24	6.0	30.03	97.30	109.62	48.07
25	5.2	30.03	50.50	83.99	50.14

The way to measure how close the fitted model to the theoretical results is the VAF (variance accounted for) estimation procedure. VAF is defined as

$$VAF = 100(1 - \frac{\sum_{i} (v_r - v_c)^2}{\sum_{i} v_r^2})\%$$
 (3.6)

where v_r is the velocity from the regression model, and v_c is the calculated velocity. From Table 3-4, a value of VAF=79.98% was obtained.

The same procedure was applied to the data recorded for the PMMA latex beads. Table 3-5 presents the results of captured particle size, laser power and particle velocity.

Table 3–6 shows results of the regression analysis. At a 95% significance level, all the parameters in linear model $v = \beta_o + \beta_1 \varrho + \beta_2 P$ are significant. While in model 2, only the parameters $\beta_o, \beta_1, \beta_2$ and β_4 are significant. Based on the F-test, it is shown that at a 95% significance level, the parameters β_3, β_4 and β_5 in model 2 but not in model 1 are not needed, but at 90% significance level, parameters β_3, β_4 and β_5 in model 2 but not in model 1 are needed. Since the parameter β_4 in model 2 is also significant by the t-test, the third model $v = \beta_o + \beta_1 \varrho + \beta_2 P + \beta_4 \varrho^2$ is chosen to fit the data. The regression analysis results are listed together in Table 3–6. By the F-test, comparing model 2 and model 3, it is shown that at a 95% significance level, those parameters β_3 and β_5 in model 2 but not in model 3 are not needed. Comparing model 1 and model 3, it was found that at a 90% significance level, parameter β_4 in model 3 but not in model 1 is needed. Therefore, model 3 is an appropriate one. We have used model 3 as the fitted model. Table 3–7 gives the results of the three velocities where the VAF is 86.04%.

Table3-5 Data of PMMA latex beads: particle size, laser power and measured velocity.

	particle radius (µm)	laser power (mW)	velocity (\mum/s)
1	7.2	80.73	214
2	6.4	80.73	90.5
3	7.2	80.73	216
4	6.4	73.96	114
5	6.8	73.96	168
6	4.8	73.96	115
7	6.4	66.36	156
8	6.0	66.36	135
9	5.6	66.36	103
10	6.0	66.36	149
11	4.4	59.17	72.1
12	5.6	59.17	107
13	4.8	59.17	83.6
14	5.2	59.17	109
15	4.8	51.14	63.0
16	6.4	51.14	119
17	5.2	51.14	61.9
18	5.2	51.14	62.2
19	5.6	44.8	72.2
20	4.8	44.8	68.9
21	6.0	44.8	72.6
22	5.2	38.04	70.7

Table 3-6: Results of regression analysis for PMMA latex beads.

		parameters	standard error	<i>t</i> –statistic	RSS	SC
first model	β_o	-162.53	37.55	26.52	•	
$v = \boldsymbol{\beta}_o + \boldsymbol{\beta}_1 \boldsymbol{\varrho} + \boldsymbol{\beta}_2 P$	β_1	31.52	8.03	11.12	1.10e+4	86.98%
	β_2	1.51	0.505	2.122	!	
second model	$oldsymbol{eta}_o$	-32.21	16.24	7.99		
$v = \beta_o + \beta_1 \varrho + \beta_2 P$	$\boldsymbol{\beta}_1$	-98.99	49.91	14.031		
	β_2	9.26	5.018	4.135		
$+\beta_3 QP + \beta_4 Q^2 + \beta_5 P^2$	β_3	-0.246	0.835	0.269	8.59e+3	90.0%
	β_4	13.45	8.07	4.733		
	β ₅	-0.056	0.042	0.273		
third model	$oldsymbol{eta}_o$	431.14	278.12	25.85		
$v = \beta_o + \beta_1 \varrho + \beta_2 P$	β_1	-170.83	94.35	17.58		
$+\beta_4 Q^2$	β_2	1.06	0.508	1.49	8.77e+3	89.7%
	β ₄	17.72	8.24	6.174		

Table 3-7: Data of the three velocities for PMMA latex beads.

	particle size	laser power	original velocity	regressed velocity	calculated velocity
	Q (μm)	P (mW)	v_o ($\mu m/s$)	ν _r (μm/s)	v_c ($\mu m/s$)
1	7.2	80.73	214.00	205.66	94.85
2	6.4	80.73	90.50	149.50	104.78
3	7.2	80.73	216.00	205.66	94.85
4	6.4	73.96	114.00	142.31	95.99
5	6.8	73.96	168.00	167.55	91.68
6	4.8	73.96	115.00	98.04	104.83
7	6.4	66.36	156.00	134.24	86.13
8	6.0	66.36	135.00	114.66	89.41
9	5.6	66.36	103.00	100.76	91.93
10	6.0	66.36	149.00	114.66	89.41
11	4.4	59.17	72.10	85.44	83.26
12	5.6	59.17	107.00	93.12	81.97
13	4.8	59.17	83.60	82.33	83.87
14	5.2	59.17	109.00	84.89	83.40
15	4.8	51.14	63.00	73.80	72.49
16	6.4	51.14	119.00	118.07	66.37
17	5.2	51.14	61.90	76.36	72.08
18	5.2	51.14	62.20	76.36	72.08
19	5.6	44.80	72.20	77.86	62.06
20	4.8	44.80	68.90	67.07	63.50
21	6.0	44.80	72.60	91.76	60.36
22	5.2	38.04	70.70	62.45	53.62

3.1.7 Discussion and Conclusions

From the observations and data analysis, the following conclusions were obtained:

- 1. Observation of the particles being attracted into the beam and accelerated upward has confirmed the existence of the transverse force and the longitudinal force.
- 2. Any transverse displacement resulted in a restoring force due to the transverse gradient force. Manipulation of the captured particles by moving the beam transversely showed that the transverse trap was relatively stable.
- 3. The regression analysis showed that the velocity is proportional to the laser power and particle size. Recall that the optical force is Q_z multiplied by $2n_mP/c$, thus the optical force is proportional to the laser power. From the theoretical results in Figure 2.3 in chapter 2, it is shown that Q_z is proportional to the particle size until the particle is as large as the beam waist size. It can be seen that the experimental data confirmed the properties of the optical scattering force.

In the experiment, some factors which could affect the results were ignored in the theoretical model:

- 1. As the particles are heavier than the water, in order to make them suspend in water, an additional tube was introduced to stir the water, thus, a turbulence was made. The turbulence will effect the motion of the particles directly. Although we took $\vec{mg} + \vec{F}_{buoy} + \vec{F}_{rand} = 0$, we can not estimate the value of the turbulence.
- 2. Thermal effects could be decreased by making the chamber as small as 20 μm. Whereas the chamber in use was 10 mm wide. The obscuring effects of thermal forces, caused by temperature gradients in the water surrounding a particle, could push the particle out of the beam [Ashkin, 1970]. The convection caused by the beam could also accelerate the particle upward. Therefore, thermal effects will affect both transverse stability and upward velocity.

3. Water absorbs light according to the relationship $I = I_0 e^{-\alpha x}$. Thus, when particles moved higher in the chamber, the light illuminated on them would be less. In most cases, there were other particles trapped in the beam at the same time. Those particles below the measured one would partially block the light reaching to the measured particle. Both of these factors would cause the particle to decelerate.

The measurement errors came from the following measurements:

- 1. The displacement of particles on screen.
- 2. The particle size.
- 3. Time period between frames.
- 4. Laser power.
- 5. The velocity obtained from a fitted curvature.

3.2 Downward Accelerating Experiment

As the thermal force and turbulence did play a role in the first experiment, the effect of the optical force may have been concealed. However, if the laser beam is reversed, what would happen? The convection and the turbulence effects should not change the direction of the motion of the particles, whereas the optical forces would. Thus, operating with a vertically downward laser beam, the behavior of small particles in the laser beam would yield some confidence to the results.

3.2.1 Apparatus

Figure 3.7 is an apparatus which guides the laser beam downward into a chamber which is filled with distilled water.

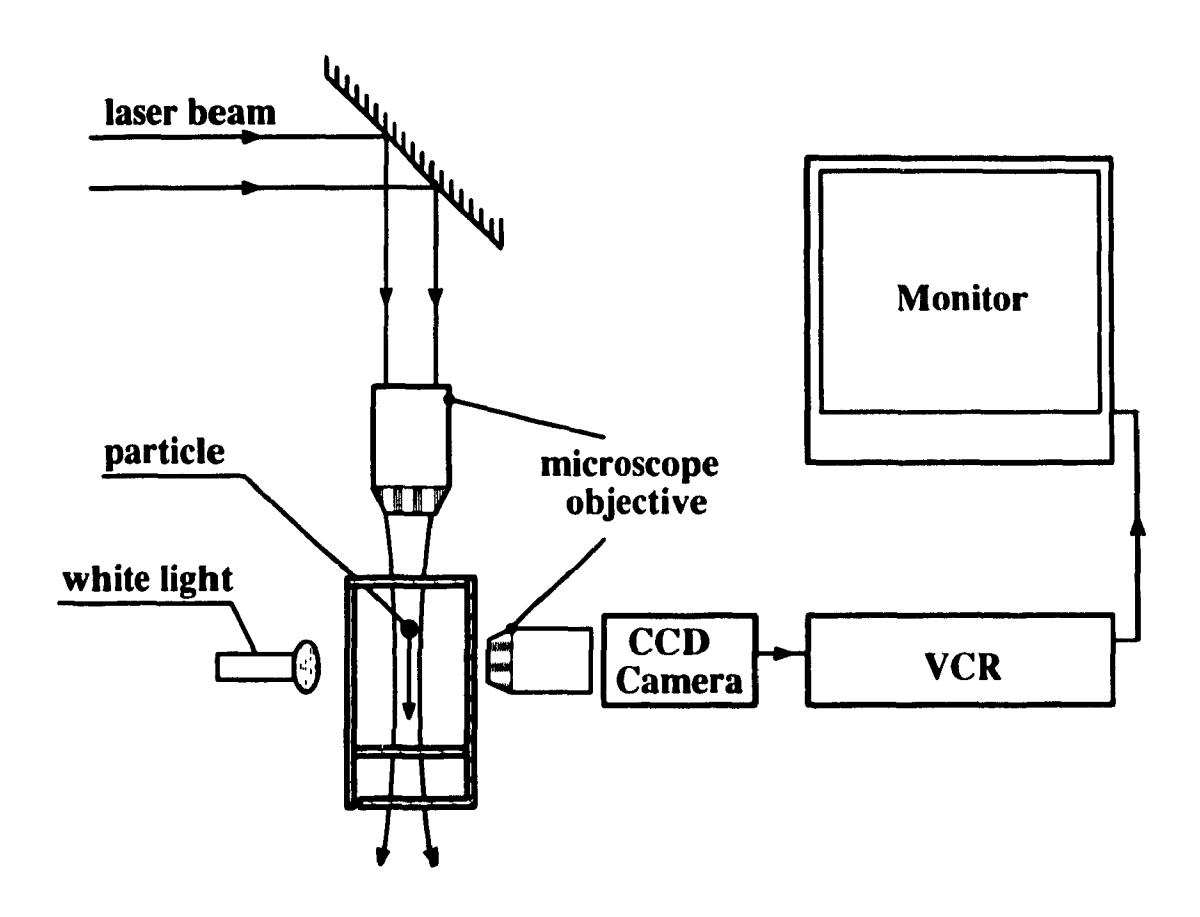


Figure 3.7: A schematic diagram of downward accelerating experiment.

3.2.2 Design Specification

In this experiment, all the elements are same as in the first experiment described in Section 3.1.2 except for the modification of the chamber.

Since the beam is directed downward into the chamber, the bottom of the chamber must be less reflective and allow the beam to go through it. If the bottom reflects some light backward, it will reduce the effect of light beam. If the bottom absorbs some light, it will become warm, heat the chamber, thus, increasing the heating affect. For this reason, the chamber was made specially as shown in Figure 3.8.

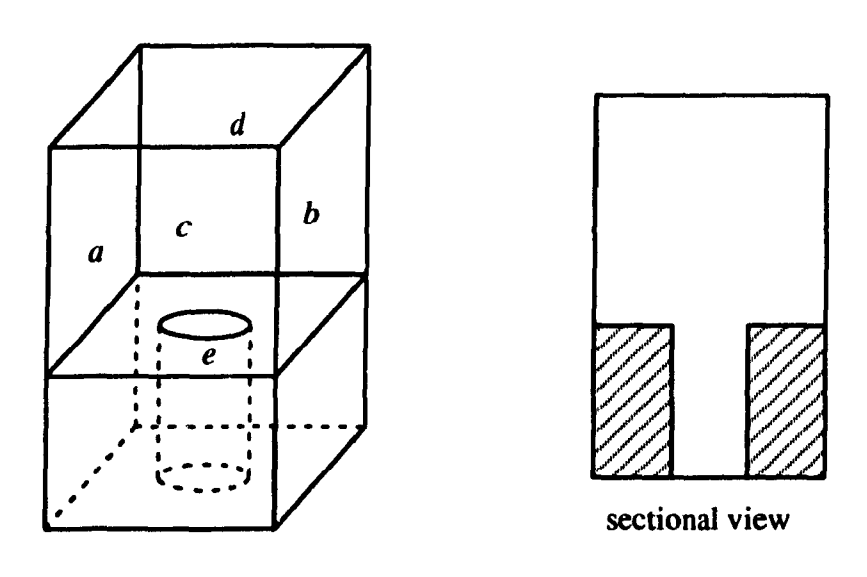


Figure 3.8: A schematic diagram of the chamber.

Side a and side b were composed of glass plates which let the objective observe the movement of particles. Side b and side d were made of plastic plates. Side e was also a glass plate, which had less reflection and less absorption of light. Below side e was a plastic block, which had a 1 mm diameter hole in it. The edge of the hole was painted black, so that, when the beam passed through the chamber, it would be less reflected and less absorbed.

3.2.3 Observation

Adjustments which are almost the same as that in the previous experiment were done in this experiment. The beam was required to pass through the hole in the chamber, and it was necessary that the view lens was focused on the laser beam.

When the laser was turned on, it was found that the captured particle, which showed a strong scattering light, moved downward as expected. Placing a filter in front of the CCD camera, the strong scattering light was obscured, it was observed that a bright dot moved down quickly while other particles wandered off. This bright dot was the captured particle. Blocking the beam stopped the captured particle, taking off the block, the particle was attracted and moved again.

Chasing of one particle by another was observed once the first particle was trapped and moved down. A second captured one, which was behind the first one, was lighted by more light than the first one, therefore, the first one moved slowly, the second one moved quickly. Thus the chasing.

Moving the laser beam transversely caused the captured particle to move with the beam.

This was caused by the gradient force.

Increasing the laser power caused the particle to move with greater velocity. Attenuating the laser power stopped the particles and even released them.

3.2.4 Data Acquisition

In order to get some quantitative results, data were recorded and processed in the exactly the same way as in the first experiment.

3.2.5 Theoretical Model

Since the particles seemed to be motionless without the laser beam, we still take:

$$\vec{mg} + \vec{F}_{buoy} + \vec{F}_{rand} = 0$$

When the beam was reversed, the optical force and the viscosity force changed direction. Take the downward direction as the positive x-axis, we have

$$F_{opt} - 6\pi \eta r \frac{dx}{dt} = m \frac{d^2x}{dt^2}$$

which is the same equation as (3.3), therefore, we have the same solution:

$$x = a + be^{-t/\tau} - b$$

where

$$a = \frac{F_{opt}}{6\pi \eta r}$$

$$b = \frac{F_{opt}m}{(6mr)^2}$$

$$\tau = \frac{m}{6\pi \eta r}$$

with the initial conditions

$$t = 0$$
, $x = 0$ and $v = 0$.

3.2.6 Data Analysis

Table 3–8 and 3–9 are the data of captured particle size, laser power and measured velocity for glass beads and PMMA latex beads respectively. The data was fitted by linear regression analysis. For the linear model and the second order model, the estimated parameters and their standard errors are listed in Table 3–10 and 3–11. The result is: for both glass beads and PMMA latex beads, at a 95% significance level, the linear model is an appropriate model. For

glass beads, at an 80% significance level, ϱ is more significant than P. For PMMA latex beads, at an 80% significance level, P is more significant than ϱ . Since the significance level is not high, both ϱ and P affect the motion of glass beads and PMMA latex beads. Table 3–12 and 3–13 are the results of the three velocities: the measured velocity, the regressed velocity and the calculated velocity. The VAF for glass beads is 81.57%, for PMMA latex beads is 97.23%.

Table 3–8: Data for glass beads: particle size, laser power and measured velocity.

	particle radius (µm)	laser power (mW)	velocity $(\mu m/s)$
1	5.2	83.9	148
2	5.6	77.71	128
3	6.4	77.71	204
4	5.6	77.71	186
5	6.9	69.77	119
6	5.6	69.77	114
7	4.75	62.26	88.5
8	4.3	62.26	62.3
9	6.92	54.75	202
10	6.49	54.75	132
11	6.49	54.75	149
12	6.49	47.25	104
13	6.92	47.25	154
14	6.49	40.62	141
15	7.35	40.62	174
16	6.9	40.62	142
17	6.48	33.56	117
18	5.6	33.56	110
19	4.75	33.56	82.2

Table 3-9: Data for PMMA latex beads: particle size, laser power and measured velocity.

	particle radius (µm)	laser power (mW)	velocity (µm/s)
1	6.9	92.29	142
2	5.6	92.29	131
3	7.8	92.29	154
4	6.49	92.29	126
5	5.6	83.90	125
6	5.2	83.90	99.8
7	4.75	83.90	82.1
8	6.05	83.90	136
9	6.9	77.71	110.3
10	4.75	77.71	88.5
11	5.75	77.71	100.8
12	6.05	68.88	121.5
13	4.75	68.88	94.4
14	4.32	68.88	94.7
15	5.19	55.19	66.4
16	5.6	55.19	92.5
17	4.75	55.19	75.4
18	4.32	47.69	74.8
19	4.75	47.69	66.9
20	6.05	47.69	82.0
21	4.75	47.69	51.2
22	4.32	32.23	43.3

Table 3-10: Regression analysis for glass beads

		parameters	standard error	<i>t</i> —statistic	RSS	SC
first model	$oldsymbol{eta}_o$	-124.66	56.69	16.556		
$v = \beta_o + \beta_1 \varrho + \beta_2 P$	β_1	32.98	7.59	11.97	1.16e+4	75.6%
	β_2	1.06	0.396	1.683		
second model	β_o	7.34	8.699	2.489		
$v = \beta_0 + \beta_1 Q + \beta_2 P$		26.38	30.86	4.749		
$+\beta_3 \varrho P + \beta_4 \varrho^2 + \beta_5 P^2$	β_2	-3.65	3.54	1.393		
+ p3Qr + p4Q + p5r =	β_3	-0.026	0.467	0.0379	1.01e+4	79.1%
	β_4	0.92	4.33	0.4423		
	β 5	0.043	0.027	0.2602		

Table 3-11: Regression analysis for PMMA latex beads

		parameters	standard error	<i>t</i> –statistic	RSS	SC
first model	$ \boldsymbol{\beta}_o $	-44.82	14.86	11.62		-
$v = \boldsymbol{\beta}_o + \boldsymbol{\beta}_1 \boldsymbol{\varrho} + \boldsymbol{\beta}_2 P$	β_1	13.40	3.31	7.37	2.55e+3	92.9%
	β_2	0.996	0.171	24.05		
second model	$oldsymbol{eta}_o$	0.692	5.34	0.299		
$v = \beta_o + \beta_1 \varrho + \beta_2 P$	$\boldsymbol{\beta}_1$	1.91	15.36	0.4868		
$+\beta_3 \varrho P + \beta_4 \varrho^2 + \beta_5 P^2$	β_2	0.755	1.44	0.6296		
+p3QF +p4Q* +p5F*	β_3	0.343	0.355	0.5752	2.43e+3	93.26%
	β_4	-1.26	3.23	0.7015		
	β_5	-111.85	0.014	0.1008		

Table 3-12: Data of the three velocities of glass beads.

	particle size Q (μm)	laser power P (mW)	original velocity $v_o \ (\mu m/s)$	regressed velocity $v_r \ (\mu m/s)$	calculated velocity v_c ($\mu m/s$)
1	5.2	83,90	148.00	135.71	140.12
2	5.6	77.71	128.00	142.34	127.73
3	6.4	77.71	204.00	168.73	120.04
4	5.6	77.71	186.00	142.34	127.73
5	6.9	69.77	119.00	176.80	101.86
6	5.6	69.77	114.00	133.93	114.68
7	4.8	62.26	88.50	97.94	104.40
8	4.3	62.26	62.30	83.11	103.11
9	6.9	54.75	202.00	161.55	79.73
10	6.5	54.75	132.00	147.37	83.80
11	6.5	54.75	149.00	147.37	83.80
12	6.5	47.25	104.00	139.42	72.32
13	6.9	47.25	154.00	153.60	68.81
14	6.5	40.62	141.00	132.39	62.17
15	7.3	40.62	174.00	160.76	55.81
16	6.9	40.62	142.00	145.92	59.30
17	6.5	33.56	117.00	124.59	51.42
18	5.6	33.56	110.00	95.57	55.16
19	4.8	33.56	82.20	67.54	56.28

Table 3-13: Data of the three velocities of PMMA latex beads.

	particle size	laser power	original velocity	regressed velocity	calculated velocity
	Q (μm)	P(mW)	v_o ($\mu m/s$)	v_r ($\mu m/s$)	ν _c (μm/s)
1	6.9	92.29	142.00	139.62	112.96
2	5.6	92.29	131.00	122.19	127.85
3	7.8	92.29	154.00	151.68	98.79
4	6.5	92.29	126.00	134.13	118.64
5	5.6	83.90	125.00	113.84	116.23
6	5.2	83.90	99.80	108.48	118.25
7	4.8	83.90	82.10	102.44	118.90
8	6.1	83.90	136.00	119.87	112.57
9	6.9	77.71	110.30	125.10	95.11
10	4.8	77.71	88.50	96.28	110.13
11	5.8	77.71	100.80	109.68	106.66
12	6.1	68.88	121.50	104.90	92.42
13	4.8	68.88	94.40	87.48	97.62
14	4.3	68.88	94.70	81.72	96.62
15	5.2	55.19	66.40	79.74	77.81
16	5.6	55.19	92.50	85.23	76.45
17	4.8	55.19	75.40	73.84	78.21
18	4.3	47.69	74.80	60.60	66.89
19	4.8	47.69	66.90	66.36	67.59
20	6.1	47.69	82.00	83.79	63.98
21	4.8	47.69	51.20	66.36	67.59
22	4.3	32.23	43.30	45.20	45.21

3.2.7 Discussion

From the observation and data analysis results, concluded that:

- 1. Although the thermal force and turbulence affected the motion of the particles, optical force did exist and played a significant role on the movement of the particles.
- 2. The transverse gradient force attracted particles into the beam and confined them moving along the beam axis.
- 3. The relationship of the optical force to the laser power and particle size has been checked by regression analysis. The optical force was confirmed quantitatively by the fact that the measurement was in rough agreement with the theoretical results.

3.3 Particles Trapped by a Single Beam

It was stated that a single big cone beam could trap particles in its focal point. In such traps, the basic scattering force and gradient force are configured to give a point of stable equilibrium located close to the beam focus. Particles in a single—beam trap are confined transversely to the beam axis by the radial component of the gradient force. Stability in the axial direction is achieved by making the beam focusing so strong that the axial gradient force component, pointing toward the beam focus, dominates over the scattering force which tries to push the particles out of the trap. This prediction was checked experimentally in the case that the beam from an argon ion laser was focused into different beam profiles. Therefore, by examining the holding stability of particles of these beams, the trapping ability of different profiles of laser beams can be determined qualitatively.

3.3.1 Apparatus

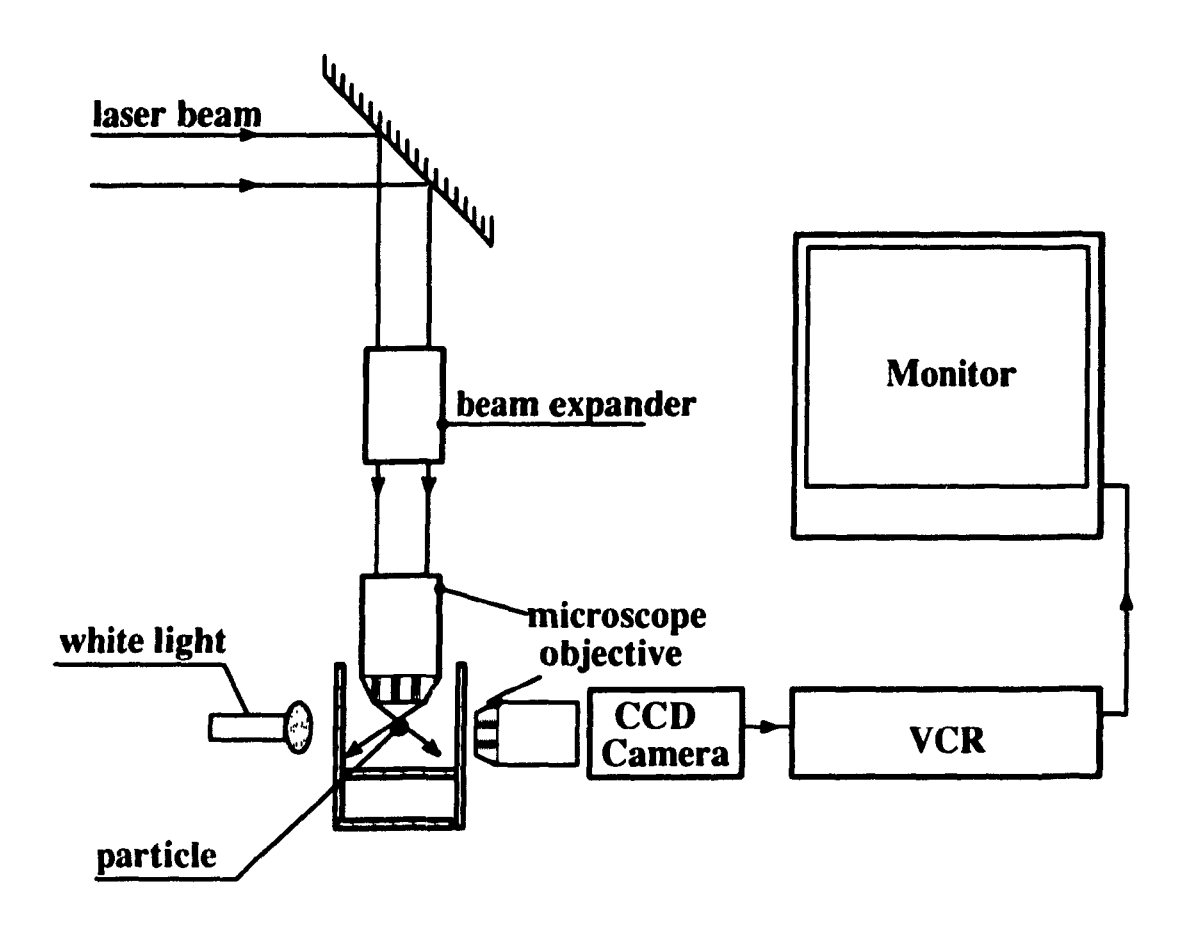


Figure 3.9: A schematic diagram of single beam trapping experiment.

Focusing the laser beam into different divergences was accomplished by expanding the beam first, then focusing the expanded beam by a high numerical aperture (N.A.) objective as shown in Figure 3.9.

The high N.A. objective had a magnification 100x, a focal length of 1.8 mm and a working distance of 0.32 mm. Its N.A. is 1.3 with oil. The beam expander consisted of two microscopic objectives having different focal lengths. The rate of the beam expanding is $M=f_2/f_1$, here the

subscript 1 stands for the first lens that the beam encounters and 2 stands for the second lens. It can be shown that $f_2/f_1=M_1/M_2$ by the formulae of the objectives, where M_1 is the magnification of the first lens, M_2 is the magnification of the second lens. Thus, $M=M_1/M_2$.

In the experiments, four different combinations of microscopic objectives were constructed as beam expanders. Table 3–14 lists the results of the beam size after beam expander, the beam spot size after focusing and the beam divergence.

Table 3–14: Results of beam size and divergence for different beam expander.

combinations	expand rate $M=M_1/M_2$	beam size (mm) $\omega' = M\omega_o$		divergence(degree) $\theta = \tan^{-1} \lambda / \pi \omega'' n$
40x + 4x	10	4.5	0.049	68.3
40x + 10x	4	1.8	0.123	45
40x + 20x	2	0.9	0.246	26.60
none	1	0.45	0.493	14.03

3.3.2 Observation

In the experiments, changing the laser power did not affect the trapping significantly, thus, the laser power was set at 78 mW for all of the combinations. The beam expander with highest rate was used first. The trapping could be seen even by the naked eye. As one particle was trapped, it was suspended in the water like a tiny light bubble. Its strong scattering ring could be seen on the optical table. Slightly moving the chamber transversely did not release the trapped particle. However, if the movement was quick, the particle was lost.

Once one particle was trapped, it remained motionless until another particle was also attracted into the trap and moved toward the equilibrium point. The first one would then be kicked out by the second one. This happened for most of the trapped particles.

It was found that on average the particle was held for 66 seconds in the trap, the longest capture time was 192 seconds.

Changing the beam expander to the second combination, it was found that the same trapping happened as the first one except that the trapped particles were easily kicked out. The average holding time was 35 seconds and the longest one was 137 seconds.

By using the third combination, it was relatively difficult to trap the particles. When they were trapped, they remained in position for a relatively short time before dropping off. The trap was not strong as compared to that in the first two experiments. Thus, a small perturbation would cause the trapped particle to move away. The average holding time with this combination was 6.5 seconds and the longest one was 14 seconds.

Applying the last combination (no beam expander), it was not possible to trap particles. Once one particle was transversely attracted into the beam, it would be accelerated in the axial direction. This happened for all of the attracted particles. None of them was found to be trapped stably.

3.3.3 Conclusions

The following conclusions are obtained from the observations and the measurements:

- 1. The possibility of trapping was strongly determined by the beam profile. The axial trap existed only in the large divergent beam.
- 2. The same divergence beam can trap particles of different sizes. This occurs because the force has the same characteristic for particles of different sizes.
- 3. The laser power did not affect the possibility of trapping, but would affect the stability of trapping.

3.4 Summary

In order to study the forces from different laser beams, three experimental stations were constructed. These stations allowed one to demonstrate the effect of a parallel beam and a cone beam.

The laser beam accelerating particles experiments showed that the gradient force did exist and could confine particles to a position on the beam axis; the scattering force could accelerate particles axially. Furthermore, the scattering force was studied quantitatively.

The single beam trapping particles experiment was performed for different beam profiles. The effect of the beam profile on the trapping was clearly observed. The relation of the beam profile to the trapping ability was confirmed to agree with the theoretical results presented in Chapter 2.

Chapter 4

Conclusions

4.1 Summary

The objectives of this thesis were:

- to develop a practical method of calculating the forces on micro-particles by a fundamental Gaussian beam, the TEM₀₀ beam,
- 2. to study the characteristics of the optical forces resulting from different laser beam profiles and to investigate the possibility of single beam trapping and
- 3. to verify the characteristics of the optical forces experimentally and qualitatively observe the stability of single beam trapping.

A simple and practical geometric optics method was described. The optical forces from a G.P.W. beam and a TEM_{oo} beam with an arbitrary shape were derived by the method. Since a G.P.W. beam is the simplest, practical plane wave with non-uniform transverse intensity distribution (it is the the approximate case of a TEM_{oo} beam when ω_o is large), it offered the possibility of studying the scattering force and the gradient force separately. A TEM_{oo} beam profile may be varied by focusing. Studying the properties of the forces resulting from various laser beam profiles showed that a single beam trap was possible if a highly focused TEM_{oo} beam was used.

Three experimental stations were designed and built. The first two confirmed the theoretical results for a G.P.W. beam: a particle captured by laser beam could be confined to the beam axis transversely by the gradient force and accelerated along the beam propagation direction by the scattering force. The scattering was studied quantitatively. The last experiment was de-

signed to test the relation of the optical force with the beam profile. It was shown that the possibility of single beam trapping was mainly determined by the beam profile, which was in agreement with the theoretical analysis.

4.2 Limitations and Recommendations for Future Work

4.2.1 Computation

The method of determination of the force on micro-particles is limited by the shape of the particles. The \vec{q} value derived in Chapter 2 is valid only for spherical particles. Furthermore, it was assumed the particles were homogeneous inside. If the method could be extended to non-spherical and inhomogeneous particles, the force on a living cell could be derived specifically.

4.2.2 Experiments

From Sections 3.1 and 3.2, it can be seen that the experimental results for PMMA latex beads were closer to their theoretical results than the glass beads. That was because the density of the PMMA latex beads is close to the density of the water, so that less turbulence was needed to make them float in the water. Therefore, in order to improve the precision of the accelerating particles experiment, particles with the same density as water are required. This would allow the particles to be suspended without the aid of turbulent forces.

Thermal affect caused by the thermal gradient could be reduced by making the chamber as small as the beam size, so that, the chamber as a whole is illuminated homogeneously by the laser beam, the thermal gradient inside the chamber is reduced to a minimum.

The experiments described in Section 3.1 and 3.2 are the simplest experiments to verify the existence of both the scattering force and the gradient force, but they do not provide an

adequate means of measuring the scattering force quantitatively. Since combination of trapped particles and particle chasing could not be avoided, there was no way to control the particles axially (they were controlled transversely). A possible solution is to fix the particle not only transversely but also axially. This can be accomplished either by an extra force, such as an electric force, or by more than one laser beam. When the particle is balanced by these forces, it will stay motionless. Thus, the optical force can be obtained versus the extra force.

1

The single beam trapping experiment was used to verify the theoretical relationship between optical force and beam profile. Since when the particle was trapped and held by the beam, the particle stayed at the position where the optical force was balanced by the particle gravity, only the force at this position could be calculated. Therefore the overall characteristics of the optical force could not be described, instead, only the stability was judged by measuring the duration that the particle was held. As discussed in Chapter 2, the force behavior at a certain range is just like a spring. Thus, $F_z \approx k(z + z_o)$ was used to describe the force properties. In order to verify experimentally the relation, the optical force F_z should be measured at different positions z. Plotting the force F_z over the position z would give the characteristics of the force. Based on this suggestion, an experiment can be considered. Instead of using neutral particles, we will use charged particles. By applying an electric field along the beam axial direction, the particle position may be controlled. The optical force may then be obtained from the voltage and the particle gravity.

The single beam trapping is a challenging research problem. Since it provides the possibility of precisely manipulating and mechanically testing of small objects, it is conceivable that laser manipulation may have wide applications to the study of the mechanical properties of single biological cells.

Appendix 1

Fresnel Coefficients

1. σ -case: \vec{E} perpendicular to the plane of incidence.

The transmission coefficient:
$$\tau_{\sigma} = \frac{2 \sin \theta' \cos \theta}{\sin(\theta' + \theta)}$$

The reflection coefficient:
$$\varrho_{\sigma} = -\frac{\sin(\theta' - \theta)}{\sin(\theta' + \theta)}$$
 with $n = \frac{\sin \theta}{\sin \theta'}$

2. π -case: \vec{E} in the plane of incidence.

The transmission coefficient:
$$\tau_{\pi} = \frac{2 \sin \theta' \cos \theta}{\sin(\theta' + \theta) \cos(\theta - \theta')}$$

The reflection coefficient:
$$\varrho_{\pi} = -\frac{\tan(\theta' - \theta)}{\tan(\theta' + \theta)}$$

Energy reflection and transmission coefficients are R and T:

For both σ -case and π -case:

$$R = |\varrho|^2$$

$$T = |\tau|^2 \frac{\cos \theta'}{n \cos \theta}$$

In the calculations in Chapter 2, we take:

$$R = \frac{1}{2}(R_{\sigma} + R_{\pi})$$

$$T = \frac{1}{2}(T_{\sigma} + T_{\pi})$$

Appendix 2

Derivation of the Angular Coordinates in the Particle Coordinate System of a Specified Ray

As shown in Figure A2.1, O-XYZ is the particle coordinate system. $O'(0, y_0, z_0)$ is the beam center. The beam axis is anti-parallel to the Z-axis and intersects with the Y-axis at point B. \vec{DC} is the direction of a ray hitting on point $C(Q, \theta, \phi)$. \vec{EF} is a diameter which is parallel to \vec{DC} . The angular expression of \vec{EF} is the same as the angular expression of \vec{DC} .

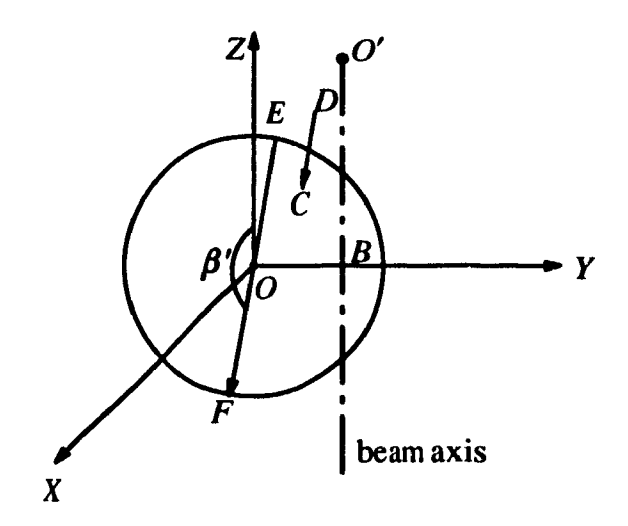


Figure A2.1: A schematic diagram of a ray incident on a sphere.

Let point I be the projection of point C on the Z=0 plane. The derivation is split into four parts according to the quadrant of point I. For each part, two cases need to be considered respectively: 1) $\beta > 0$, 2) $\beta < 0$. β is the angle of \overrightarrow{DC} with the beam axis $\overrightarrow{O'B}$. If $\beta > 0$, the ray arriving at point C is diverging away from the beam axis. If $\beta < 0$, the ray arriving at point

C is converging toward to the beam axis. First of all, we will discuss the case $\beta > 0$ for all the four parts. Since \vec{EF} is parallel to \vec{DC} , it is clear that $\beta' = 180^o - \beta$ for all the parts.

1) $0 < \phi < 90^o$ (*l* is in the first quadrant)

1

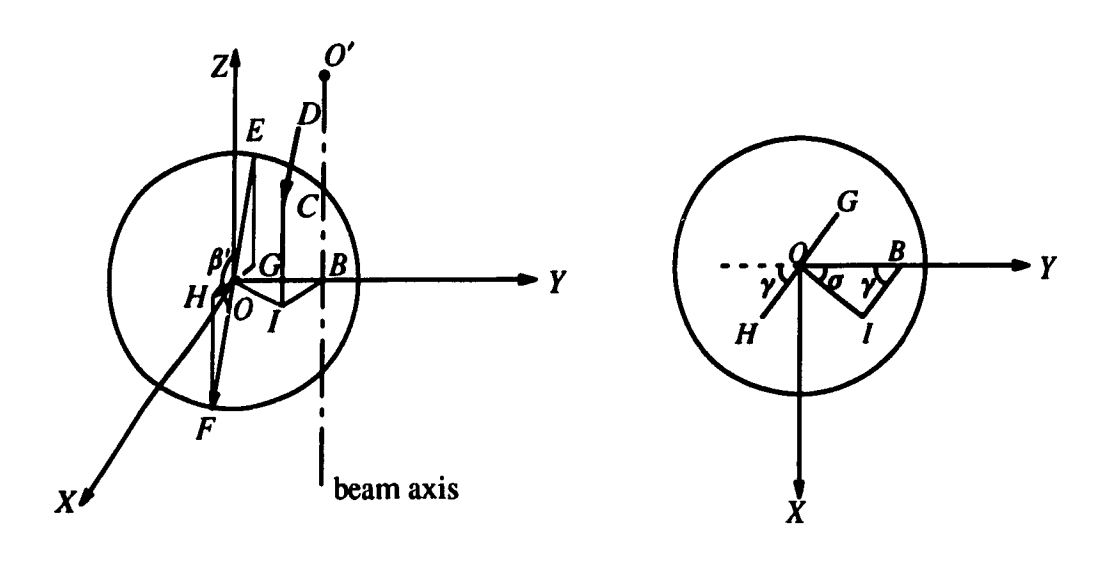


Figure A2.2: A schematic diagram of the system of a ray incident on a sphere and its sectional drawing when point *I* is in the first quadrant.

As shown in Figure A2.2, \vec{GH} is the projection of \vec{EF} on the Z=0 plane. I is the projection of point C on the Z=0 plane. Since DC and the beam axis O'B are on the same plane, BI is parallel to GH. Thus, angle γ in the triangle OBI is the angle of OH with the negative Y-axis, $\alpha' = 270^{\circ} + \gamma$. From the triangle OBI, we have:

by the sine law,
$$\frac{\sin \gamma}{|\vec{OI}|} = \frac{\sin \sigma}{|\vec{IB}|}$$
 where $\sigma = 90^{\circ} - \phi$
thus $\sin \gamma = \varrho \sin \theta \cos \phi / r$ $\gamma = a \sin (\frac{\varrho \sin \theta \cos \phi}{r})$
and $\alpha' = 270^{\circ} + a \sin (\frac{\varrho \sin \theta \cos \phi}{r})$

2) $90^{\circ} < \phi < 180^{\circ}$ (I is in the second quadrant)

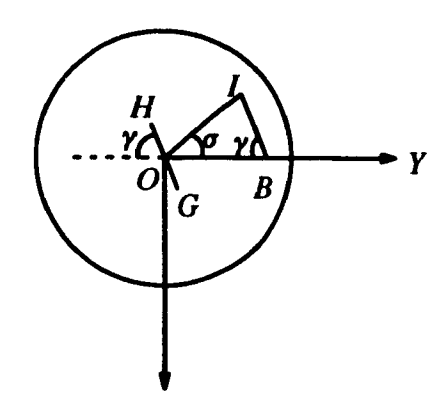


Figure A2.3: A sectional drawing for the case where I is in the second quadrant.

As shown in Figure A2.3,

$$\frac{\sin \gamma}{|\vec{OI}|} = \frac{\sin \sigma}{|\vec{IB}|}$$

where

$$\sigma = \phi - 90^\circ$$

$$\sigma = \phi - 90^{\circ}$$
 $|\vec{OI}| = \varrho \sin \theta$ and $|\vec{IB}| = r$

$$|\vec{IB}| = r$$

thus

$$\sin \gamma = -\varrho \sin \theta \cos \phi / r$$

$$\alpha' = 270^o - \gamma = 270^o + a\sin(\frac{\varrho \sin\theta \cos\phi}{r})$$

3) $180^{\circ} < \phi < 270^{\circ}$ (*I* is in the third quadrant)

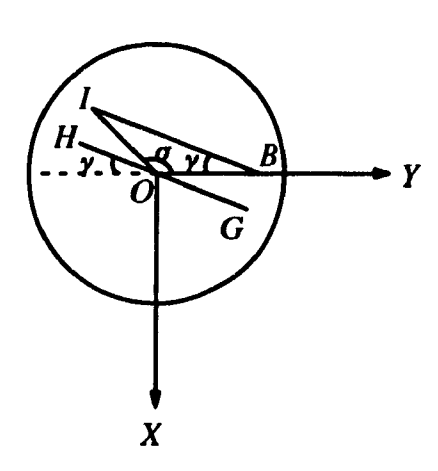


Figure A2.4: A sectional drawing for the case where I is in the third quadrant.

As shown in Figure A2.4, from the triangle OIB, we have:

$$\frac{\sin \gamma}{|\vec{OI}|} = \frac{\sin \sigma}{|\vec{IB}|}$$
where $\sigma = \phi - 90^{\circ}$ $|\vec{OI}| = \varrho \sin \theta$ and $|\vec{IB}| = r$
thus $\sin \gamma = -\varrho \sin \theta \cos \phi / r$

 $\alpha' = 270^{\circ} - \gamma = 270^{\circ} + a\sin(\frac{\varrho \sin\theta \cos\phi}{r})$

4) $180^{\circ} < \phi < 270^{\circ}$ (I is in the fourth quadrant)

and

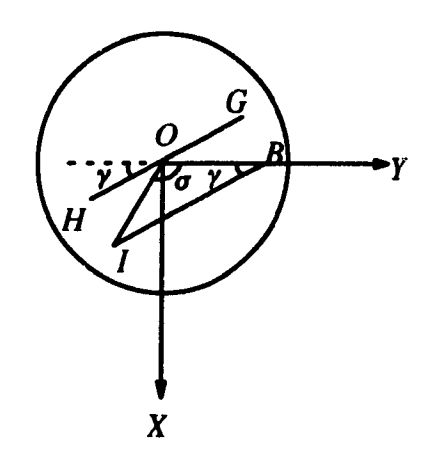


Figure A2.5: A sectional drawing for the case where I is in the fourth quadrant.

From the triangle OIB in Figure A2.5, we have:

$$\frac{\sin \gamma}{|\vec{OI}|} = \frac{\sin \sigma}{|\vec{IB}|}$$
where $\sigma = 360^{\circ} - \phi + 90^{\circ}$ $|\vec{OI}| = \varrho \sin \theta$ and $|\vec{IB}| = r$
thus $\sin \gamma = \varrho \sin \theta \cos \phi / r$
and $\alpha' = 270^{\circ} + \gamma = 270^{\circ} + a \sin(\frac{\varrho \sin \theta \cos \phi}{r})$

Summarizing of the above, it can be seen that for $\beta > 0$, independent of the quadrant of point $I, \alpha' = 270^{\circ} + a\sin(\varrho \sin \theta \cos \phi/r)$ and $\beta' = 180^{\circ} - \beta$.

Consider the case $\beta < 0$. As shown in Figure A2.6, \vec{EF} is equivalent to that of the case, \vec{EF} is rotating 180^o about the Z-axis, and \vec{GH} is equivalent to \vec{GH} in magnitude, but reversed in direction. Thus, independent of the quadrant of point I, we have:

$$\beta' = 180^{\circ} - (-\beta) = 180^{\circ} + \beta.$$

and

$$\alpha' = 270^o + a\sin(\frac{\varrho \sin\theta \cos\phi}{r}) - 180^o = 90^o + a\sin(\frac{\varrho \sin\theta \cos\phi}{r})$$

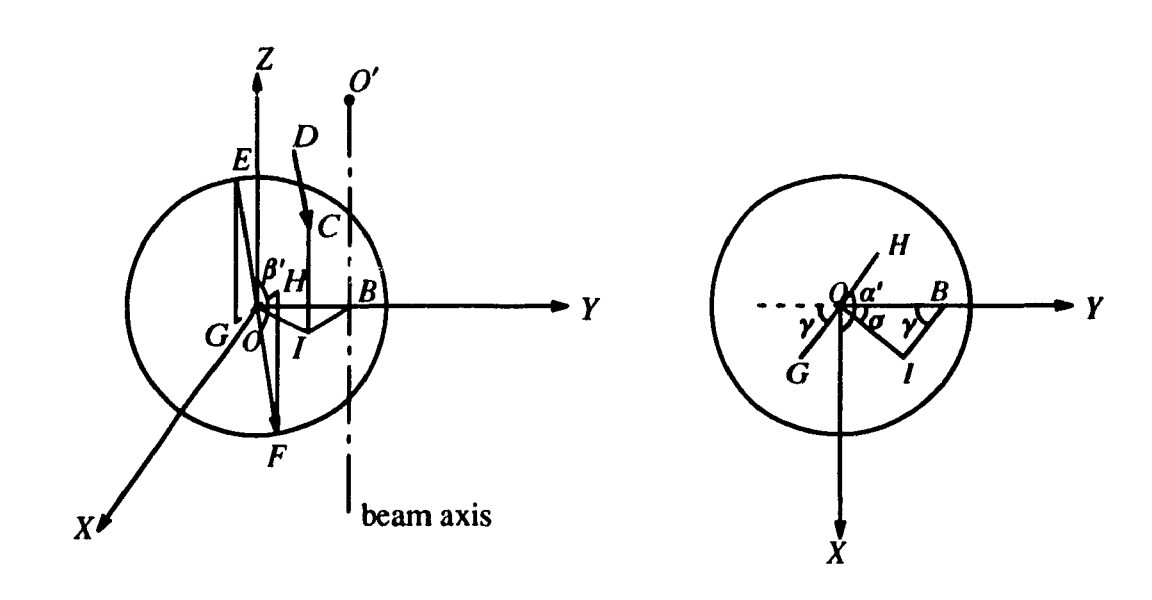


Figure A2.6: A schematic diagram of the system of a ray incident on a sphere with $\beta < 0$.

Appendix 3

Computer Programs

1. FORTAIN Programms for Numerical Calculation of the force for a G.P.W.

```
c CALCULATING THE Z-COMPONENT
c PROGRAM MAIN
   DIMENSION FA(30,4)
   A2=0.00
   DO 10 J=1,10
          DO 20 J=1,4
            RN=FLOAT(J)*0.2+1.
            A1=0.1*FLOAT(I)
     FA(I,J)=FORCE(A1,A2,RN)
     CONTINUE
      WRITE(*,13)(FA(I,J),J=1,4)
13
      FORMAT(1X,4(F6.3,1X))
      CONTINUE
     END
  FUNCTION FORCE(A1,A2,RN)
C INTEGRATION OVER PHI BY SIMPSON RULE
  IRPT=0
  N=1
  TWO=0.0
  D=1.
  A=0.
  B=8.*ATAN(1.)
  STEP=ABS(A-B)/2.
  FT=FORC1(A,A1,A2,RN)+FORC1(B,A1,A2,RN)
  FOUR=FORC1(A+STEP,A1,A2,RN)
  Y1=(FT+4.*FOUR)*STEP/3.
C REPEAT CALCULATION
10 IF(D.GT.1.0E-5.AND.IRPT.LT.20) THEN
    Y0=Y1
    TWO=TWO+FOUR
    FOUR=0.0
    STEP=STEP/2.0
   N=2*N+1
```

```
DO 20 I=1.N.2
          FOUR=FOUR+FORCI(A+FLOAT(I)*STEP,A1,A2,RN)
20
    CONTINUE
          Y1=(FT+4.0*FOUR+2.0*TW\;)*STEP/3.0
          D=ABS(Y1-Y0)
          IRPT=IRPT+1
    GOTO 10
    ENDIF
   FORCE=Y1
    RETURN
   END
  FUNCTION FORC1(FI,A1,A2,RN)
C INTEGRATION OVER THETA BY SIMPSON RULE
  IRPT=0
  N=1
  TWO=0.0
  D=1.
  A=0.
  B=2.0*ATAN(1.)
  STEP=ABS(A-B)/2.
  FT=CFUN(A,FI,A1,A2,RN)+CFUN(B,FI,A1,A2,RN)
  FOUR=CFUN(A+STEP,FI,A1,A2,RN)
  Y1=(FT+4.*FOUR)*STEP/3.
C REPEAT CALCULATION
10 IF(D.GT.1.0E-5.AND.IRPT.LT.10) THEN
    Y0=Y1
   TWO=TWO+FOUR
    FOUR=0.0
    STEP=STEP/2.0
   N=2*N+1
   DO 20 I=1,N,2
   FOUR=FOUR+CFUN(A+FLOAT(I)*STEP,FI,A1,A2,RN)
20 CONTINUE
    Y1=(FT+4.0*FOUR+2.0*TWO)*STEP/3.0
   D=ABS(Y1-Y0)
    IRPT=IRPT+1
    GOTO 10
    ENDIF
   FORC1=Y1
   RETURN
   END
   FUNCTION CFUN(X,FI,A1,A2,RN)
 C INTEGRATE FUNCTION
    RL=ASIN(SIN(X)/RN)
    RP=(RN*COS(X)-COS(RL))/(RN*COS(X)+COS(RL))
    RS=(COS(X)-RN*COS(RL))/(COS(X)+RN*COS(RL))
```

```
r=0.5*(RP*RP+RS*RS)
           t=1-r
     F1=-2.*(A1*A1*SIN(X)*SIN(X)+A2*A2-2.*A1*A2
           *SIN(X)*SIN(FI))
     F2=A1*A1*EXP(F1)
           FR=COS(2.0*(X-RL))+R*COS(2.0*X)
           FR1=1.0+R*R+2.0*R*COS(2.0*RL)
           FRT=T*T*FR/FR1
           FRT1=R*COS(2.0*X)+1.0-FRT
           CFUN=F2*FRT1*SIN(X)*COS(X)
     RETURN
     END
                                      -End-
c CALCULATING THE Y-COMPONENT
C PROGRAM MAIN
   DIMENSION FA(30,4)
   RN=1.5/1.3
   DO 10 I=1,30
           DO 20 J=1,4
            A1=FLOAT(J)*0.25+0.25
            A2=FLOAT(I)*0.1
      FA(I,J)=FORCE(A1,A2,RN)
20
       CONTINUE
            WRITE(*,13)(FA(I,J),J=1,4)
13
      FORMAT(1X,4(F5.3,1X))
 10
      CONTINUE
      END
  FUNCTION FORCE(A1,A2,RN)
C INTEGRATION OVER PHI BY SIMPSON RULE
   IRPT=0
   N=1
   TWO=0.0
   D=1.
   A=0.
   B=8.*ATAN(1.)
   STEP=ABS(A-B)/2.
  FT=FORC1(A,A1,A2,RN)+FORC1(B,A1,A2,RN)
  FOUR=FORC1(A+STEP,A1,A2,RN)
   Y = (FT+4.*FOUR)*STEP/3.
C REPEAT CALCULATION
```

10 IF(D.GT.1.0E-5.AND.IRPT.LT.20) THEN

```
Y0=Y1
   TWO=TWO+FOUR
   FOUR=0.0
   STEP=STEP/2.0
   N=2*N+1
   DO 20 I=1,N,2
     FOUR=FOUR+FORC1(A+FLOAT(I)*STEP,A1,A2,RN)
   CONTINUE
   Y1=(FT+4.0*FOUR+2.0*TWO)*STEP/3.0
   D=ABS(Y1-Y0)
   IRPT=IRPT+1
   GOTO 10
   ENDIF
   FORCE=Y1
   RETURN
   END
 FUNCTION FORC1(FI,A1,A2,RN)
C INTEGRATION OVER THETA BY SIMPSON RULE
  IRPT=0
  N=1
  TWO=0.0
  D=1.
  A=0.
  B=2.0*ATAN(1.)
  STEP=ABS(A-B)/2.
  FT=CFUN(A,FI,A1,A2,RN)+CFUN(B,FI,A1,A2,RN)
  FOUR=CFUN(A+STEP,FI,A1,A2,RN)
  Y1=(FT+4.*FOUR)*STEP/3.C
  REPEAT CALCULATION
10 IF(D.GT.1.0E-5.AND.IRPT.LT.10) THEN
   Y0=Y1
   TWO=TWO+FOUR
   FOUR=0.0
   STEP=STEP/2.0
   N=2*N+1
   DO 20 I = 1, N, 2
   FOUR=FOUR+CFUN(A+FLOAT(I)*STEP,FI,A1,A2,RN)
   CONTINUE
   Y1=(FT+4.0*FOUR+2.0*TWO)*STEP/3.0
   D=ABS(Y1-Y0)
   IRPT=IRPT+1
   GOTO 10
   ENDIF
   FORC1=Y1
   RETURN
   END
```

```
FUNCTION CFUN(X,FI,A1,A2,RN)
C INTEGRATE FUNCTION
  RL=ASIN(SIN(X)/RN)
 RP=(RN*COS(X)-COS(RL))/(RN*COS(X)+COS(RL))
 RS=(COS(X)-RN*COS(RL))/(COS(X)+RN*COS(RL))
  R=0.5*(RP*RP+RS*RS)
   T=1-R
 FI=-2.*(AI*AI*SIN(X)*SIN(X)+A2*A2-2.*AI*A2
       *SIN(X)*SIN(FI))
 F2=A1*A1*EXP(F1)
       FR=SIN(2.0*(X-RL))+R*SIN(2.0*X)
       FR1=1.0+R*R+2.0*R*COS(2.0*RL)
       FRT=T*T*FR/FR1
       FRT1=FRT-R*SIN(2.0*X)
 CFUN=F2*FRT1*SIN(X)*COS(X)*SIN(FI)
  RETURN
  END
```

-END-

2. C Programs for Calculating the Force for a TEM_{oo} Beam

```
/*************************
                                                          */
    Routines to find the force component Q_z applied on a
                                                          */
    particle in the Laser beam.
                                                          */
/* cc -o zforce zforce.c -lm
/* Hongyan Zhao
                       Jan. 18, 1991
                                                          */
#include <math.h>
#include <stdio.h>
#define PI 3.1415926535897932
double ly0,z0,rh,om,rn;
/****** The meaning of ly0,z0,rh,om,rn **********************/
/* ly0: the y-coordinate of laser beam to the center of the sphere
                                                          */
/* z0; the z-coordinate of laser beam to the center of the sphere
                                                          */
/* rh: the radius of the sphere;
                                                          */
/* om: the waist of laser beam;
                                                          */
/* rn: the ratio of the refractive index of the particle to its surroundings.
/*********************
main()
1
double force();
double fa[201][4];
int i,j;
lv0=0.;
rn=1.5/1.3;
om=5.;
for(i=0;i<=200;i++){
for(j=0;j<=3;j++){
rh=j+2.;
z0=i*2-200.;
fa[i][j]=force();
```

```
printf("%10.8f ",fa[i][j]);
 printf("\n");
 double force()
 double cfun();
long int irpt=0,n=1,i;
double a=0.,d=1.0;
double b,step,ft,two=0.0,four,y1,yy;
if(rh \le z0)
b=PI/2.;
   }
else(
b=PI:
step=fabs(a-b)/2.;
ft=cfun(a)+cfun(b);
four=cfun(a+step);
y1=(ft+4.0*four)*step/3.;
while( irpt < 12) {
yy≈y1;
two=two+four;
four=0.;
step=step/2.0;
n=2*n+1;
for(i=1; i \le n; i=i+2){
four=four+cfun(a+i*step);
  }
y1=(ft+4.0*four+2.0*two)*step/3.0;
d=fabs(y1-yy);
irpt++;
  }
return(y1);
```

```
/*************** integrate function **********************
double cfun(th)
double th;
#define al 0.5145
double z,rxy,zw,p,q,pq,be,ga,be1,be2,ap1,ap2;
double tb,rl,ab,ac,rp,rs,r,t;
double fc,fs,fr,ftc,fts,fz,fy,ff,wz2,f2,f3;
z=rh*cos(th);
rxy=rh*sin(th);
zw=1.3*PI*om*om/al;
if(z==z0)\{be=0.;\}
else{
p=1+zw*zw/((z-z0)*(z-z0));
q=1-zw*zw/((z-z0)*(z-z0));
pq=rxy/(z0-z);
be=atan(pq/(p-q*pq*pq/(2*p)));
 }
tb=th+be;
if(tb \geq=PI/2.) return(0.0);
rl=asin(sin(tb)/rn);
ab=rn*cos(tb)+cos(rl);
ac=cos(tb)+rn*cos(rl);
if(ab==0. \parallel ac==0.) printf("AB=%f,AC=%f\n",ab,ac);
rp=(rn*cos(tb)-cos(rl))/ab;
rs=(cos(tb)-rn*cos(rl))/ac;
r=0.5*(rp*rp+rs*rs);
t=1-r:
fc=cos(2.0*(tb-rl))+r*cos(2.0*tb);
fs=sin(2.0*(tb-rl))+r*sin(2.0*tb);
fr=1.0+r*r+2.0*r*cos(2.0*rl);
ftc=t*t*fc/fr;
fts=t*t*fs/fr;
fz=r*cos(2.*tb)+1.-ftc;
fy=fts-r*sin(2*tb);
ff= fz*cos(be)-fy*sin(be);
wz2=om*om*(1.0+(z-z0)*(z-z0)/(zw*zw));
f2=rh*rh*exp(-2.0*rxy*rxy/wz2)/wz2;
f3=2*PI*f2*ff*sin(th)*cos(tb);
```

```
/*
                                                     */
/*
    Routines to find the force component Q_v applied on a
                                                     */
/*
    particle in the Laser beam.
                                                     */
/*
                                                     */
  cc -o yforce yforce.c -lm
                                                     */
/* Hongyan Zhao
                     Jan. 18,1991
                                                     */
                                                     */
/***********************
#include <math.h>
#includ <stdio.h>
#define PI 3.1415926535897932
double ly0,z0,rh,om,rn;
/* ly0: the y-coordinate of laser beam to the center of the sphere
                                                     */
/* z0: the z-coordinate of laser beam to the center of the sphere
                                                     */
/* rh: the radius of the sphere:
                                                     */
/* om: the waist of laser beam:
                                                     */
/* rn: the index of refraction ratio of the sphere to its
                                                     */
/*
    surounding.
                                                     */
main()
{
double force();
double fa[40][4];
int i,j;
z0=0.;
```

```
rn=1.5/1.3;
om=0.1
for(i=0;i<=39;i++){
for(j=0;j<=3;j++){
rh=j+2.;
ly0=i*0.25;
fa[i][j]=force();
printf("%10.8f ",fa[i][j]);
printf("\n");
   }
/******* Integration over phi and theta *********************/
/* Integrate phi */
double force()
double force1();
long int irpt=0,n=1,i;
double a=0.,d=1.0, b=2.0*PI;
double step,ft,two=0.0,four,y1,yy;
step=fabs(a-b)/2.;
ft=force1(a)+force1(b);
four=force1(a+step);
y1=(ft+4.0*four)*step/3.;
while(irpt < 10) {
yy=y1;
two=two+four;
four=0.;
step=step/2.0;
n=n*2+1;
for(i=1; i \le n; i=i+2){
 four=four+force1(a+i*step);
  }
y1=(ft+4.0*four+2.0*two)*step/3.0;
d=fabs(y1-yy);
irpt++;
  }
return(y1);
}
```

```
double force1(ph)
   double ph;
 {
 double cfun();
long int irpt=0,n=1,i;
 double a=0.,d=1.0;
double b,step,ft,two=0.0,four,y1,yy;
if(rh \le z0)
b=PI/2.;
   }
else{
b=PI;
  }
step=fabs(a-b)/2.;
ft=cfun(a,ph)+cfun(b,ph);
four=cfun((a+step),ph);
y1=(ft+4.0*four)*step/3.;
while (irpt < 10) {
yy=y1;
two=two+four;
four=0.;
step=step/2.0;
n=2*n+1;
for(i=1; i \le n; i=i+2){
four=four+cfun((a+i*step),ph);
y1=(ft+4.0*four+2.0*two)*step/3.0;
d=fabs(y1-yy);
irpt++;
return(y1);
double cfun(th,ph)
double th,ph;
#define al 0.488
double x,y,z,rxy,zw,p,q,pq,be,ga,be1,ap;
```

```
double ttb,tb,rl,ab,ac,rp,rs,r,t,r2;
double fc,fs,fr,ftc,fts,fz,fy,ff,wz2,f1,f2,x1,y1;
x=rh*sin(th)*cos(ph);
y=rh*sin(th)*sin(ph);
z=rh*cos(th);
r2=x*x+(y-ly0)*(y-ly0)
rxy = sqrt(r2);
zw=1.3*PI*om*om/al;
if(z==z0)\{be=0.;\}
  else{
p=1+zw*zw/((z-z0)*(z-z0));
q=1-zw*zw/((z-z0)*(z-z0));
pq=rxy/(z0-z);
be=atan(pq/(p-q*pq*pq/(2*p)));
  }
if(rxy !=0.)
if(ly0!=0.){
x1=ly0*ly0+r2-rh*rh*sin(th)*sin(th);
else {x1=-cos(ph);}
y1=rh*sin(th)*cos(ph)/rxy;
ga=atan2(y1,x1);
  }else {ga=0.;}
if(be >= 0.){
ap=1.5*PI+ga;
 }
 else{
ap=PI/2+ga;
 }
be1=PI-fabs(be);
ttb=-sin(th)*sin(be1)*cos(ap-ph)-cos(th)*cos(be1);
if(ttb \leq 0.) return(0.0);
tb=acos(ttb);
rl=asin(sin(tb)/rn);
ab=rn*cos(tb)+cos(rl);
ac=cos(tb)+m*cos(rl);
if(ab==0. \parallel ac==0.) printf("AB=%f,AC=%f\n",ab,ac);
rp=(rn*cos(tb)-cos(rl))/ab;
rs=(cos(tb)-rn*cos(rl))/ac;
r=0.5*(rp*rp+rs*rs);
t=1-r;
```

r War

```
fc=cos(2.0*(tb-rl))+r*cos(2.0*tb);
fs=sin(2.0*(th-rl))+r*sin(2.0*tb);
fr=1.0+r*r+2.0*r*cos(2.0*rl);
ftc=t*t*fc/fr;
fts=t*t*fs/fr;
fz=r*cos(2.*tb)+1.-ftc;
fy=fts-r*sin(2*tb);
if(sin(tb)==0.){f1=0}
 else{
f1=(\sin(th)*\sin(ph)+ttb*\sin(be1)*\sin(ap))/\sin(tb);
 }
ff=fz*sin(be1)*sin(ap1)+fy*f1;
wz2=om*om*(1.0+(z-z0)*(z-z0)/(zw*zw));
f2=rh*rh*exp(-2.0*rxy*rxy/wz2)/wz2;
return(f2*ff*sin(th)*ttb);
}
```

- END -

Bibliography

- Ashkin, A., Acceleration and Trapping of Particles by Radiation Pressure, Phys. Rev. Lett., Vol. 24, No. 4, 156-159, 1970.
- Ashkin, A. and J. M. Dziedzic, *Optical Levitation by Radiation Pressure*, Applied Physics Letters, Vol. 19, No. 8, 283–285, 1971.
- Ashkin, A. and J. M. Dziedzic, Optical Levitation of Liquid Drops by Radiation Pressure, Science, Vol. 187, 1073–1075, 1975.
- Ashkin, A. and J. M. Dziedzic, Feedback Stabilization of Optically Levitated Particles, Applied Physics Letters, Vol. 30, No. 4, 202-204, 1977.
- Ashkin, A. and J. M. Dziedzic, Observation of Resonances in the Radiation Pressure on Dielectric Spheres, Phys. Rev. Lett., Vol. 38, No. 23, 1351–1354, 1977.
- Ashkin, A., Trapping of Atoms by Resonance Radiation Pressure, Phys. Rev. Lett., Vol. 40, No. 12, 729-732, 1978.
- Ashkin, A. and J. M. Dziedzic, Observation of Light Scattering from Nonspherical Particles Using Optical Levitation, Applied Optics, Vol. 19, No. 5, 660–668, 1980(1).
- Ashkin, A., Applications of Laser Radiation Pressure, Science, Vol. 210, No. 4474, 1081–1087, 1980(2).
- Ashkin, A. and J. M. Dziedzic, Observation of Radiation-pressure Trapping of Particles by Alternating Light Beams, Phys. Rev. Lett. Vol. 54, No. 12, 1245-1248, 1985.
- Ashkin, A., J. M. Dziedzic, J. E. Bjorkholm and S. Chu, Observation of a Single-beam Gradient Force Optical Trap for Dielectric Particles, Optics Letters, Vol. 11, No. 5, 288-290, 1986.
- Ashkin, A. and J. M. Dziedzic, *Optical Trapping and Manipulation of Viruses and Bacteria*, Science, Vol. 235, 1517–1520, 1987.
- Ashkin, A. and J. M. Dziedzic, Optical Trapping and Manipulation of Single Living Cells Using Infra-Red Laser Beams, Phys. Chem., Vol. 93, 254–260, 1989(1).
- Ashkin, A. and J. M. Dziedzic, *Internal Cell Manipulation Using Infrared Laser Traps*, Cell Biology, Vol. 86, 7914–7918, 1989(2).
- Balykin, V. I., V. S. Letokhov and A. I. Sidorov, Focusing Atomic Beams by the Dissipative Radiation Pressure Force of Laser Light, JETP Lett., Vol. 43, No. 4, 217–220, 1986.
- Balykin, V. I., V. S. Letokhov and V. G. Minogin, Laser Control of the Motion of Neutral Atoms and Optical Atomic Traps, Physica Scripta, Vol. T22, 119–127, 1988.
- Berns, M. W., et al., Laser Microsurgery in Cell and Developmental Biology, Science, Vol. 213, No. 31, 505-513, 1981.

- Bjorkholm, J. E., R. R. Freeman, A. Ashkin and D. B. Pearson Observation of Focusing of Neutral Atoms by the Dipole Forces of Resonance-radiation Pressure, Phys. Rev. Lett., Vol. 41, No. 20, 1361-1364, 1978.
- Block, S. M., D. F. Blair and H. C. Berg, Compliance of Bacterial Flagella Measured with Optical Tweezers, Nature, Vol. 338, 514-517, 1989.
- Burns, M. M., J. Fournier and J. A. Golovchenko, Optical Matter: Crystallization and Binding in Intense Optical Fields, Science, Vol. 249,749–249, 1990.
- Chang, S. and S. S. Lee, Optical Torque Exerted on a homogeneous Sphere Levitated in the Circularly Polarized Fundamental—mode Laser Beam, J. Opt. Soc. Am. B, Vol. 2, No. 11, 1853–1860, 1985.
- Grehan, G. and G. Gouesbet, Optical Levitation of a Single Particle to Study the Theory of the Quasi-elastic Scattering of Light, Applied Optics, Vol. 19, No. 15, 2485–2487, 1980.
- Hunter, I. W., S. Lafontaine, P. M. F. Nielsen, P. Hunter and J. M. Hollerbach, *Manipulation and Dynamic Mechanical Testing of Microscopic Objects Using a Tele-micro-robot System*, IEEE Control Systems, Vol. 10, No. 2, 3-8, 1990.
- Jackson, J. D., Classical Electrodynamics, John Wiley & Sons, New York, 1975.
- Kim, J. S. and S. S. Lee, Scattering of Laser Beams and the Optical Potential Well for a Homogeneous Sphere, J. Opt. Soc. Am., Vol. 73, No. 3, 303–312, 1983.
- Klein, M. V. and T. Furtak, Optics, John Wiley & Sons, New York, 1986.
- Lettieri, T. R., W. D. Jenkis and D. A. Swyt, Sizing of individual Optically Levitated Evaporating Droplets by Measurement of Resonances in the Polarization Ratio, Applied Optics, Vol. 20, No. 16, 2799–2805, 1981.
- Park, S. O. and S. S. Lee, Forward Far-field Pattern of a Laser Beam Scattered by a Water-suspended Homogeneous Sphere Trapped by a Focused Laser Beam, J. Opt. Soc. Am. A, Vol. 4, No. 3, 417-422, 1987.
- Roosen, G., Optical Levitation by Means of Two Horizontal Laser Beams: A Theoretical and Experimental Study, Physics Letters, Vol. 59A, No. 1, 6-8, 1976.
- Roosen, G., A theoretical and Experimental Study of the Stable Equilibrium Positions of Spheres Levitated by Two Horizontal Laser Beams, Optics Communications, Vol. 21, No. 1, 189–194, 1977.
- Roosen, G., The TEM₀₁ Mode Laser Beam a Powerful Tool for Optical Levitation of Various Types of Spheres, Optics Communications, Vol. 26, No. 3, 432–436, 1978.
- Roosen, G. and S. Slansky, Influence of the Beam Divergence on the Exerted Force on a Sphere by a Laser Beam and Required Conditions for stable Optical Levitation, Optics Communications, Vol. 29, No. 3, 341–346, 1979.

- Seber, G. A. F., Linear Regression Analysis, John Wiley & sons, New York, 1977.
- Self, S. A., Focusing of Spherical Gaussian Beams, Appl. Optics, Vol. 22. No. 5, 658-661, 1983.
- Shen, Y., The Principles of Nonlinear Optics, John Wiley & sons, New York, 1984.
- Siegman, A. E., Lasers, University Science Books, Mil Valley, California, 1986.
- Thurn, R., and W. Kiefer, Raman-Microsampling Technique Applying Optical Levitation by Radiation Pressure., Applied Spectroscopy, Vol. 38, No. 1, 78-83, 1984.
- Thurn, R., and W. Kiefer, Observations of Structural Resonances in the Raman Spectra of Optically Levitated Dielectric Microspheres, Journal of Raman Spectroscopy, Vol. 15, No. 6, 1984.
- Yariv, A., Optical electronics, Holt, Rinehart and Winston, New York, 1985.